Extrinsic and Intrinsic Factors Impacting Local Circuit Inhibition in the Neocortex

HARVARD UNIVERSITY
Graduate School of Arts and Sciences

DISSERTATION ACCEPTANCE CERTIFICATE

The undersigned, appointed by the

Division of Medical Sciences

Program in Neuroscience

have examined a dissertation entitled

Extrinsic and Intrinsic Factors Impacting Local Circuit Inhibition in the Neocortex

presented by Zhanlei Ye

candidate for the degree of Doctor of Philosophy and hereby certify that it is worthy of acceptance.

Signature: Jeffrey D. Macklis

Typed Name: Dr. Jeffrey Macklis

Signature: Chinfei Chen

Typed Name: Dr. Chinfei Chen

Signature: Pat

Typed Name: Dr. Pat Levitt

Dr. Rosalind Segal, Program Head *Date:* December 02, 2016

Dr. David Lopes Cardozo, Director of Graduate Studies

Extrinsic and Intrinsic Factors Impacting Local Circuit Inhibition in the Neocortex

A dissertation presented

by

Zhanlei Ye

to

The Division of Medical Sciences

in partial fulfillment of the requirements
for the degree of
Doctor of Philosophy
in the subject of
Neurobiology

Harvard University
Cambridge, Massachusetts

December 2016

Dissertation Advisor: Professor Takao K. Hensch Zhanlei Ye

Extrinsic and Intrinsic Factors Impacting
Local Circuit Inhibition
in the Neocortex

Abstract

Neuronal circuits controlling our perception and behaviors are radically shaped by experiences during early critical periods. For example, early life stress (ELS) has been linked to enduring negative behavioral consequences in humans and compromised structure/function of the prefrontal cortex (PFC). Parvalbumin (PV) expressing interneurons are particularly vulnerable to genetic and environmental insults associated with cognitive disorders. The maturation of PV inhibition is also pivotal for initiating critical periods in primary sensory cortices. The goal of this thesis is to examine how the functional maturation of PV inhibition is affected by intrinsic and extrinsic factors with a particular focus on the developing mouse medial PFC (mPFC).

First, I examined cell-intrinsic and extrinsic factors that might regulate the maturation and organization of local circuit inhibition. Assisting Yohei Kobayashi, we demonstrated that PV cell-intrinsic *Clock* genes underlie the maturational trajectory of PV cell-mediated inhibition and hence critical period timing. In collaboration with Mohammed A. Mostajo-Radji from Paola Arlotta's lab, using the approach of *in vivo* reprogramming of cortical pyramidal neurons, we showed that postsynaptic projection

neuron identity instructs afferent connectivity from inhibitory PV inputs in a pyramidal class-specific manner.

Next, I established models for studying the impact of ELS in both C57BL/6J and monogamous, bi-parental wild mice (*Peromyscus polionotus*). Based on anatomical and physiological results, we discovered sex-specific effects of poor parental care on PV interneurons in the mPFC, and their potential involvement in regulating anxiety behaviors in females. Our lab had previously defined a critical period for the anxiolytic benefits of acquiring an acoustic preference in the mPFC upon early music exposure. Here, I found the emergence of PV-cells in the mPFC normally matches this critical period window.

Finally, I tested whether PV-cell maturation controls such critical period plasticity in the mPFC by examining acoustic preference formation in two genetic models (Otx2, BDNF Val/Met) exhibiting delayed developmental trajectories. In contrast, the anxiolytic window for early music exposure was shifted earlier in females experiencing ELS. Notably, this effect was replicated in both mice and humans, suggesting a conserved mechanism and potential opportunity for therapeutic intervention after ELS.

Table of Contents

Acknowledgements

To my advisor, Takao, for continuous support of my research and career development

To my parents and brother, for keeping me grounded

To my husband, Mu, for motivating me to run and fly

Chapter 1

Introduction

Developmental brain dysfunctions arise from complex interactions between genetic and environmental factors. Developmental timing, namely, critical periods, regulates the environment's impacts on the reorganization of neural circuits. A classic example is amblyopia, in which condition the visual cortex permanently loses response to a deprived eye during a limited developmental time window (Hubel et al., 1976; Shatz and Stryker, 1978; Wiesel, 1982; Wiesel and Hubel, 1963). Another example is that passive simple tone exposure during postnatal day (P) 12-P15 (but not later) can shift the tonotopic map in the mouse primary auditory cortex (Barkat et al., 2011). Mis-wiring of circuits in cortical regions that control higher-order cognitive functions, mainly in the prefrontal cortex (PFC), is related to aberrant behaviors observed in psychological disorders including schizophrenia, sociopathy, obsessive-compulsive disorder, depression, and drug abuse (Heidbreder and Groenewegen, 2003).

Early social adversities, including abuse and neglect, have been associated with an increased risk for mental disorders in humans. A well-known example comes from studies on children subjected to early socio-emotional deprivation in Romanian orphanages during their first two years of life (Nelson et al., 2007). Adoptees show lower intelligence quotient (IQ), poor cognitive performance and social interaction in their later ages compared with normally raised subjects. The abnormalities in their brain anatomy and function include glucose hypometabolism in limbic and paralimbic structures (the orbital frontal gyrus, infralimbic prefrontal cortex, hippocampus/amygdala, lateral

temporal cortex) (Chugani et al., 2001); and reduced structural integrity of the uncinate fasciculus, which connects the anterior temporal lobe and the frontal lobe(Eluvathingal et al., 2006). These results reveal that the PFC is susceptible to early social experiences. Understanding how the PFC can be affected by experiences and the mechanisms regulating critical period plasticity in the PFC may provide insight into probing the developmental origins of mental illness.

Inhibitory parvalbumin (PV)+ circuits as a trigger for critical period plasticity in primary sensory modalities

Given the advantages of relatively clear input, output, and the pathway in between, maturation of receptive field properties in primary sensory modalities have been the main systems studied for critical period regulation. Examples include ocular dominance (OD) plasticity in the primary visual cortex (V1), whisker tuning in the somatosensory cortex (S1) and tonotopic map plasticity in the primary auditory cortex (A1). Although both the intrinsic maturation courses and the external stimuli differ across sensory modalities, one common feature is that inhibitory parvalbumin (PV)+ circuits serve as a trigger for critical period plasticity.

Maturation of local inhibition is shown to be both necessary and sufficient to trigger the onset of the critical period for OD plasticity in mouse V1. Glutamic acid decarboxylase 65 (GAD65, a synaptically localized isoform of γ-Aminobutyric acid GABA synthetic enzyme) knockout mice are insensitive to monocular deprivation, suggesting that they never enter the critical period for OD plasticity (Hensch et al., 1998). The sensitivity can be restored by infusing diazepam, an allosteric modulator of $GABA_A$

receptor, into V1 to enhance local inhibition (Hensch et al., 1998). It is further shown that diazepam infusion is able to initiate an early critical period in P15 wild-type (WT) mice (Fagiolini and Hensch, 2000). A more general notion is that local excitation/inhibition (E/I) balance controls the timing of critical periods.

Among all cortical interneurons, the specific PV+ neuron network plays a critical role in controlling critical period onset. In α1(H101R) specific mutant mice, in which $GABA_A$ receptors are insensitive to diazepam, monocular deprivation fails to produce OD shifts in a pre-critical period after diazepam administration (Fagiolini et al., 2004). $GABA_A$ receptor α1 subunits are preferentially enriched at somatic synapses innervated by PV+ fast-spiking (FS) large basket cells (Freund and Katona, 2007; Klausberger et al., 2002). Also, mature PV+ cells are preferentially enwrapped by perineuronal nets (PNN) containing chondroitin sulfate proteoglycans (CSPGs) (Hartig et al., 1999; Luth et al., 1992). CSPG degradation with chondroitinase-ABC (ChABC) re-opens the critical period for OD plasticity in adult rats (Pizzorusso et al., 2002). Finally, Otx2, a homeoprotein recognized by PNNs and internalized by PV+ cells, is shown to regulate the onset of the critical period for OD plasticity (Beurdeley et al., 2012; Sugiyama et al., 2008).

The maturation timing of PV+ cells varies across different cortices (del Rio et al., 1994), which is correlated with the timing of critical periods in corresponding cortical areas. In S1, an increase in PV+ neurons and PNNs in neighboring deprived barrel was observed after univibrissa rearing (McRae et al., 2007; Nowicka et al., 2009). Although not conclusive, this may suggest that the PV+ neuron network is also involved in regulating the critical period plasticity in somatosensory cortex. It is also shown that

maturation of PV+ neurons controls multiple sensory integration in mouse insular cortex (Gogolla et al., 2014)

The maturation of the PV+ neuron network is also experience-dependent. In layer 4 (L4) of primary sensory cortices, PV+ neurons receive direct inputs from corresponding thalamic nuclei. Withholding sensory experience by dark-rearing animals from birth delays the maturation of PV+ cells (Tropea et al., 2006) in V1, thus keeping V1 functionally immature and delaying critical period onset (Fagiolini et al., 1994). In A1, rearing young rats to spectrally-limited noise can prevent the maturation of PV+ neurons in the cortical area corresponding to the frequency range of noise, and delay critical period window for tonotopic plasticity (de Villers-Sidani et al., 2008). Exposing adult animals to noise reduces PV expression in A1 and restores tonotopic plasticity (Zhou and Merzenich, 2012; Zhou et al., 2011)

Mechanisms of critical period initiation

Why the onset of critical period plasticity is controlled by the maturation of inhibition, especially PV+ interneuron-mediated inhibition?

Several forms of plasticity are shown to have larger magnitude during critical period, compared with later stages. For example, long-term potentiation (LTP) evoked from the white matter in the visual cortex (Kirkwood et al., 1995), and inhibitory LTD (iLTD) recorded in layer 2/3 (L2/3) pyramidal neurons evoked in L4 (Jiang et al., 2010), are age and experience- dependent. Both are stronger in immature (or sensory-deprived) animals, and are absent after critical period. And sensory inputs during critical period can change the threshold for LTD-LTP switch (Kirkwood et al., 1996).

Besides the changes in plasticity, theoretical modeling and *in vivo* recording show that maturation of inhibition during critical period increases signal-to-noise ratio by preferentially suppressing spontaneous neuronal activities relative to evoked responses (Toyoizumi et al., 2013). The effect of monocular deprivation can be explained by broadening of deprived-eye spatial correlations, based on modeling using Hebbian learning rule and homeostatic plasticity (Toyoizumi et al., 2013).

Somatic feedforward inhibition by PV+ interneurons is important for these two hypotheses regarding the mechanisms of critical period initiation. Feedforward inhibition mechanisms in thalamorecipient layers after sensory stimulation via PV+ fast-spiking interneurons have been reported in vitro (Cruikshank et al., 2007) and in vivo (Swadlow, 2003; Wehr and Zador, 2005) in primary sensory cortices. PV+ interneurons and excitatory neurons receive direct inputs from the thalamus. PV+ interneurons also inhibit excitatory neurons. Compared with pyramidal neurons, the excitatory post-synaptic currents (EPSCs) in PV+ neurons are larger, and PV+ neurons show a higher responsiveness. Thus feed-forward inhibition is functionally important for filtering input information at the first stage of processing.

Somatic feedforward inhibition onto pyramidal neurons provides inhibition after excitation with a short time delay. It enforces precise coincidence detection in the soma (Pouille and Scanziani, 2001), thus enables PV+ neurons to control the potentiation of synapses between pyramidal neurons and their afferent fibers. Maturation of inhibition limits the temporal window that allows spike-timing dependent plasticity (STDP) (Kuhlman et al., 2010). In addition, suppressing spontaneous firing activity will prevent

the backpropagation of "unwanted" spikes into the dendrites that could result in STDP (Hensch, 2005).

E/I balance on a circuit level

Recent efforts in understanding the mechanisms of critical period plasticity are to investigate the E/I balance on a circuit level. A disinhibition microcircuit, namely, activation of pyramidal neurons by inhibiting inhibitory PV+ interneurons, has been shown to be crucial for cortical plasticity. A rapid but transient disinhibition due to decreased excitation onto PV+ neurons after MD only presents during the critical period for OD plasticity, and is necessary for the expression of OD (Kuhlman et al., 2013). In Nogo receptor 1 knockout (NgR1-KO) animals that show adult critical period plasticity for OD, similar disinhibition process was also observed (Stephany et al., 2016).

Neuromodulators also regulate cortical E/I balance by disinhibition via increased inhibitory inputs onto PV+ interneurons. Oxytocin has been shown to have a rapid effect in disinhibiting the auditory cortex. The pairing of oxytocin and pup calls enhances responses of pyramidal neurons by balancing excitation and inhibition, which is involved in maternal retrieval behavior (Marlin et al., 2015). Acetylcholine (ACh) activates L1 inhibitory neurons through nicotinic ACh receptors (nAChRs), which inhibit L2/3 PV+ neurons. This process is shown to be important for associative fear learning in the auditory cortex (Letzkus et al., 2011). It is also reported that disinhibition can be achieved via inhibitory inputs from vasoactive intestinal peptide (VIP)+ interneurons in upper layers to inhibit somatostatin (SST)+ interneurons in deeper layers(Fu et al., 2014; Stryker, 2014).

However, little is known about the pairing of interneurons and pyramidal neurons in the developing cortex. Interneurons have distinct laminar positions in the neocortex (Lodato et al., 2011). When immature medial ganglionic eminence (MGE)-derived interneurons were transplanted into the postnatal cortex, they migrated to their appropriate laminar locations and integrated into local circuits (Southwell et al., 2014; Tang et al., 2014). Previous work from our lab and the Arlotta lab has shown that the lamination of interneurons was disturbed in brains that lacked corticospinal motor neurons in L5 (Lodato et al., 2011). These findings suggest that the laminar location of interneurons may be affected by the presence of specific classes of pyramidal neuron partners. However, within cortical layers, interneurons target many of their neighboring pyramidal neurons (Fino and Yuste, 2011; Packer and Yuste, 2011). Thus the specificity of the interneuron-pyramidal neuron paring was not detectable due to the dense connectivity. These findings have led to the hypothesis of a nonspecific "blanket of inhibition" across pyramidal neurons in the cortex (Karnani et al., 2014). Whether interneurons selectively modulate their interactions with individual pyramidal neurons according to the pyramidal neuron subtype is not understood. Recent work has shown that different populations of pyramidal neurons within L5 of the mouse medial prefrontal cortex (mPFC) receive differing excitatory and inhibitory inputs (Lee et al., 2014), suggesting that the identity of pyramidal neurons may have a role in the establishment of their afferent connectivity. Consistent with this hypothesis, in L2 of the medial entorhinal cortex (MEC), cholecystokinin-expressing (CCK+) GABAergic basket cells specifically target pyramidal neurons that project to the contralateral EC, while avoiding neighboring pyramidal neurons (Krook-Magnuson et al., 2012; Varga et al., 2010). However, it

remains unknown whether interneurons make appropriate cell-type specific synapses based on the identity of pyramidal neuron partners.

Circadian modulation of E/I balance

Functional and structural synaptic plasticity is circadian dependent (see review (Frank and Cantera, 2014)). In humans, cortical excitability, measured by the evoked response to transcranial magnetic stimulation (TMS), is significantly modulated by circadian phase (Ly et al., 2016). Modeling of human EEG recording data also suggests that cortical E/I balance oscillates with circadian dynamics (Chellappa et al., 2016). In particular, TMS experiments reveal a morning peak of GABA-mediated intracortical inhibition, which decreases during the course of the day (Lang et al., 2011).

The stress hormone cortisol also follows a circadian rhythm. The secretion of cortisol shows an early morning peak, and then gradually declines during the course of the day (Edwards et al., 2001; Kirschbaum and Hellhammer, 1989). The cortisol circadian rhythm develops until age 15 in humans (Shirtcliff et al., 2012). And it can be affected by early life experiences. Higher levels of early postnatal maternal anxiety are associated with flatter cortisol declines in children (Simons et al., 2015). Flattened cortisol rhythm is reported in psychiatric disorders such as post-traumatic stress disorder (PTSD), depression, bipolar disorder, antisocial aggressiveness, addiction and so on (see review (Jeanneteau and Chao, 2013)). In rats, sleep patterns and EEG activities can be affected by early life stress (Mrdalj et al., 2013).

The oscillation of cortisol modulates spine plasticity, possibly via interactions with brain-derived neurotrophic factor (BDNF) (Jeanneteau and Chao, 2013). However, it remains unclear how circadian rhythms could directly regulate critical period plasticity.

Brakes for critical period closure

The closure of critical period is controlled by active processes that limit plasticity. Structural confinements, including PNN and myelin, mature during development, and limit the extent of circuit remodeling. Degradation of PNN with chondroitinase-ABC (ChABC) can re-open the critical period for OD plasticity in adult rats (Pizzorusso et al., 2002). And the critical period for OD plasticity opens normally and remains open in NgR knockout animals (McGee et al., 2005). In addition, molecular brakes are turned on towards the end of critical periods to limit further plasticity. For example, Lynx1, an endogenous antagonist to the nicotinic acetylcholine receptors (nAChR) (Miwa et al., 1999), has an increased expression after the critical period in V1. And removal of Lynx1 causes a non-closed critical period for OD plasticity in mice (Morishita et al., 2010).

The critical period in the mouse mPFC

The PFC in general plays a critical role in cognitive control due to its ability to coordinate thought and action in accordance with internal motivations (Miller and Cohen, 2001). The mouse mPFC in this thesis refers to the prelimbic (PrL) and the infralimbic (IL) cortex. To some extent, it is homologous to the orbital PFC (area 13, ventral part of area 12) and the medial PFC (area 25 and 32) in primates (Uylings and van Eden, 1990). One common feature of their connectivity is that they are directly connected with limbic

structures including the amygdala, hippocampus, hypothalamus and associated cortices (Miller and Cohen, 2001; Uylings and van Eden, 1990). Thus, functionally, the mPFC is suggested to play a central role in the mediating emotional, attentional, motivational, social, and cognitive behaviors (Heidbreder and Groenewegen, 2003; Vogt et al., 1992).

The PFC is believed to have a later and more prolonged development than other cortical areas. In humans, the PFC shows no sign of myelination until one month after birth, while primary sensory or motor areas attain an adult-like myelination pattern at birth (Flechsig Of Leipsic, 1901; Giedd and Rapoport, 2010). It is further inferred that the myelination in the PFC continues into late childhood and does not stabilize until the fourth decade of life (Yakovlev and Lecours, 1967). The late maturation of the PFC agrees with the proposed cascades of critical periods (Hensch, 2004), among which the critical periods for higher-order cognition may open later, and continue into adolescence (Year 12 to 18 in humans, and P28-P42 in rodents (Spear, 2000)).

Critical periods for cognitive function around adolescence have long been suggested. This hypothesis was formulated mainly based on correlations across increasing age, development of brain physiology and developmental changes in behaviors during adolescence (see review (Spear, 2000)). Such internal maturational events may trigger an individual's sensitivity to external experiences (Colombo, 1982).

But, in order to define a critical period in the mouse mPFC, one should also identify the essential critical external stimuli, both the positive (or normal) experiences that are considered necessary for triggering further development into later stages of life (Lorenz, 1937), and the noxious experiences to which individuals show the greatest

vulnerability (Stockard, 1921). Using this criterion, several recent studies have mapped out possible critical period(s) in the mouse mPFC.

Pattwell et al. (Pattwell et al., 2012) reported that human adolescents (12-17 years old) showed attenuated fear-extinction learning compared to adults (>18 y old) and children (5-11 y old). Similar results were also observed in mice. P29 mice showed significantly decreased fear-extinction compared to adult and P23 mice. In P23 and adult mice, L5 pyramidal neurons in the mPFC showed an increase in c-Fos activation and spontaneous excitatory post-synaptic current (sEPSC) frequency and amplitude after fear-extinction learning. But in P29 mice, no change in these parameters was detected. Our lab (Yang et al., 2012) reported that the acoustic preference behaviors in the mice could be reversed from their innate bias towards silence by music exposure between P15 and P24, but not after P60. Early music-exposed animals showed more c-Fos activation in the mPFC to brief exposure to the music in adulthood. And the formation of music preference was coupled with anxiolytic effect. Makinodan et al. (Makinodan et al., 2012) reported that mice that were isolated during P21 to P35 showed a decrease in social interaction and a deficit in working memory, in company with reduced myelination in the mPFC. Similar results have been shown in rats that isolation between P25 and P45 produced an irreversible effect upon object contact (Einon and Morgan, 1977).

It should be noted that the above studies adapted different behavior paradigms to test various aspects of cognitive function, which are emotion learning, acoustic preference (and anxiolytic benefit) and social behavior, respectively. Nevertheless, the mPFC is commonly engaged in these functions/behaviors, and changes in the mPFC after altered experiences were examined in all of these studies. Furthermore, the critical

periods proposed in these studies overlap in the time window P20-P30, suggesting common mechanisms underlying the critical periods in the mPFC.

However, it has not reached a common understanding how critical periods in the mPFC are regulated. Luckily, the critical period systems in primary sensory modalities have been intensively studied, which may provide an inspiration for studying the mechanisms underlying critical period plasticity in the mPFC.

PV+ neurons in the mouse mPFC

The PV+ fast-spiking large basket inhibitory neurons in the mPFC are functionally important. Dysfunction of the PV+ neuron network in the mPFC has been suggested to be involved in the pathophysiology of psychiatric disorders including autism (see review (Gogolla et al., 2009)) and schizophrenia (see review (Lewis et al., 2012)). Briefly, deficits in cognitive control could be caused by impaired prefrontal gamma oscillations, as a result of hypofunction of PV+ neuron network (Lodge et al., 2009; Sohal et al., 2009). Imbalance of excitation and inhibition in the mouse mPFC leads deficits in social behaviors (Yizhar et al., 2011).

Developmental changes in PV inhibition in the mPFC have also been reported. The subunit composition of $GABA_A$ receptors changes during development (Caballero and Tseng, 2016). In developing non-human primate dorsolateral PFC, α1 subunit expression increases in company with a reduction of α2 and α5 subunits (Duncan et al., 2010; Hashimoto et al., 2009; Hoftman and Lewis, 2011). The changes in postsynaptic receptor composition suggest a possible shift in the function and plasticity of PV+ neurons in the mPFC during development. For example, mice with early postnatal

ablation of N-methyl-D-aspartate receptor (NMDA) receptor subunit NR1 only in PV+ neurons showed selective cognitive impairments, including deficits in habituation, working memory and associative learning. The mutant mice have enhanced baseline cortical gamma rhythms, and impaired gamma rhythm induction after optogenetic drive of PV+ interneurons (Carlen et al., 2012). But post-adolescent deletion of NR1 does not result in such behavioral abnormalities (Belforte et al., 2010). Interestingly, decreased expression of α1 subunit has also been reported in Schizophrenia (Duncan et al., 2010), suggesting potential developmental origins for psychiatric disorders.

Is there a connection between psychiatric disorders and critical period plasticity? Do PV+ neurons in the mPFC regulate critical period plasticity in a similar way as in primary sensory areas? How are PV+ neurons in the mPFC affected by early experiences? Are there any rules for PV+ interneuron-pyramidal neuron connection?

The goal of my thesis is to examine how the functional maturation of PV inhibition is affected by intrinsic and extrinsic factors, with a particular focus on the developing mouse mPFC.

To answer the questions raised, I employed the following strategy:

1. I examined how PV cell-intrinsic *Clock* genes modulate cortical inhibition and critical period plasticity in the visual cortex;

2. I demonstrated that postsynaptic projection neuron identity instructs afferent connectivity from inhibitory PV inputs in a pyramidal class-specific manner, using the approach of *in vivo* reprogramming of cortical pyramidal neurons;

3. I examined the effects of early life stress (ELS) on behaviors and PV inhibition in the mouse mPFC;

4. I tested critical period plasticity in animal models with disrupted PV network in the mPFC.

Overall, I seek to provide anatomical, physiological and behavioral readouts for local circuit inhibition in the neocortex. By doing so, I hope to present evidence of cell-intrinsic, extrinsic and environmental impacts on PV circuits in the developing cortices.

Chapter 2

Materials and Methods

Animals

Animal information for Chapter 3 was published (Kobayashi et al., 2015). In detail, C57BL/6J (JAX no. 000664), ClockΔ5-6 (JAX no. 010925) (Debruyne et al., 2006), Pvalb-2A-Cre (PV-Cre) (JAX no. 012358) (Madisen et al., 2010), Clockflox (JAX no. 010490) (Debruyne et al., 2006), and Bmal1flox (JAX no. 007668) (Storch et al., 2007) mice were purchased from Jackson Laboratory. Original PV-GFP mouse breeders were kindly provided by H. Monyer (Heidelberg Univ.) (Meyer et al., 2002). TLCN-Cre mice (TLCN3.9-Cre Line D) were kindly provided by Y. Yoshihara (RIKEN Brain Science Institute) (Mitsui et al., 2007). All mice were on a C57BL/6J background.

Information on animals used in Chapter 4 can be found in our published paper (Ye et al., 2015). PV-IRES-Cre mice were generated by Hippenmeyer and colleagues (Hippenmeyer et al., 2005). Ai32 (ChR2(H134R)-EYFP) mice were generated by Madisen and colleagues (Madisen et al., 2012). Timed-pregnant CD-1 mice for *in utero* electroporation were obtained from Charles River Laboratories (Wilmington, MA).

In Chapter 5, *Peromyscus polionotus* (PO) were originally purchased from the Peromyscus Genetic Stock Center (PGSC), and maintained in Hopi Hoekstra's lab in Harvard University. POs are housed with 16 h of light and 8 h dark to mimic their nature habitat (Weber et al., 2013). BDNF Val/Met animals were kindly provided by Francis Lee (Weill Medical College of Cornell University) (Chen et al., 2006). C57BL/6J (JAX

no. 000664) mice were purchased from Jackson Laboratory and maintained in the lab for breeding and early life stress experiments.

In Chapter 6, the Otx2-AA mouse line was generated through a knock-in approach, as described previously (Bernard et al., 2014). In brief, the targeting molecule was produced by modification of a previous construct through PCR-mediated mutagenesis (Acampora et al., 2009). The mouse line was generated by C57BL/6 blastocyst injection and the removal of the selectable neo cassette was performed using a Cre-deleter mouse strain. PV-Cre (JAX no. 008069) and α1f/f (JAX no. 004318) mice were purchased from Jackson laboratory.

C57 mice were maintained on a 12 h:12 h light:dark cycle and allowed free access to regular chow and water. Mice were randomly assigned to the experimental groups. All procedures were approved by the Harvard University Institutional Animal Care and Use Committee and performed in accordance with institutional and federal guidelines.

Behavior Tests

Parental Separation in POs

Parental separation was performed according to published literature (Millstein and Holmes, 2007), but with 2-hr separation according to our approved protocol. One male and one female POs were housed together during breeding and continued till the weaning of the pups. The date of birth was denoted as postnatal day (P) 0. Litters were randomly selected for parental separation during postnatal (P) 2 to P14 with 2 hours per day at a random time during the light cycle. Pups were separated from parents and placed in a

separate room for 2hrs. Parental behaviors were monitored for 15min after returning the pups.

Fragmented Care in C57s

Fragmented care procedures were performed according to the published literature (Ivy et al., 2008). In Brief, 2nd-time pregnant females were single housed. Starting from P2, dam and pups were transferred to a new cage with 2g of shredded cardboard bedding on a mesh wire. Animals were returned to the normal housing at P9 and pups were weaned at P21.

Enriched Environment (using Marlau cage)

Standardized enrichment cages (Marlau Enrichment Cages) were purchased from Viewpoint Life Sciences. Environmentally enriched (EE) cages were furnished with rodent enrichment devices from Bioserv. Items were switched and moved around the cage daily. All items were cleaned with clidox and 70% ethanol before being placed in the cages. Pregnant C57 females were transferred into the EE cages and delivered there the litters. As the animals reach P21, males and females were separated in two different EE cages, with no more than 18-25 mice/EE cage. Cages were changed weekly.

Acoustic preference behavior

Mice were assessed for acoustic preference, first naïvely then again after music-exposure (2 weeks, Beethoven Symphony #1). The acoustic preference test (Yang et al.,

2012) was conducted using a Phenotyper 4500 (Noldus Information Technology), a 45 cm (width)×45 cm (depth)×45 cm (height) open arena with clear plastic walls viewed by means of a ceiling-mounted video camera and infrared lights and filters. Two diagonally opposing corners of the Phenotyper 4500 were chosen randomly and furnished with red, opaque plastic shelters bearing a side entrance. A small loudspeaker (1.6 cm diameter×1 cm height) was installed on the ceiling of each shelter (6 cm high), where nesting and bedding materials were provided at the bottom. To minimize ambient noise interference, the entire test setup was placed in an anechoic sound isolation chamber [inner dimensions: 55 cm (width)×49 cm (depth)×66 cm (height); Industrial Acoustics Company] with an ambient light source (8 W).

Each test was initiated by placing mice in the center of the arena and was monitored for 3 h consecutively. The animals' behavior was recorded by video camera, tracked, and analyzed using Ethovision XT software (Noldus Information Technology). Tests were conducted between 0900 and 1700 hours during the light phase to promote mouse dwelling in the shelters. All components of the test setup were wiped clean twice with Clidox solution, followed by 70% ethanol/30% purified water and ddH_2O, and then air-dried between each trial. The positions of shelters and sound playback were randomized on each trial.

To assay preference, time spent in each shelter during the final 30 min was measured. Mice spending most (80%) of their time in open areas within the test arena but outside either shelter were labeled as having made "no choice" and dropped from further analysis. Preference for silence or for music was calculated, respectively, as (percentage) 100×(time in silent shelter/total time in both shelters) or 100×(time in music shelter/total

time in both shelters). Animals spending 75% or more of their time in silent shelter were classified as ‘silence’ while those spending 75% or more in music shelter were classified as ‘music’ and the remaining are as ‘equal’.

Open field (OF) test

The open field test was performed in the same arena in an anechoic sound isolation chamber described above. Overall activity in the open field was measured by center dwell dime, distance (cm) moved, and the number of center crossings during the first 30 min via video recording and quantified by Ethovision XT software. The center was denoted as a 15cm X 15cm square in the center of the arena.

Elevated plus maze (EPM)

The EPM apparatus was purchased from Med Associates, Inc (part no. ENV-560A). EPM was performed during the dark phase of the light cycle. Animals were habituated to the behavior room for at least 30min before testing. Animals were left on the apparatus for 15min, and their behaviors were recorded using a camera and analyzed using Ethovision XT software (Noldus Information Technology) offline. The apparatus was cleaned with 70% Ethanol, followed by ddH_2O, and air-dried for 10min between trials. Open arm preference was calculated as the time spent in the open arms over the sum of the time spent in the open and closed arms.

3-chamber social test

The 3-chamber test was performed according to the published literature (Yang et al., 2011), in a 60 cm × 40 cm open arena equally divided into 3 chambers separated by transparent walls (25cm tall) with doors connecting the chambers. Animals were habituated to the behavior room for at least 30min before the test. For each testing animal, the trial contains 3 episodes: 5min exploration in the center chamber, 10min exploration in all 3 chambers, and 10min interaction with the newly introduced object and target mouse. During the 3rd episode, the novel object and mouse were placed separately in the 2 side chambers. Young adult 129S1 (JAX no. 002448) mice of the same sex and approximate body weight were used as target mice. Target mice were habituated to the wired cup for 2 15min-sessions one day before testing. We rotated through target mice to avoid over stimulation of target mice within a short period of time. Animals' behaviors were recorded using a camera, and analyzed using Ethovision XT software (Noldus Information Technology) offline. The apparatus was cleaned with 70% Ethanol, followed by ddH_2O, and air-dried for 10min between trials. The half chamber area with the object/mouse was considered the proximity to the object/mouse.

In vitro **electrophysiology**

Voltage-Sensitive Dye Imaging (VSDI) of A1 tonotopy

Mouse pups and mothers were placed in a sound-attenuating chamber and passively exposed to 7 kHz tones (100-ms pulses at 5 Hz for 1 s, followed by 2 s of silence, 80 dB SPL). Tones were generated by Audacity software.

The brain was sectioned peri-horizontally (600μm, 15°) to preserve the ventral medial geniculate (MGBv) and its projection to the auditory cortex (A1) (Barkat et al.,

2011). Thalamocortical brain slices were incubated for at least 90 minutes in the voltage-sensitive dye, Di-4-ANEPPS (Invitrogen D-1199, 5 μg/l). Six sites in the MGBv were activated with a glass pipette along the latero-medial axis (5 mA, 1 ms pulse; Iso-Flex, A.M.P.I.; spaced at 100μm). Fluorescence signals (1 ms frame rate; 512 ms) were imaged from regions of interest (130 x 130 μm) along the rostro-caudal axis of A1 at a fixed distance from a reference (rostral point of hippocampus) and at constant depth from the pia, corresponding to upper layer IV (L4). Excitation light from a shuttered LED (BrainVision) was reflected toward the slice. Emitted fluorescence was imaged using a MiCam Ultima CMOS-based camera (SciMedia). Fluorescence changes were normalized to resting fluorescence (ΔF/F0). Peak amplitude was defined as the maximum response across all L4 locations averaged across ten trials (MiCam Ultima analysis software). Individual time course traces were exported to Igor Pro (WaveMetrics) for analysis.

Brain slice preparation for electrophysiology

Mice were anesthetized using isoflurane and quickly decapitated. The brains were rapidly dissected and 350 μm thick coronal sections were collected using a blade microtome (Microm HM 650V, Thermo Scientific) in oxygenated (95% O_2, 5% CO_2) ice-cold cutting solution. In Chapter 3, coronal sections containing V1 visual area (Distance from lambda: -0.5mm – 0.5 mm) were collected from postnatal day (P) 26-P30 animals (at the peak of the visual critical period). Recordings were performed in the dark phase of the light cycle. In Chapter 4, coronal sections containing the M1 motor area (Distance from bregma: 1.42 – 0.74 mm) were collected from P22-P26 mice. In Chapter 5, coronal sections containing the mPFC area (Distance from bregma: 1.98 – 1.60 mm)

were collected from >P90 mice. Slices were incubated in artificial CSF (ACSF) at 34°C for 30 min and allowed to cool to room temperature. ACSF contained (in mM): 125 NaCl, 2.5 KCl, 1.25 NaH_2PO_4, 2 $CaCl_2$, 1 $MgCl_2$, 25 Glucose and 25 $NaHCO_3$. Cutting solution contained (in mM): 125 NaCl, 2.5 KCl, 1.25 NaH_2PO_4, 2 $CaCl_2$, 10 $MgCl_2$, 10 Glucose, 25 $NaHCO_3$ and 4 Ascorbate.

Recording and data acquisition

Recordings were made at room temperature (22-25°C). Slices were kept under constant (2 ml/min) bath perfusion using a peristaltic pump (MINIPULS 3, Gilson). Neurons were visualized in NIS-Elements microscope imaging software (Nikon), using an upright microscope (Eclipse FN1, Nikon) with a CCD camera (CoolSNAP EZ, Photometrics). Cortical layers were identified based on cell density and distance from pia (in V1, ~300- 400 μm for L4; in M1, ~100-400 μm for L2/3 and ~400-800 μm for L5; in mPFC, ~300-500 μm for L5). Cells expressing fluorescent protein (eGFP or tdTomato) were first identified under fluorescence light illumination (X-cite 120, Lumen Dynamics). Endogenous L2/3 and L5 pyramidal neurons were identified based on cell body size and morphology.

Recording pipettes (2.5-3.5 MΩ) were pulled from borosilicate glass capillaries using a DMZ-universal puller (Zeitz Instruments, Munich, Germany). Whole-cell recordings were amplified using a Multiclamp 700B amplifier (Axon Instruments) and acquired using Clampex 10 and a Digidata 1440A board (Axon Instruments). Recordings were filtered at 10kHz and digitized at 20kHz. Liquid junction potentials were not

compensated. Series resistance (5-12 MΩ) was closely monitored during recording. A recording was discarded if series resistance changed by >15%.

To assess the intrinsic properties, whole cell recordings were performed with internal solution containing (in mM) 130 K-gluconate, 4 KCl, 2 NaCl, 10 HEPES, 0.2 EGTA, 10 Phosphocreatine-Tris, 4 Mg-ATP, 0.3 Na_3-GTP (Osmolarity 290 mOsm, pH=7.2). For miniature inhibitory post-synaptic currents (mIPSCs), internal solution contained (in mM) 100 KCl, 40 K-gluconate, 8 NaCl, 2 $MgCl_2$, 10 HEPES, 0.1 EGTA, 2 Mg-ATP, 0.3 Na3-GTP and 1 lidocaine derivative QX-314 (Osmolarity 290mOsm, pH=7.2).

Miniature IPSC events were recorded at holding potential of -60 mV, with 20 μM CNQX (6-Cyano-7-nitroquinoxaline-2,3-dione disodium) (Tocris Biosciences, 1045), 50 μM AP-5 (D-(-)-2-Amino-5-phosphonopentanoic acid) (Tocris Biosciences, 0106) and 1 μM TTX (tetrodotoxin) (Tocris Biosciences, 1069) added to bath solution to block AMPA, NMDA receptors, and voltage-gated sodium channels, respectively. Traces at least 150 s-long were collected 3 min after break-in for mIPSC analysis. For pharmacological analysis, Zolpidem (Sigma-Aldrich, Z103) was dissolved in DMSO (Dimethyl sulfoxide) in stock solution (5mM). The final fraction of DMSO was 0.02%. Vehicle DMSO at the same concentration was present before Zolpidem application. For analysis of the effect of Zolpidem, mIPSC traces at least 150 ms long were collected before application of Zolpidem and 3 min after.

Optogenetics

For optogenetic experiments, a 473 nm laser (IKE-473-100-OP, IkeCool) was used to deliver light to brain slices via an optical fiber (core diameter of 200 μm). The fiber was placed ~3.5mm away from the slice surface, at a 45° angle, centered at recording sites. 20 μM CNQX and 50 μM AP-5 were applied to block excitatory inputs. Post-synaptic inhibitory responses were evoked by 2-msec light pulses, with a 10-sec inter-stimulation interval. Minimal responses were evoked at average threshold power of 190 μW for PV-IRES-Cre;Ai32 slices, at which level both successes and failures were observed. Repeated recordings of IPSC from 0.1 Hz light stimulation of a given cell showed high stability (no depression or facilitation was observed); this is consistent with stable stimulation parameters. At minimal stimulation, both successes and failures were observed, as expected. Maximal responses were evoked at power levels >1000 μW.

Data analysis

Passive membrane properties and action potentials were analyzed in Clampfit 10 (Axon Instruments). The 12 parameters were measured as follows: CThr (current threshold), current injection required to elicit an action potential; Vm (resting potential), membrane resting potential; Rm (input resistance), slope of steady state voltage responses to current injection of -100 pA, -50 pA and 0 pA; tau (membrane time constant), decay constant of the membrane with single exponential fit of the membrane response to a -100 pA current injection; Cm (membrane capacitance), calculated from Cm = tau/Rm; Vsag (voltage sag), measured as the sum of the voltage sag and rebound depolarization in response to a hyperpolarizing current pulse of -100 pA; VThr (action potential voltage threshold), the membrane voltage when $dV/dt \geq 20$; APamp (action potential amplitude),

amplitude of the action potential from baseline; APhw (half width), half width of action potential; fAHP (fast-afterhyperpolarization), amplitude of the hyperpolarization after the action potential spike measured from threshold voltage, APr (AP Rising time), time of 10–90% rising phase of action potential; APd (AP decay time), time of 90-20% decay phase of action potential. Properties of action potentials were measured from action potentials evoked at the current threshold.

mIPSCs were after-filtered at 2k Hz and analyzed in Mini Analysis Program (Synaptosoft). Decay time was calculated as the time between peak and 0.37 (1/e) of peak during decay, as an approximation for the decay constant of single exponential decay. In Chapter 4 for weighted tau, 90%-10% of the decay phase of each event was fitted with two exponentials. Fittings with R^2 less than 0.99 were not included. The weighted tau is calculated as: $\tau_w = \frac{A_1\tau_1 + A_2\tau_2}{A_1 + A_2}$

Biocytin Filling and Reconstructions

Recording of mIPSCs and voltage sag was done as described above except that high KCl internal solution with 0.3% (w/v) biocytin was used. After recording, neurons were held for 30 min to allow complete filling with biotin. Slices were then fixed in 4% PFA in PBS at 4 degrees overnight. After washing in PBS (3 x 15 min), slices were incubated in PBS / 0.2% Triton X-100 with Alexa Fluor 546-conjugated streptavidin (Life Technologies, diluted 1:500) for 4 hrs at room temperature, followed by washing in PBS / 0.1% Triton X-100 (3 x 15 min). Slices were then mounted in Fluoromount-G Slide Mounting Medium (SouthernBiotech). Image stacks were acquired using a confocal microscope (Zeiss 710) with a 10X objective lens. Neurons were traced in VAST Lite

and segmentations were exported to ImageJ for average-intensity z-projection. The width of the dendritic apical tuft was taken as the maximum horizontal span of the tuft measured parallel to the pia.

Algorithmic classification of reprogrammed vs non-reprogrammed cells (Chapter 4)

We prepared an algorithm to classify Fezf2-overexpressing cells based on their electrophysiological characteristics using a custom program written in MatLab (Mathworks, Natick, MA). A logistic-regression-based classifier was trained using 60% of control data (endogenous L2/3 CPNs and control GFP-CPNs vs. endogenous L5 CFuPNs) using a new random selection for each run, tested on the remaining 40% of control data, and then applied to classify Fezf2-overexpressing cells. The performance of the classifier on the test data set was measured by Precision (true positive over test positive), Recall (true positive over condition positive), F-score (2*Precision*Recall / (Precision+Recall)) and Accuracy (true positive and true negative) over 1000 test runs on independent random subsets of the training data. The classification algorithm was applied 1000 times.

In vivo **physiology**

Monocular Deprivation (MD) and Visual Evoked Potential (VEP)

The procedures and recording in Chapter 3 were performed by Yohei Kobayashi (Kobayashi et al., 2015).

Eyelid margins were trimmed by iris scissors and eyelids sutured shut under isoflurane anesthesia, as described (Fagiolini et al., 2004; Fagiolini and Hensch, 2000;

Sugiyama et al., 2008). Eyes were closed for 4 days from P25-P26 for critical period studies and from P60-P90 for adult studies. The integrity of the suture was checked daily and mice were used only if the eyelids remained closed throughout the duration of the deprivation period.

VEPs were recorded under nembutal/chlorprothixene anesthesia using standard techniques in mice (Fagiolini and Hensch, 2000; Porciatti et al., 1999). A tungsten electrode (9-12 MΩ) was inserted into V1b, where the maximal VEP response is located within the visual field 20° from the vertical meridian (3.0 mm from lambda) (Porciatti et al., 1999). Electrodes were advanced to a depth of 100-400 μm from the pial surface, where VEPs exhibit their maximal amplitude. Signals were band-pass-filtered (0.1-100 Hz), amplified, and fed to a computer for analysis. In brief, at least 30 events were averaged in synchrony with abrupt stimulus contrast reversal (1Hz). Transient VEPs were evaluated in the time domain by measuring the peak-to-baseline amplitude of the major negative component. Visual stimuli were horizontal sinusoidal gratings of different spatial frequencies at 100% contrast. Visual acuity was obtained by extrapolation to zero amplitude of the linear regression through the data points along a curve of VEP amplitude plotted against log spatial frequency. Ocular dominance was assessed by calculating the ratio of VEP amplitudes recorded by stimulating the eye contralateral and ipsilateral to the visual cortex where recording was performed.

Auditory brain stem response (ABR, performed by Henry Hing Cheong Lee)

Mice at P60 were anesthetized with a mixture of ketamine (100mg/Kg) and xylazine (10mg/Kg) and were kept on a heating pad at 37^{o}C. ABRs were measured using

a TDT system III with RZ6 multiprocessors and BioSigRZ software (Tucker Davis Technologies). Tone signals were calibrated using a 0.25 inch PCB microphone (PCB-FF-1/4) connected to the RZ6 multiprocessor analog / digital input. Calibrated and attenuated tone pips sinusoidal signals (0.5 ms rise time, 5 ms duration) were fed into an MF-1 magnetic speaker using the digital/analog output of the multi-processor (200 kHz sampling rate). The MF-1 magnetic speaker was placed in front of the right ear canal opening. Frequencies tested were 5.6, 8, 11.3, 16, 22.6, 32 kHz with sound pressure level (dB SPL, relative to 20 μPa) attenuated in a 5 dB steps between 10 and 80 dB SPL.

ABR waveforms were recorded using needles placed below the right ear pinna, while needles located at the vertex of the skull and at the base of the tail served as reference and ground electrodes respectively. The needles were connected to a low-impedance head stage (RA4LI; Tucker Davis Technologies) and fed into the optical port of the RZ6 multiprocessor through a preamplifier (RA4PA, gain 20x; Tucker Davis Technologies). ABR waveforms were averages obtained from 512 presentations of the tone in alternating phase and were band pass filtered (300 to 3k Hz). Thresholds in the ABR tuning curves were defined as the minimum dB SPL of atone that elicited a wave I above the noise level. All experiments were conducted in a sound booth (Industrial Acoustic Company Model 120A double wall).

Electroencephalography (EEG, chapter 6, performed by Henry Hing Cheong Lee)

Adult mice (>P60) were anesthetized by isoflurane and EEG electrodes were implanted onto cranial surface near prefrontal region (bregma +1.5mm, lateral 1mm) while reference and ground electrodes near visual region (bregma -4mm, lateral 1.5mm)

and secured by screws and dental cement. Two electromyogram (EMG) electrodes were implanted under the nuchal muscles to monitor muscular activities. During EEG recording, mice were placed inside a circular recording chamber containing bedding, food and water. A camera was also used to monitor the activities of the mice inside recording chamber. After 30 min habituation to the recording arena, a continuous recording of 2-hours were performed where signals were amplified 100x by a preamplifier (Pinnacle), filtered (1-1kHz) and transferred to a computer for recording (VitalRecorder). A HumBug was used to further remove noise. EEG data were processed by fast fourier transform using SleepSign software and the power between 1-80Hz was directly used for comparison. Data from awake stages, which was defined by active muscular activities, were used.

Immunohistochemistry

Detailed methods of immunohistochemistry for chapter 3 (Kobayashi et al., 2015) and chapter 4 (Ye et al., 2015) were published.

In brief, mice were perfused transcardially with 0.9% NaCl followed by 4% paraformaldehyde prepared in 1X PBS. Brains were dissected, post-fixed overnight at 4°C in 4% paraformaldehyde, cryopreserved in 30% (wt/vol) sucrose in 1X PBS for over 24hrs, embedded in OCT compound (Sakura Finetek USA Inc.), and sectioned on a Cryostat (Leica). Immunohistochemistry was performed on free-floating sections (40μm). Sections were blocked for 3hr in room temperature, incubated with primary antibodies overnight at 4°C, intensively washed at room temperature and further incubated with corresponding Alexa Fluor-conjugated secondary antibodies for 3 hour at

room temperature. The following primary antibodies were used: anti-Otx2 (mouse monoclonal, in house), anti-cFos (rabbit polyclonal, 1/500, Santa Cruz), and anti-PV (rabbit polyclonal, 1/500, Swant). Secondary antibodies were used as follows: anti-mouse Alexa Fluor 488 (1/1000-2000, Molecular Probes), anti-rabbit Alexa Fluor 546 (1/1000-2000, Molecular Probes) and anti-rabbit Alexa Fluor 488 (1/1000-2000, Molecular Probes) Biotinylated WFA (1/100, Sigma-Aldrich) was used to reveal perineuronal nets and streptavidin-conjugated Alexa Fluor 633 (1/2000, Molecular Probes) was used for its detection. Stained sections were mounted in Fluoromount medium (Southern Biotech) and image stacks were acquired with a confocal microscope (Leica SP5 or Zeiss 710).

Image analysis

Staining intensity analysis and cell counting were then carried out using ImageJ software. The mouse mPFC was first confirmed by direct inputs from to basolateral amygdala (BLA) (Figure 2.1, (Paxinos, 2001)). A virus (pAAV-CAG-GFP) was injected into BLA to label its fibers. In brief, images were thresholded to subtract signals against background. Size and circularity filters were applied to remove structures that were counted false-positively. DAPI counterstain was further used to visually confirm that the analyzed structures were cells. For extracellular WFA staining, the mean intensity of the entire image was analyzed, to quantify staining on both the cell body and its projections. Average PV intensity was taken as the average value in a cortical area. Co-localization of different antibodies stains was quantified manually.

Figure 2.1. The mouse medial prefrontal cortex (mPFC)

(A-B) The mouse mPFC according to the brain atlas (Paxinos, 2001). (C) Co-staining of BLA fibers and PV in the mPFC sections. PrL: prelimbic cortex. IL: Infralimbic cortex. Scale bar: 200 μm

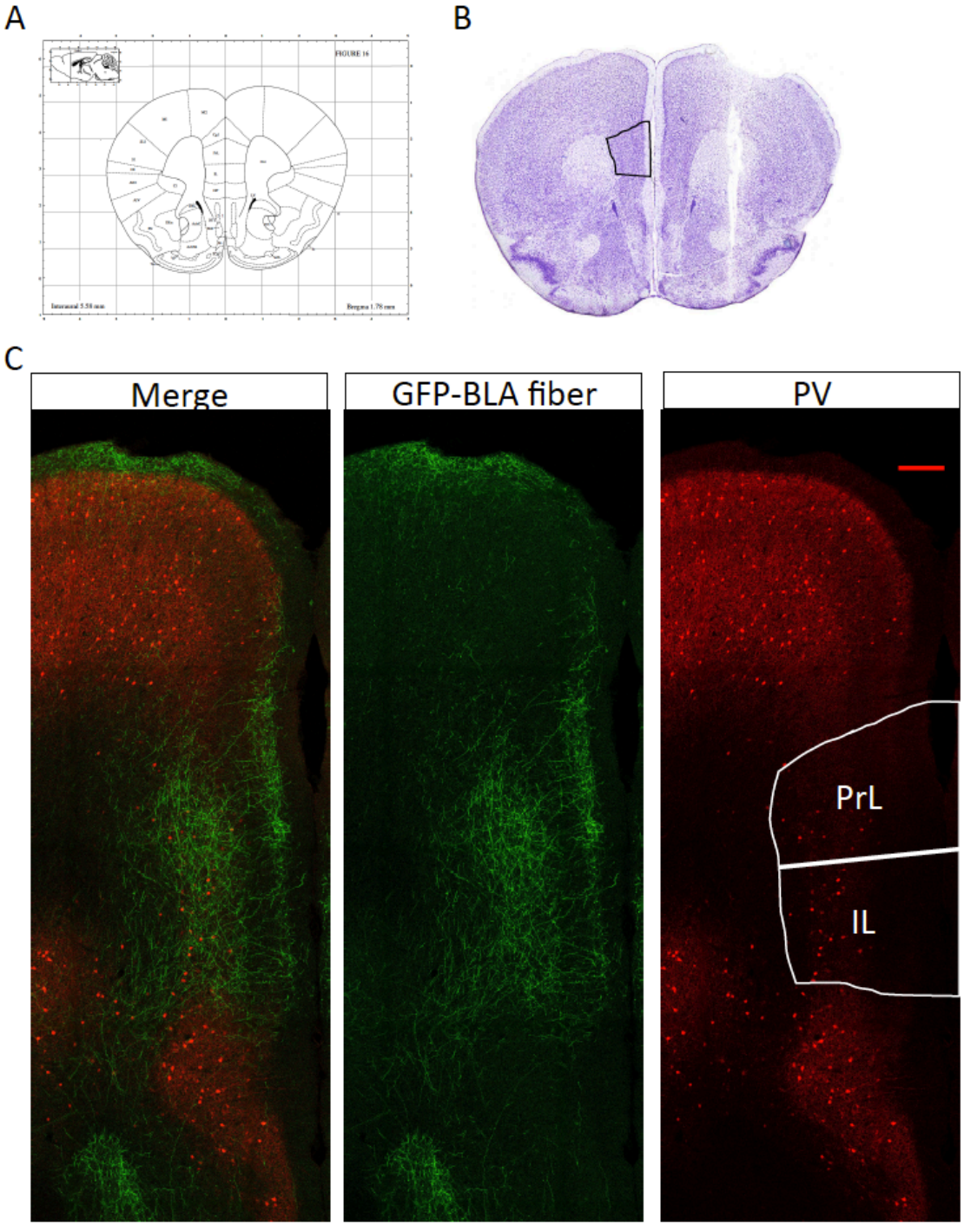

Figure 2.1 (Continued)

In utero electroporation

Detailed methods were published (Ye et al., 2015). (Chapter 4, performed by Mohammed A. Mostajo-Radji)

The Cdk5r-Fezf2-IRES-eGFP (Cdk5r-Fezf2^{eGFP}) and Cdk5r-empty-IRES-eGFP (Cdk5r-Ctl^{eGFP}) constructs (Rouaux and Arlotta, 2013) and the CAG-GFP construct (Zhao et al., 2006) have been previously described. The Cdk5r-Fezf2^{colorless} construct was generated by removing the eGFP sequence from the Cdk5r-Fezf2^{eGFP} cassette. The CAG-tdTomato construct was kindly donated by the Macklis lab. *In utero* electroporation was performed as previously described (Molyneaux et al., 2005). Briefly, 0.8 μl of endonuclease-free purified DNA (2 μg/μl) in sterile PBS mixed with 0.005% Fast Green was injected into the lateral ventricle of embryonic day 14.5 mice under ultrasound guidance (Vevo 770, VisualSonics). Five 35 volt pulses of 50 ms duration at 1 s intervals were delivered outside the uterus in appropriate orientation using 1-cm-diameter platinum electrodes and a CUY21EDIT square-wave electroporator (Nepa Gene). For the molecular, electrophysiological and pharmacological analysis, Cdk5r-Fezf2^{eGFP} or Cdk5r-Ctl^{eGFP} were coelectroporated with CAG-GFP into CD1 embryos (Charles River Laboratories). For optogenetic experiments, Cdk5r-Fezf2^{colorless} was coelectroporated with CAG-tdTomato into PV-IRES-Cre;Ai32 embryos.

mRNA analysis

Reverse transcription and qPCR

Cortical tissue micro-dissection was carried out as previously described(Saxena et al., 2012). In brief, dissected tissues were snap frozen in liquid nitrogen, lysed in trizol

reagent at 4°C and RNA extracted using the RNeasy Mini extraction kit (Qiagen). Genomic DNA was digested before elution from column. Isolated RNA was then subject to quantification and checked for purity using Nanodrop. The same amount of RNA was subject to reverse transcription using high capacity RNA-to-cDNA kit (Applied Biosystems) to obtain cDNA. qPCR reactions were set up using Taqman Universal Master Mix (Applied Biosystems). Taqman probes used were as follows: *BDNF*(Mm04230607_s1), and *GABRA1*(Mm00439046_m1). Both probes were FAM-conjugated except *GAPDH* which was VIC-conjugated serving as internal control. PCR reactions were performed using StepOnePlus™ Real-Time PCR system (Applied Biosystems) in 96-well plates using standard curve protocol. All results were internally normalized to the *GAPDH* expression.

Single Cell Gene Expression Profiling (Chapter 4, performed by Mohammed A. Mostajo-Radji and Juliana R. Brown.)

Detailed methods were published (Ye et al., 2015).

Cortical neurons of CD1-mice electroporated at E14.5 with either Cdk5r-Fezf2eGFP or Cdk5r-CtleGFP were dissociated at postnatal day 15 as previously described (Brewer and Torricelli, 2007). Briefly, tissue was digested with papain in HibernateA medium (BrainBits LLC, HA) with B27 supplement (Gibco, 17504-044). For the GABA receptor expression experiment described in Figure 4.6, the cell suspension was then purified by OptiPrep (Sigma-Aldrich, 1556) density gradient centrifugation.

Individual GFP-positive neurons visualized under a dissecting microscope were aspirated using a hand-pulled glass micropipette and ejected directly into 4 µl of lysis

buffer composed of DNA Suspension Solution (Teknova, T0221) with 100U/ml SUPERase•In RNase Inhibitor (Ambion, AM2696) and 0.5% NP40 (Thermo Scientific, PI-28324). The entire lysate was reverse transcribed using qScript™ cDNA SuperMix (Quanta Biosciences, 95048-100) according to manufacturer's instructions, except that the reaction volume was reduced to 5 µl. Specific target amplification (STA) was performed using HotStarTaq Plus DNA Polymerase (Qiagen, 203605) and 0.02X each TaqMan® Gene Expression Assays as follows: initial heat activation: 5 minutes at 95oC; followed by 2-step cycling: 5 seconds at 95oC, 6 minutes at 60oC for 20 cycles. The PCR product was cleaned using Exonuclease I (New England Biolabs, M0293S) according to manufacturer's protocol. Samples were then prescreened for the genes indicated below by standard qPCR using TaqMan probes. High-density microfluidic chip-based quantitative PCR was performed using TaqMan® Gene Expression Assays (probed listed in (Ye et al., 2015)), Fluidigm 96.96 Dynamic Array Chip for Gene Expression, and the Biomark HD System, following Fluidigm's protocols.

Raw data from the Biomark assay chips was processed with the Fluidigm Real-Time PCR Analysis software (Fluidigm). For reactions marked by the software as failed, amplification curves were inspected and reactions showing exponential amplification were manually passed. Subsequent data analysis was performed using R 3.1.2 (R Development Core Team, 2015) with the RStudio 0.98.1102 interface (RStudio, 2014) and the cited packages, GraphPad Prism 5.0f (GraphPad Software, Inc.), and STATA 13.1 (StataCorp LP).

Statistics

Various methods for statistical testing were used in this thesis. They were selected based on the question and the nature of the data encountered. Detailed methods were described in Chapter 3-6 text and figures. Values are mean ± sem. * $p<0.05$, ** $p<0.01$, *** $p<0.001$ and **** $p<0.0001$. n.s. (not significant) $p>0.05$

Chapter 3

Clock Genes Control Cortical Critical Period Timing

Author contribution

Yohei Kobayashi, Zhanlei Ye, and Takao K. Hensch

Y.K. designed, performed and analyzed *in vivo* recording and immunohistochemistry experiments. Z.Y. performed *in vitro* slice electrophysiology. T.K.H. supervised the project. This work has been published in Neuron (Kobayashi et al., 2015).

Summary

Circadian rhythms control a variety of physiological processes, but whether they may also time brain development remains largely unknown. Here, we show that circadian clock genes control the onset of critical period plasticity in the neocortex. Within visual cortex of Clock-deficient mice the maturation of inhibitory parvalbumin (PV)-cell networks slowed. Loss of visual acuity in response to brief monocular deprivation was concomitantly delayed and rescued by direct enhancement of GABAergic transmission. Conditional deletion of Clock or Bmal1 only within PV-cells recapitulated the results of total Clock-deficient mice. These data demonstrate a developmental role for circadian clock genes outside the suprachiasmatic nucleus, which may contribute mis-timed brain plasticity in associated mental disorders.

Introduction

Circadian rhythms are approximately 24-hour biological clocks which drive daily patterns of gene expression, physiology and behavior in most organisms (Dibner et al., 2010; Masri and Sassone-Corsi, 2010; Takahashi et al., 2008). In mammals, the central oscillator is located in the hypothalamic suprachiasmatic nucleus (SCN) and is generated by an auto-regulatory genetic feedback loop driven by the transcription factors CLOCK and BMAL1 (Lowrey and Takahashi, 2011) (Figure 3.1). This transcriptional loop can be observed not only in the SCN but also in nearly all mammalian tissues (Dibner et al., 2010; Takahashi et al., 2008). Notably, the majority of brain regions exhibit circadian rhythmicity by the same oscillatory machinery (Wakamatsu et al., 2001; Yan et al., 2000). However, the purpose of circadian clocks outside the SCN, especially their link to higher-order functions such as information processing in the cerebral cortex remains poorly understood.

Circadian oscillations in the visual cortex are established with onset of the visual critical period (Kobayashi et al., 2015), we hypothesize that they have a direct impact upon cortical plasticity during early postnatal life. To examine such a developmental role, we took advantage of mutant mice whose circadian gene expression is dampened. Among the two core clock components, CLOCK and BMAL1, we chose *Clock*-deficient ($Clock^{-/-}$) mice (Debruyne et al., 2006), because total *Bmal1*-deficient animals exhibit a variety of defects including reduced total activity and age-dependent weight loss (Bunger et al., 2000; Kondratov et al., 2006), which could affect brain functions independently.

In this study, we investigated a role for circadian clock genes in the binocular zone of mouse V1. We show that the intrinsic clock genes within PV-cells coordinate

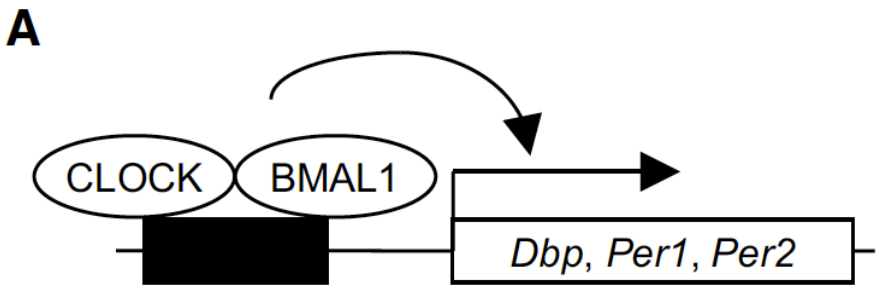

Figure 3.1. Schematic of CLOCK:BMAL1-mediated circadian gene expression

postnatal maturation of their networks and consequently the onset of critical period plasticity.

Results

CLOCK determines critical period timing

To assess the impact of *Clock* deletion on critical period plasticity, we measured visual acuity following 4 days monocular deprivation (MD) using visual-evoked potential (VEP) recordings, as reported previously in mice (Beurdeley et al., 2012; Carulli et al., 2010; Kang et al., 2013; Morishita and Hensch, 2008). VEP amplitudes were measured in response to various stimulus spatial frequencies, and visual acuity was calculated by linear extrapolation (log coordinates) to zero amplitude.

Upon MD during the critical period starting from P25-P26, visual acuity of the deprived eye was significantly reduced (i.e. amblyopia) in $Clock^{+/+}$ mice, indicating strong plasticity at this age (Figure 3.2 A). However, visual acuity was not changed in $Clock^{-/-}$ mice (Figure 3.2 A). Instead, after MD in adulthood starting from P60-P90, visual acuity remained typically unchanged in $Clock^{+/+}$ mice, but was significantly reduced in $Clock^{-/-}$ mice (Figure 3.2 B).

Since maturation of cortical inhibitory networks in the postnatal brain is important for initiating this critical period (Fagiolini and Hensch, 2000; Sugiyama et al., 2008), we hypothesized that inhibition might be compromised in $Clock^{-/-}$ mice. Thus, we attempted to rescue critical period timing by enhancing GABAergic transmission using benzodiazepine agonists (Fagiolini and Hensch, 2000). Amblyopia was induced fully by diazepam treatment concurrent with MD at P25-P26 in $Clock^{-/-}$ mice (Figure 3.2 C).

Figure 3.2. Delayed critical period plasticity in *Clock*$^{-/-}$ mice is restored by enhanced GABA signaling

(A) Monocular deprivation (MD) performed for 4 days during the typical CP from P25-P26. Average visual acuity evaluated by VEP recording in *Clock*$^{+/+}$ (noMD and MD, 5 mice each) and *Clock*$^{-/-}$ mice (noMD, 5 mice; MD, 6 mice) ***$P < 0.001$; ns, not significant (t-test). Values are mean ± SEM

(B) MD performed for 4 days in adulthood (P60-P90). Average visual acuity evaluated by VEP recording in *Clock*$^{+/+}$ (noMD and MD, 5 mice each) and *Clock*$^{-/-}$ mice (noMD and MD, 5 mice each). **$P < 0.01$; ns, not significant (t-test). Values are mean ± SEM

(C) *Clock*$^{-/-}$ mice treated with diazepam (DZ, 5 mice) or vehicle solution (Veh, 4 mice) starting one day before and concurrent with MD for 4 days from P25-P26. Average visual acuity evaluated by VEP recording. **$P < 0.01$ (t-test). Values are mean ± SEM

(D) Visual acuity in *Clock*$^{-/-}$ mice treated with DZ (6 mice) or Veh (4 mice) from P23 to P33 prior to 4 days MD at P60-P90. *$P < 0.05$. Values are mean ± SEM

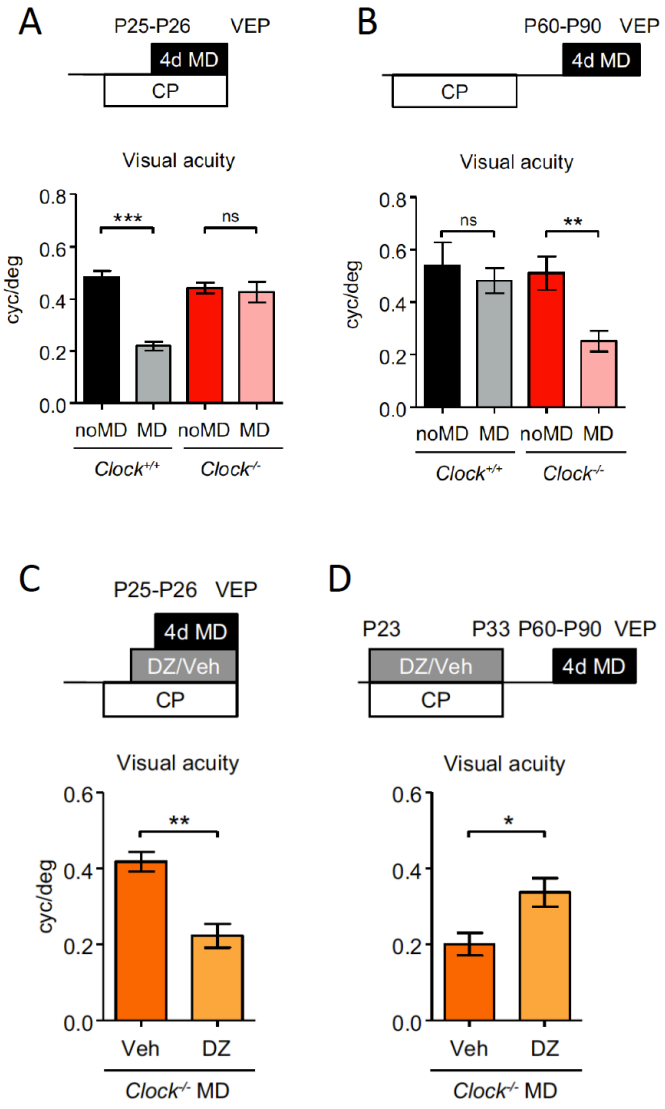

Figure 3.2 (Continued)

Moreover, mimicking a critical period by 10-day injection (P23-P33) of diazepam (Fagiolini and Hensch, 2000) prevented later adult plasticity in *Clock*$^{-/-}$ mice (Figure 3.2 D). These data suggested a reduced inhibition within local cortical circuits in the total absence of CLOCK (Hensch et al, 1998).

CLOCK regulates maturation of PV-cell circuits

To examine the maturation of inhibition in *Clock*$^{-/-}$ mice, we first recorded directly from PV+ cells to measure their intrinsic properties in PV-GFP X *Clock*$^{-/-}$ mice. Intrinsic electrophysiological properties of PV-cells were unaffected by *Clock* deletion (Figure 3.3 and Table 3.1). Detailed analysis revealed PV-positive puncta onto layer 4 pyramidal neurons to be decreased in size and number in *Clock*$^{-/-}$ mice (Figures 3.4 A-C). Moreover, we analyzed another marker for PV puncta, Synaptotagmin-2 (Syt2), which is not activity-dependent (Sommeijer and Levelt, 2012). Syt2 puncta were also decreased in size and number in *Clock*$^{-/-}$ mice (Figures 3.4 D-F). Consistent with these anatomical changes, the frequency (but not amplitude) of miniature inhibitory post-synaptic currents (mIPSCs) was significantly reduced within layer 4 pyramidal neurons (Figures 3.4 G-I). Taken together, CLOCK is important for the functional maturation of PV-cell circuits.

PV-cell-intrinsic Clock genes set critical period timing

To determine whether the role of circadian clock genes on PV-cell maturation is cell-autonomous, we performed conditional deletion of *Clock* from PV-cells using *Clock*^{flox} mice (Debruyne et al., 2006) crossed to a *PV-Cre* line expressing Cre recombinase driven by the parvalbumin promoter (Madisen et al., 2010).

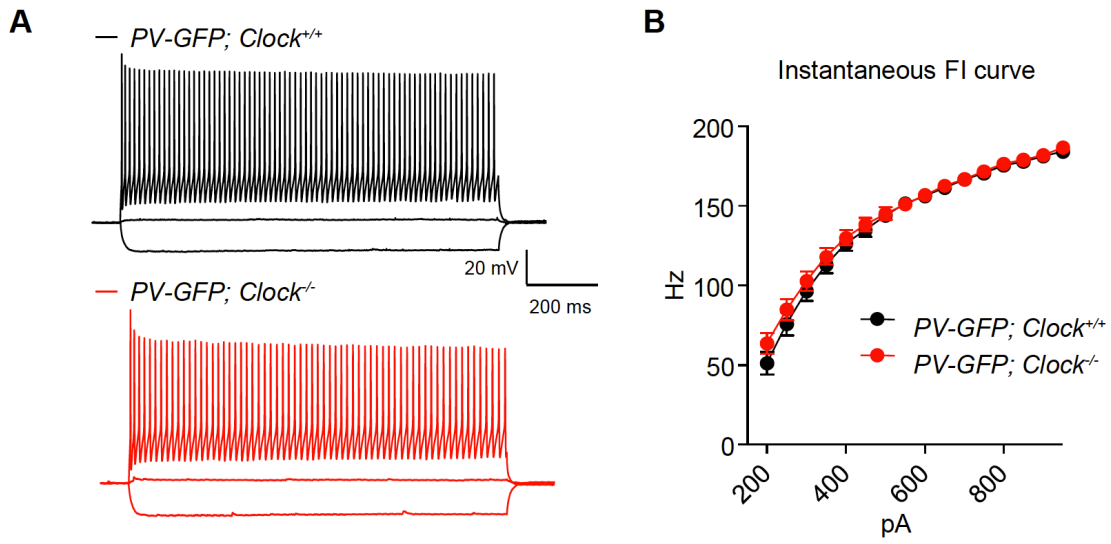

Figure 3.3. No change in intrinsic properties of PV+ neurons in Clock-/- mice

(A) Current steps (-100, 10, 300 pA) in representative PV-cells from *PV-GFP; Clock*$^{+/+}$ or *PV-GFP; Clock*$^{-/-}$ mice at CP (P28).

(B) PV-cell instantaneous FI curves (inverse of first inter-spike interval) for *PV-GFP; Clock*$^{+/+}$ (23 cells) or *PV-GFP; Clock*$^{-/-}$ mice (25 cells) at CP (P26-P30). Values are mean ± SEM

Table 3.1. Electrophysiologcial peroperties of PV+ interneurons

Parameter	Clock+/+	Clock-/-
Max Firing Rate(Hz)	184.60±2.51	187.00±3.19
Threshold Current (pA)	131.90±13.97	129.90±11.07
Resting Potential (mV)	-63.73±0.58	-63.77±0.59
AP Threshold (mV)	-37.04±1.02	-35.65±0.93
AP Amplitude (mV)	79.31±1.79	80.21±1.02
AP fAHP (mV)	23.94±0.70	25.10±0.66
AP Half-width (ms)	0.72±0.02	0.72±0.01
Time to Hyper Peak (ms)	1.90±0.08	1.91±0.05
Membrane time constant (ms)	8.15±0.42	8.30±0.47
Input Resistance (MΩ)	140.50±8.87	151.40±11.06
Capacitance (pF)	44.69±2.71	45.29±2.46

Figure 3.4. Functionally weakened PV-circuits in *Clock*$^{-/-}$ mice

(A-C) Immature PV puncta onto pyramidal neurons in layer 4 of V1b in *Clock*$^{-/-}$ mice at CP (P29) (A). Cumulative plots for mean PV puncta size per soma (B) and PV puncta number per soma (C), and their mean values (insets) in *Clock*$^{+/+}$ (90 cells from 4 mice) and *Clock*$^{-/-}$ mice (92 cells from 4 mice).

(D-F) Immature Syt2 puncta onto pyramidal neurons in layer 4 of V1b in *Clock*$^{-/-}$ mice at CP (P29) (D). Same analyses as in (B) and (C) in *Clock*$^{+/+}$ (86 cells from 4 mice) and *Clock*$^{-/-}$ mice (102 cells from 4 mice). Scale bar, 5 mm. *$P < 0.05$; **$P < 0.01$; ***$P <$ 0.001 (K-S test for cumulative plots; Mann-Whitney test for insets). Values are mean ± SEM

(G-I) mIPSC traces from pyramidal neurons in layer 4 of V1b in *Clock*$^{+/+}$ (21 cells from 3 mice) and *Clock*$^{-/-}$ mice (23 cells from 3 mice) at CP (P26-P28) (G). Cumulative plots for mIPSC amplitude (H) and inter-event interval (I) from all events, and their mean values from all cells (insets). ****$P < 0.0001$ (K-S test); *$P < 0.05$ (Mann-Whitney test for insets); ns, not significant. Values are mean ± SEM

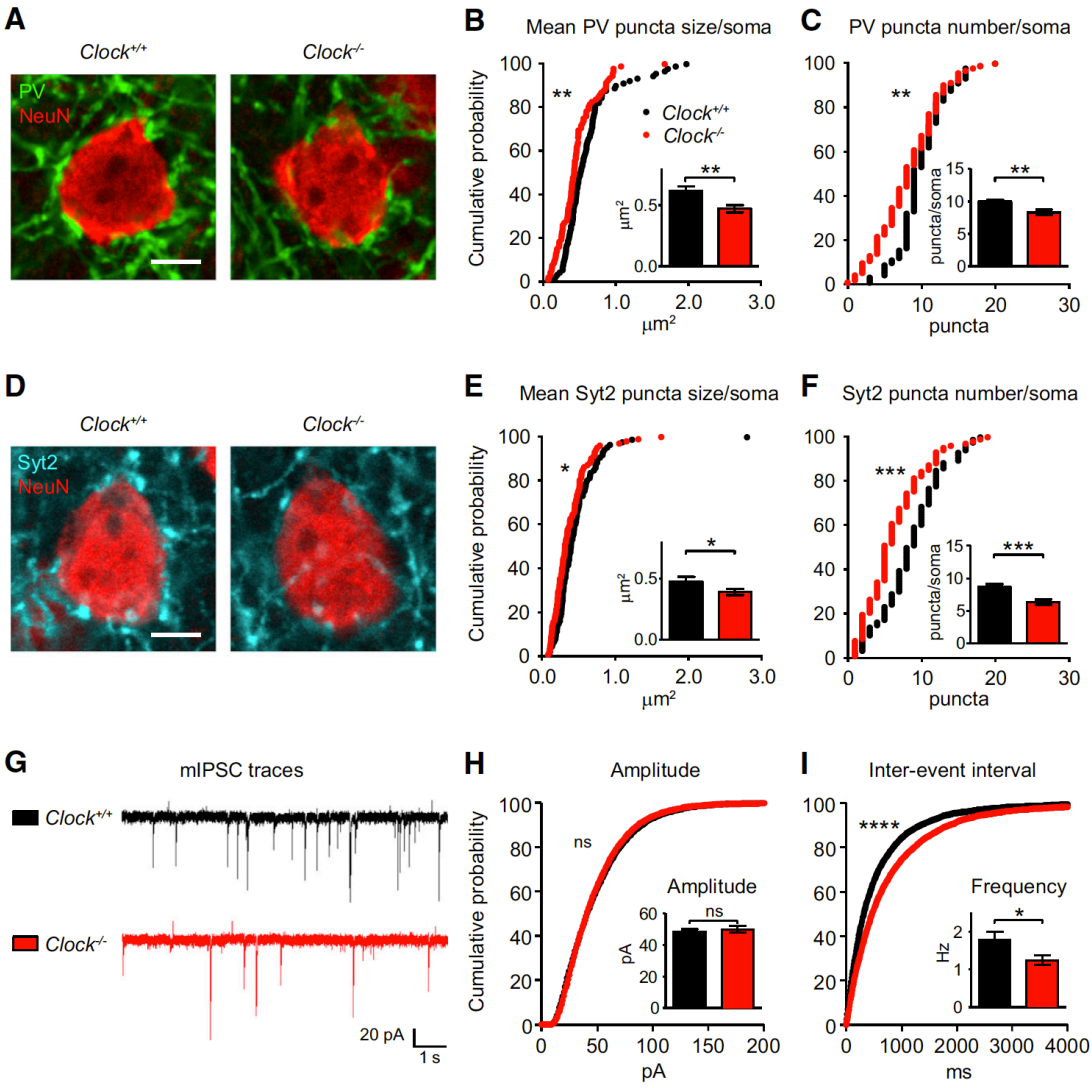

Figure 3.4 (Continued)

Immunohistological analysis confirmed specific loss of CLOCK expression within cortical PV-cells at typical critical period age (Figure 3.5A). Importantly in the SCN, PV was not expressed, leaving CLOCK expression intact by our conditional deletion (Figure 3.5B). While amblyopia was then induced as expected by brief MD in *PV-Cre* control littermates only at critical period, visual acuity was significantly reduced in *PV-Cre; Clock*$^{f/f}$ mice by brief MD only in adulthood (Figure 3.5C).

To verify these results, we deleted another core clock component, BMAL1 (Figure 3.1A), just from PV-cells using *Bmal1*^{flox} mice (Storch et al., 2007), which caused neither gross abnormalities associated with global deletion (Bunger et al., 2000; Kondratov et al., 2006). Visual acuity again remained unchanged by MD at typical critical period ages (Figure 3.5D), but was reduced significantly in adulthood in *PV-Cre; Bmal1*$^{f/f}$ mice (Figure 3.5C). These results recapitulate delayed onset of plasticity identified in global *Clock*$^{-/-}$ mutants by selective deletion of *Clock* or *Bmal1* only from PV-cells.

For comparison, we also generated excitatory neuron-specific *Bmal1* deletion using *TLCN-Cre* mice in which Cre recombinase is expressed only in forebrain pyramidal neurons (Mitsui et al., 2007). As opposed to PV-cell-specific deletion, the removal of *Bmal1* from the more numerous excitatory neuron population did not delay critical period plasticity (Figure 3.5D). Taken together, intrinsic clock genes within pivotal PV-cells are important for their maturation and subsequent timing of critical period plasticity (Figure 3.6).

Figure 3.5. Delayed plasticity by PV-cell-specific *Clock* or *Bmal1* deletion

(A) Conditional *Clock* deletion in V1b at P27 of *PV-Cre; Clock*$^{f/f}$ mice. Arrows, CLOCK-expressing PV-cells. Arrowheads, CLOCK-depleted PV-cells. Scale bar, 100 μm.

(B) CLOCK expression in the SCN at P66. Scale bar, 100 μm.

(C) Reduced visual acuity after 4 days of monocular deprivation (MD) in *PV-Cre* controls during the CP (noMD and MD, 6 mice each) but not in adulthood (noMD and MD, 5 mice each). In contrast, a delayed CP plasticity is seen in adult *PV-Cre; Clock*$^{f/f}$ and *PV-Cre; Bmal1*$^{f/f}$ mice (noMD and MD, 5 mice each). $^{**}P < 0.01$; $^{***}P < 0.001$; ns, not significant (t-test). Values are mean ± SEM

(D) Brief monocular deprivation (MD) for 4 days during the typical CP (P25-26). Visual acuity evaluated in *Bmal1*$^{f/f}$, *TLCN-Cre; Bmal1*$^{f/f}$ and *PV-Cre; Bmal1*$^{f/f}$ mice (noMD and MD, 5 mice each). $^{**}P < 0.01$; $^{***}P < 0.001$; ns, not significant (t-test). Values are mean ± SEM

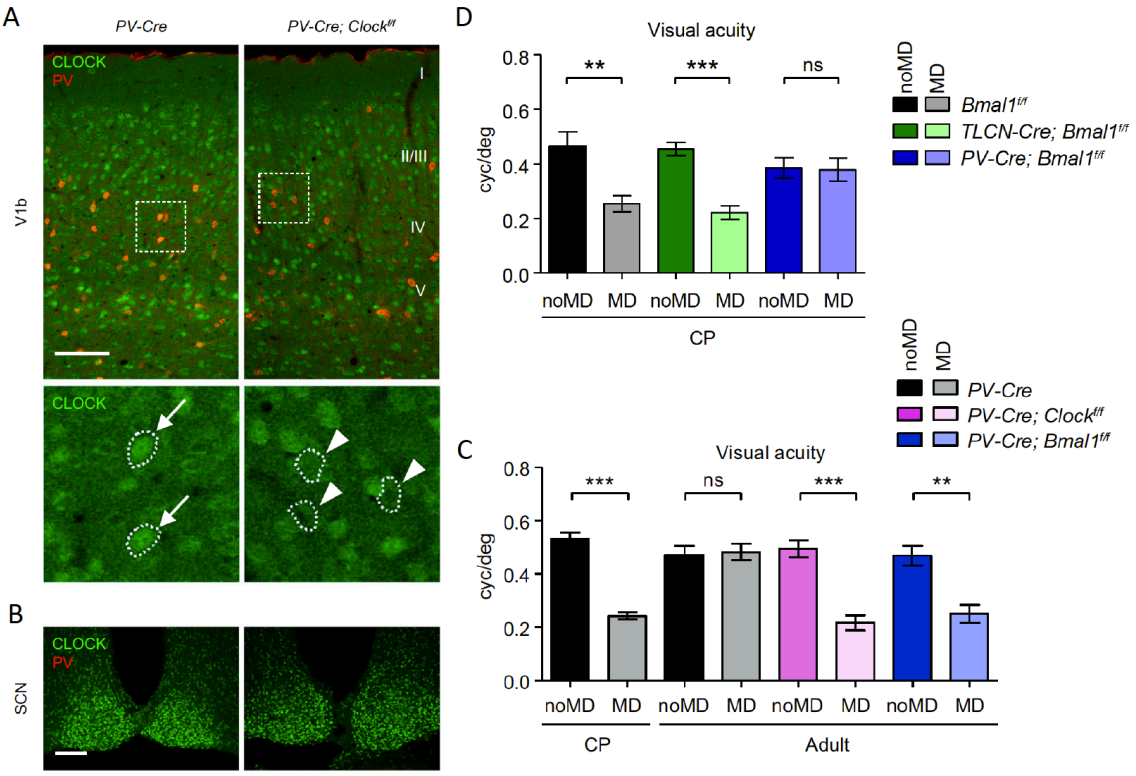

Figure 3.5 (Continued)

Figure 3.6. Cell-intrinsic circadian Clock genes promote PV-circuit maturation and critical period timing

Normally, PV-cell function in mouse V1 emerges after eye opening and reaches a plateau near the end of the CP (P23-P33), setting the time course of plasticity (Hensch 2005). When circadian clock machinery within PV-cells is disrupted, PV-circuit maturation and CP timing are delayed.

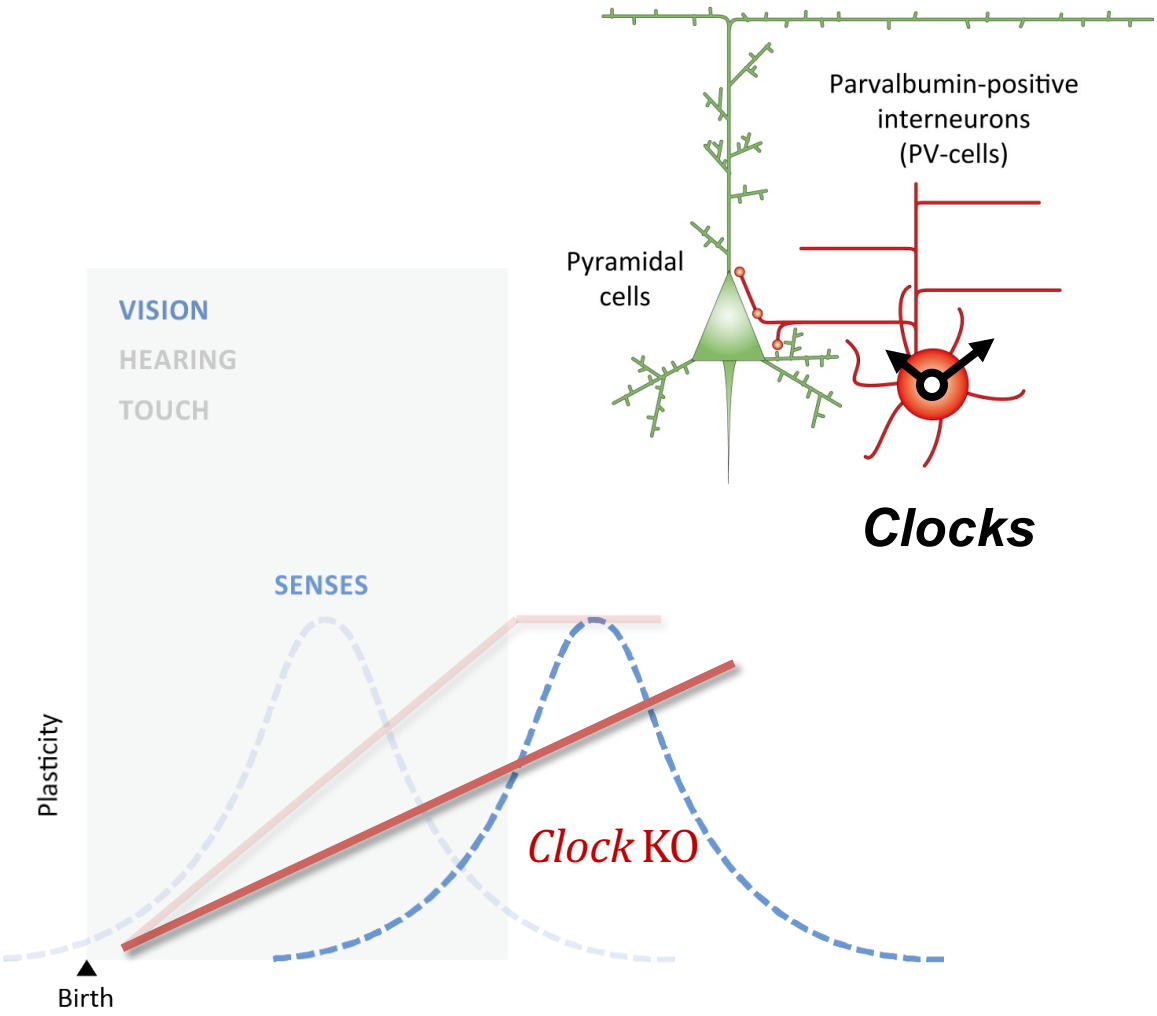

Figure 3.6 (Continued)

Discussion

Circadian rhythms have been shown to control not only daily biological processes but also the timing of other physiological events outside the diurnal cycle. For example, there is a link between circadian timing mechanisms and seasonal, photoperiodic driven changes in an organism's physiology and behavior (Golombek et al., 2014). However, there is little evidence to date demonstrating a role of the circadian system in timing of developmental processes.

In this study, we showed that circadian clock genes time postnatal brain development. Moreover, the necessary clockwork is cell-intrinsic to specific interneurons known to play a pivotal role in critical period plasticity (Hensch, 2005). PV-cell maturation was anatomically and functionally slowed by disruption of the molecular clock. Concomitantly, the onset of critical period plasticity was delayed, but restored by pharmacological enhancement of GABAergic transmission.

The developmental delay observed here is not likely due to loss of systemic circadian rhythms, since *Clock*$^{-/-}$ mice exhibit normal behavioral rhythms under a conventional light:dark cycle (Debruyne et al., 2006), and PV-cell-specific *Clock* or *Bmal1* conditional knock-out mice also exhibited delayed critical period timing despite an intact master clock in the SCN (Figure 3.5). However, it is important to keep in mind that the levels and/or activity of CLOCK:BMAL1 are tightly linked to circadian oscillations, which are disrupted by pulsed-light exposure or sleep deprivation suppressing CLOCK:BMAL1-mediated transcription (Grone et al., 2011; Mongrain et al., 2011). Thus, these environmental influences even during normal development may still impact timing of critical period plasticity through the mechanisms described here.

What is the molecular machinery underlying PV-circuit maturation? Because CLOCK:BMAL1-mediated transcription targets a variety of genes in different cellular contexts across tissues (Janich et al., 2011; Marcheva et al., 2010; Paschos et al., 2012; Yu et al., 2013), PV-cell specific target genes or other mechanisms controlled by the clock machinery should be considered. PV-cell specific microarray (Kobayashi et al., 2015) analysis identified unique sets of genes mis-regulated in *Clock*$^{-/-}$ mice that are potentially responsible for the immature PV-cell circuits. It is likely that these genes are involved in maturation and/or maintenance of PV-cell circuits rather than earlier events such as cell migration. Notably, the delayed deletion of *Clock* or *Bmal1* once PV-cells have already appeared induced similar phenotypes as seen by constitutive *Clock* deletion. Here, we discuss three potential mechanisms that might then influence PV-circuit maturation.

First, clock machinery could directly control synaptic input and/or output of PV-cells. Enhancing neuromodulatory action, such as acetylcholine or serotonin, has been shown to reopen adult plasticity (Maya Vetencourt et al., 2008; Morishita et al., 2010). Reduced expression of *Lynx1* or *Htr2a* observed in *Clock*-deleted PV-cells (Kobayashi et al., 2015) may then alter excitatory/inhibitory (E/I) balance in the surrounding circuitry. Lynx1-mediated dampening of cholinergic signaling would normally limit adult plasticity (Morishita et al., 2010). Altered 5-HT_{2A}-mediated serotonin signaling within PV-cells may likewise modulate E/I balance by adjusting spontaneous IPSC frequency onto pyramidal neurons (Weber and Andrade, 2010).

As for PV-cell output, presynaptic neurexins (NRXNs) bind to neuroligins (NLGNs) expressed on the target postsynapic site and mediate signaling across the

synapse (Sudhof, 2008). Disruption of specific NRXN-NLGN complexes weakens inhibitory synapses formed by PV-cells (Chubykin et al., 2007). Interestingly, *Nrxn* transcripts display circadian oscillations in the SCN (Shapiro-Reznik et al., 2012), suggesting a direct involvement of CLOCK:BMAL1-mediated transcription. Altered expression of NRXNs (*Nrxn1*, *Nrxn2*, *Nrxn3*) in *Clock*-deleted PV-cells (Kobayashi et al., 2015) may underlie the reduced inhibitory output onto pyramidal neurons observed in $Clock^{-/-}$ mice (Figure 3.4).

Second, circadian clock genes may preserve PV-cell integrity. Circadian rhythms have been shown to regulate redox homeostasis in the brain, and disruption of circadian genes causes neuronal oxidative damage (Musiek et al., 2013). Notably, fast-spiking PV-cells are highly metabolically active with a hallmark of abundant mitochondrial molecules (Plessy et al., 2008) and are particularly vulnerable to redox dysregulation as compared to other neuronal types, resulting in their enhanced oxidative stress and loss of PNNs (Cabungcal et al., 2013a; Cabungcal et al., 2013b),b). Direct cell autonomous redox dysregulation by deletion of the primary antioxidant (glutathione) synthetic enzyme (*Gclc*) only within PV-cells is sufficient to prolong critical period plasticity (Morishita et al., 2015). Altered expression of genes downstream of CLOCK related to the respiratory chain (e.g. *Cox* and *Nduf* family genes) and redox regulation (e.g. *Gpx4*) (Kobayashi et al., 2015) may thus jeopardize the integrity of redox homeostasis. Another important PV-circuit maturation and maintenance factor in this context is Otx2 (Beurdeley et al., 2012; Spatazza et al., 2013; Sugiyama et al., 2008). How this non-cell autonomous molecule interacts with PV cell-intrinsic clocks will be of great interest, as

Otx2 has been suggested to reciprocally interact with CLOCK in a positive regulatory loop in *Xenopus* embryos (Green et al., 2001; Morgan, 2002).

Third, apart from the molecular targets above, the clock system itself may act as a PV cell-intrinsic timer. Intracellular maturational programs in addition to the local cortical milieu may regulate the development of GABAergic circuits (Bartolini et al., 2013). Supporting this idea, when embryonic precursors of GABA neurons are transplanted into the postnatal visual cortex of mice, an ectopic critical period is induced once sufficient maturational time has elapsed for the transplanted cells (Southwell et al., 2010). Curiously, embryonic stem cells, which do not exhibit circadian rhythmicity, acquire their oscillatory machinery during neural differentiation (Yagita et al., 2010). Emergence of full circadian oscillations (i.e. over a certain number of cycles) may positively drive postnatal PV-cell development. The three roles above are not mutually exclusive, and may independently or coordinately aid proper maturation of PV-cell circuits.

Lastly, our findings offer a neurodevelopmental link between circadian disruption and mental illness. Linkage studies in human patients have implicated circadian gene mutations and behavioral changes (e.g. sleep disturbances) in psychiatric disorders, such as autism and schizophrenia (Chemerinski et al., 2002; Wulff et al., 2010), which are in turn marked by impaired PV-cell circuits (Gogolla et al., 2009; Le Magueresse and Monyer, 2013; Maeda, 2015; Marin, 2012). It has been shown that a set of genes mis-regulated in our *Clock*-deleted PV-cells are associated with autism (*Kcnma1*, *Nrxn1-3*, *Prkcb*, *Slc24a2*, *Cacna1c*, *Ptpn11*, *Htr2a*, *Abat*) and schizophrenia (*Cacna1c*, *Htr2a*) (Allen et al., 2008; Basu et al., 2009). Understanding the cell-specific role of molecular

clocks within developing PV-cells may offer novel therapeutic approaches and insights into the etiology of mental illness as a reflection of critical period dysregulation.

Chapter 4

Instructing Perisomatic Inhibition by Direct Lineage Reprogramming of Neocortical Projection Neurons

Author contribution:

Zhanlei Ye, Mohammed A. Mostajo-Radji, Juliana R. Brown, Caroline Rouaux, Giulio Srubek Tomassy, Takao K. Hensch, and Paola Arlotta

P.A., T.K.H., Z.Y., M.A.M, J.R.B., and C.R. conceived the experiments. Z.Y. performed electrophysiological recordings and analysis. M.A.M. and C.R. performed surgical manipulations. M.A.M., J.R.B. and G.S.T. performed molecular studies and quantification. This work has been published in Neuron (Ye et al., 2015).

Summary

During development of the cerebral cortex, GABAergic inhibitory interneurons recognize and pair with excitatory projection neurons to ensure the fine excitatory-inhibitory balance essential for proper local circuit function. Whether projection neuron class-specific identity has a role in the establishment of afferent inhibitory synapses is debated. Here, we report that direct *in vivo* lineage reprogramming of layer 2/3 (L2/3) callosal projection neurons (CPNs) into induced corticofugal projection neurons (iCFuPNs) increases inhibitory input onto the converted neurons to levels similar to those of endogenous CFuPNs of layer 5 (L5). iCFuPNs recruit increased numbers of inhibitory perisomatic synapses from parvalbumin (PV)-positive interneurons, with single-neuron

resolution and despite their ectopic location in L2/3. The data show that individual reprogrammed excitatory projection neurons extrinsically modulate afferent input by local PV+ interneurons, suggesting that projection neuron class-specific identity can actively control the wiring of the cortical microcircuit.

Introduction

The correct balance between glutamatergic excitatory projection neurons (PNs) and GABAergic inhibitory interneurons (INs) is crucial for the proper function and plasticity of the cerebral cortex, and its misregulation is implicated in a variety of neurodevelopmental disorders (Rossignol, 2011).

PNs and INs are two extremely diverse classes of neurons that interact in the neocortex to form complex local circuits. PNs are broadly divided into two main subgroups, which contain a variety of neuronal subtypes (Greig et al., 2013; Lodato et al., 2015). Commissural PNs, including callosal PNs (CPNs), are largely located in layer 2/3 (L2/3) and send their axons to the contralateral hemisphere, striatum, and frontal cortex. Corticofugal PNs (CFuPNs) are located in L5 and L6 and connect to subcortical targets including the thalamus, superior colliculus, pons, and spinal cord. The activity of all PNs is modulated by local GABAergic INs, which are classified into distinct subtypes based on molecular identity, morphology, electrophysiological properties, and the location of their synaptic connections (DeFelipe et al., 2013; Markram et al., 2004; Petilla Interneuron Nomenclature et al., 2008). Among IN subtypes, parvalbumin (PV)-positive cells largely synapse onto the soma of PNs (Buhl et al., 1994), and are the major source of miniature inhibitory post-synaptic currents (mIPSCs) (Soltesz et al., 1995).

Little is known about the mechanisms underlying the recognition and pairing of INs and PNs in the developing cortical circuit. Once in their final position, INs form dense connectivity with many neighboring PNs (Fino et al., 2013). However, paired recordings have also shown that connection probabilities among PNs or between PNs and INs depends on the identity of the pre- and post-synaptic partners (Brown and Hestrin, 2009; Lee et al., 2014; Otsuka and Kawaguchi, 2009). Different populations of PNs within L5 receive differing excitatory and inhibitory inputs, and emerging evidence suggests that the strength of inhibition from PV+ cells varies between PN subtypes in L5 (Lee et al., 2014). Similarly, INs selectively innervate PNs with distinct long-distance targets (Krook-Magnuson et al., 2012; Lee et al., 2014; Varga et al., 2010). Together, these results suggest that PN identity might have a role in the establishment of specific afferent connectivity.

In vivo direct lineage reprogramming can become a valuable tool to investigate the role of cellular identity in biological phenomena, as it can be used to create sparsely distributed cells within an ectopic context. In the neocortex, *Fezf2,* a terminal selector gene capable of instructing CFuPN identity in otherwise-fated progenitors (Lodato et al., 2014; Molyneaux et al., 2005; Rouaux and Arlotta, 2010; Zuccotti et al., 2014), has also been shown to reprogram postmitotic L2/3 CPNs and L4 spiny interneurons into induced CFuPNs (iCFuPNs) (De la Rossa et al., 2013; Rouaux and Arlotta, 2013). These iCFuPNs acquire molecular properties and long-distance axonal connectivity of endogenous CFuPNs (Rouaux and Arlotta, 2013).

Here, we further demonstrate that individual reprogrammed iCFuPNs also acquire the global molecular signature, somato-dendritic morphology and intrinsic

electrophysiological properties of endogenous CFuPNs. Notably, despite being distributed among L2/3 CPNs, iCFuPNs receive a frequency of perisomatic inhibition comparable to endogenous L5 CFuPNs, and significantly higher than neighboring L2/3 CPNs. This was at least partly due to a larger number of PV+ synapses onto iCFuPNs, and was independent of IN lamination. The data demonstrate that reprogramming PN class-specific identity is sufficient to shape PV+ inhibitory input *in vivo*.

Results

Reprogramming L2/3 CPNs induces molecular programs and intrinsic electrophysiological traits of CFuPNs

We previously showed that *Fezf2* overexpression in postmitotic L2/3 CPNs is sufficient to induce expression of selected CFuPN markers (Rouaux and Arlotta, 2013). In order to use reprogramming as a tool to probe IN-PN interactions, we first more broadly characterized the extent of molecular reprogramming in this system.

We assembled a broad panel of class-specific signature genes which show differential expression at either embryonic or postnatal stages of PN differentiation (Arlotta et al., 2005; Molyneaux et al., 2007; Molyneaux et al., 2015); *in toto,* 40 CFuPN and 36 CPN genes.

We overexpressed either *Fezf2*-GFP or control empty-GFP constructs in cortical progenitors under the postmitotic neuronal promoter Cdk5r (Rouaux and Arlotta, 2013) via *in utero* electroporation at E14.5. Single GFP^+ neurons were isolated at postnatal day 15 (P15) and profiled for a panel of 88 genes (76 markers and 12 controls) using single-cell, fluidics-based quantitative RT-PCR (Figure 4.1B).

Figure 4.1. iCFuPNs acquire molecular identity of CFuPNs

(A) Timeline of experiments performed. In utero electroporation at E14.5; single-cell gene-expression profiling at P15; electrophysiology at P22-26; histological analysis at P28. (B-C) mRNA expression analysis of CPN and CFuPN markers in single Fezf2-OE PNs and GFP-CPNs at P15 shows that a subset of Fezf2-OE cells acquire a CFuPN-like molecular identity. Fezf2-OE n = 70, GFP-CPN n= 57. (B) Gene expression heatmap of 88 genes assayed by high-density qPCR demonstrates acquisition of a global CFuPN-like signature in a subset of Fezf2-OE neurons. Sample clustering by PAM identified 2 clusters (green/orange and chartreuse/red bars). Top row of blue bars: item consensus (IC) values, a metric of cluster assignment stability. Correlated gene expression modules were identified by WGCNA (M1-M4: Module 1 through Module 4, N: not assigned to a module). Bolding indicates genes with significant expression differences (>2-fold and $p<0.05$); arrows indicate direction of change in Cluster 2. Gene color-coding: red, CFuPN marker; green, CPN marker; purple, synaptic; blue, normalization control; orange, other control. (C) PCA of gene expression data demonstrates that Clusters 1 and 2 separate along PC1. Also see Figure 4.2.

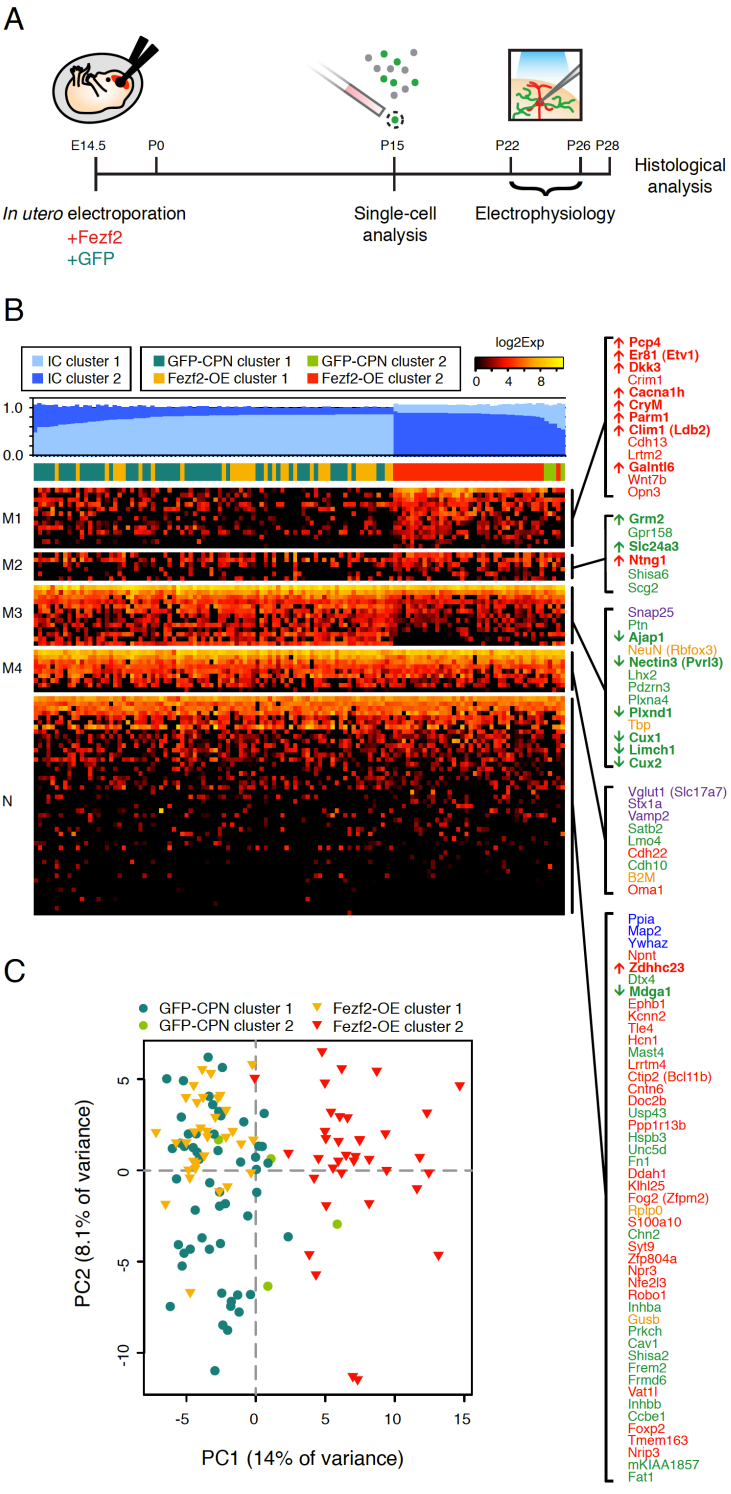

Figure 4.1 (Continued)

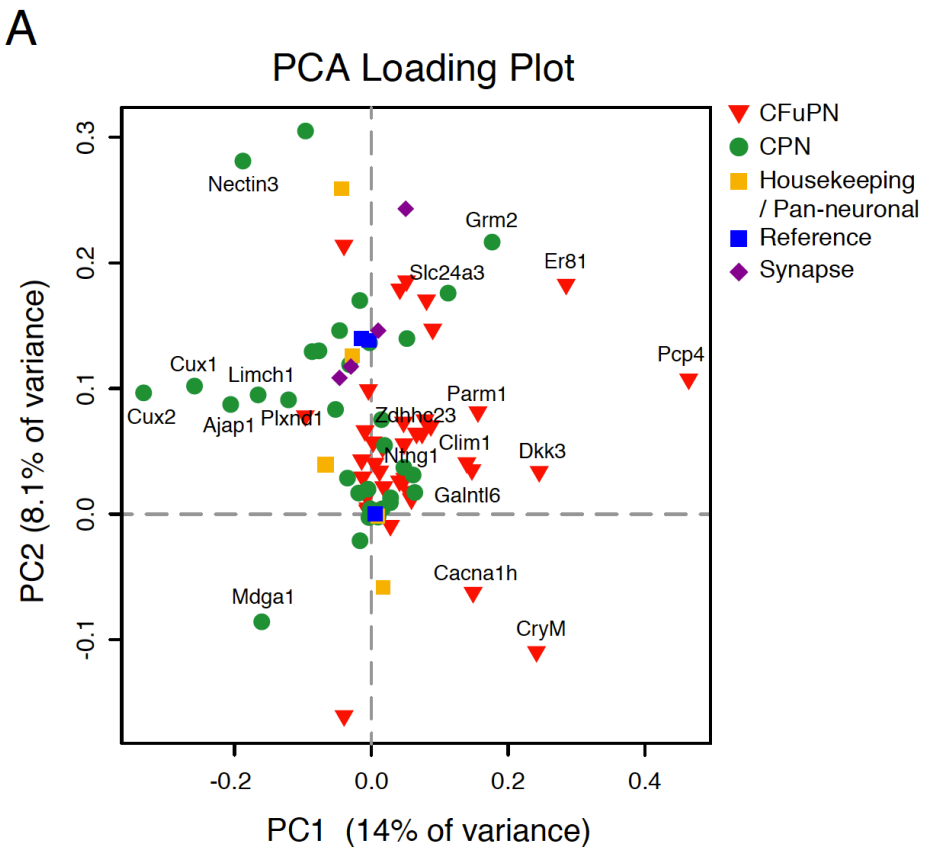

Figure 4.2. Genes Contributing to be the separation of endogenous CPNs and reprogrammed CPNs

(A) PCA loading plot showing the contribution of individual genes to the first and second PCA axes; distance from the origin along each axis corresponds to strength of contribution to that axis. CFuPN and CPN markers show opposite contributions to the primary axis of variation (PC1).

Samples were partitioned using Partitioning Around Medoids (PAM) and consensus clustering (Monti et al., 2003), and genes were clustered using weighted gene co-expression network analysis (WGCNA) (Langfelder and Horvath, 2008). PAM identified two sample clusters (Figure 4.1B); Cluster 1 contained the majority of GFP-overexpressing control cells (GFP-CPN) (54/57) and 33/70 Fezf2-overexpressing cells (Fezf2-OE), and Cluster 2 contained the remaining 37 Fezf2-OE cells and 4 GFP-CPNs. Principal component analysis (PCA) confirmed this cluster division (Figure 4.1C). WGCNA identified four gene modules (Figure 4.1B). Module 1 contained CFuPN genes (13/13) that were predominantly upregulated in Cluster 2 (8/13; $p<0.05$ and >2-fold expression change). Module 3 contained predominantly CPN genes (10/13); half of the genes in this module were downregulated in Cluster 2 (6/13). Importantly, Modules 1 and 3 were significantly anti-correlated within individual cells (Spearman correlation of module eigengenes: $r=-0.478$, $p=<0.0001$), indicating coordinate induction of CFuPN markers and repression of CPN markers rather than a mixed cell identity. Overall, 10/12 genes upregulated in Cluster 2 were CFuPN-associated and 7/7 downregulated genes were CPN-associated. These results closely resembled the list of genes that were significantly associated with PC1 in the sample PCA (Figure 4.2A). We conclude that approximately half of Fezf2-OE neurons are molecularly reprogrammed into iCFuPNs, acquiring a global CFuPN-like gene expression profile that is distinct from GFP-expressing CPNs and that persists for at least 3 weeks after initial conversion.

We next assessed whether iCFuPNs acquire appropriate subtype-specific electrophysiological properties. Using whole-cell patch clamp recording in acute brain

slices (P22-P26), we measured 12 intrinsic parameters: 5 related to passive membrane properties and 7 to action potential generation (Table 4.1).

We confirmed that GFP overexpression did not alter any of these parameters (GFP-CPNs vs. endogenous L2/3 CPNs) (Figure 4.4); therefore, to improve the power of analysis, the 8 endogenous L2/3 CPNs and 24 control GFP-CPNs were combined as a single group, hereafter collectively referred to as L2/3 CPNs (Table 4.1 and Figures 4.3E-K). As expected, the intrinsic properties of L2/3 CPNs were distinct from endogenous L5 CFuPNs (identified by cell size) (Figure 4.3 and Table 4.1) (Mason and Larkman, 1990).

We found that Fezf2-OE cells differed significantly from GFP-CPNs in current threshold (CThr), resting potential (Vm), voltage sag (Vsag), membrane decay constant (Tau), and input resistance (Rm) (Figure 4.4 and Table 4.1). They also showed a wider distribution in Vm, Vsag, Tau, Rm, and membrane capacitance (Cm), suggesting population heterogeneity (Figure 4.4). Indeed, two firing patterns were observed: one similar to L5 CFuPNs (iCFuPNs), and the other to L2/3 CPNs (Fezf2-non-reprogrammed; Fezf2-NR) (Figure 4.3A). PCA on these data also separated Fezf2-OE cells into two groups (Figures 4.3B-C, 4.4C and Table 4.2); the histogram of Fezf2-OE cells on the major axis of variation (PC1, accounting for 41% of the total variance) was best fitted by a two-component Gaussian model (Log-likelihood ratio test, LRT, $p=0.017$) (Figure 4.3B). In contrast, the PC1 histograms of L2/3 CPNs and L5 CFuPNs were best fitted with one-component Gaussian distributions, suggesting single populations.

We employed supervised machine learning to unbiasedly classify Fezf2-OE cells based on their electrophysiological properties (Figure 4.4D). Averaging over 1000 runs of the classifier, 14/33 Fezf2-OE PNs were classified as L5 CFuPNs (~42%; iCFuPNs),

Figure 4.3. iCFuPNs in L2/3 acquire electrophysiological properties of L5 CFuPNs

(A) Representative current steps at -100, 50, and 350 pA. iCFuPNs show a firing pattern similar to L5 CFuPNs, whereas Fezf2-NR neurons resemble endogenous L2/3 CPNs and L2/3 GFP-CPNs. Scale bar: 500 ms (horizontal), 20 mV (vertical). (B-C) PCA on 12 intrinsic electrophysiological properties separates algorithmically identified iCFuPNs from Fezf2-NR neurons. Also see Figure 4.4. (B) Histogram of cell distribution along PC1 shows bimodal distribution of Fezf2-OE cells. Dotted lines: fits to single (L2/3 CPN, L5 CFuPN) or mixed (Fezf2-OE) Gaussian distributions. PDF: probability density function. (C) PCA analysis clusters the Fezf2-NR and iCFuPN populations with L2/3 CPNs and L5 CFuPNs, respectively. Color-coding as in A. Dotted circles: threshold where PDF=0.02 after fitting to 2D Gaussian distribution. (D-K) Intrinsic properties of algorithmically identified iCFuPNs and Fezf2-NRs resemble L5 CFuPNs and L2/3 CPNs, respectively. (D) Firing-current curves (spike numbers in 2 seconds vs. current injection). Asterisks indicate p values (Black, L5 CFuPN vs. L2/3 CPN; Red, iCFuPN vs. L2/3 CPN; Gold, L5 CFuPN vs. iCFuPN): * $p<0.05$, ** $p<0.01$, *** $p<0.001$. Color-coding as in A. (E-G) Quantification of passive membrane properties: (E) Vm, (F) Vsag, and (G) Tau. (H-K) Quantification of action potentials: (H) Sample traces of action potentials, (I) CThr, (J) VThr and (K) fAHP. Endogenous L2/3 CPN n=8, GFP-CPN n=24, L5 CFuPN n=11, iCFuPN n=14, Fezf2-NR n=21. Error bars: mean ± SEM.

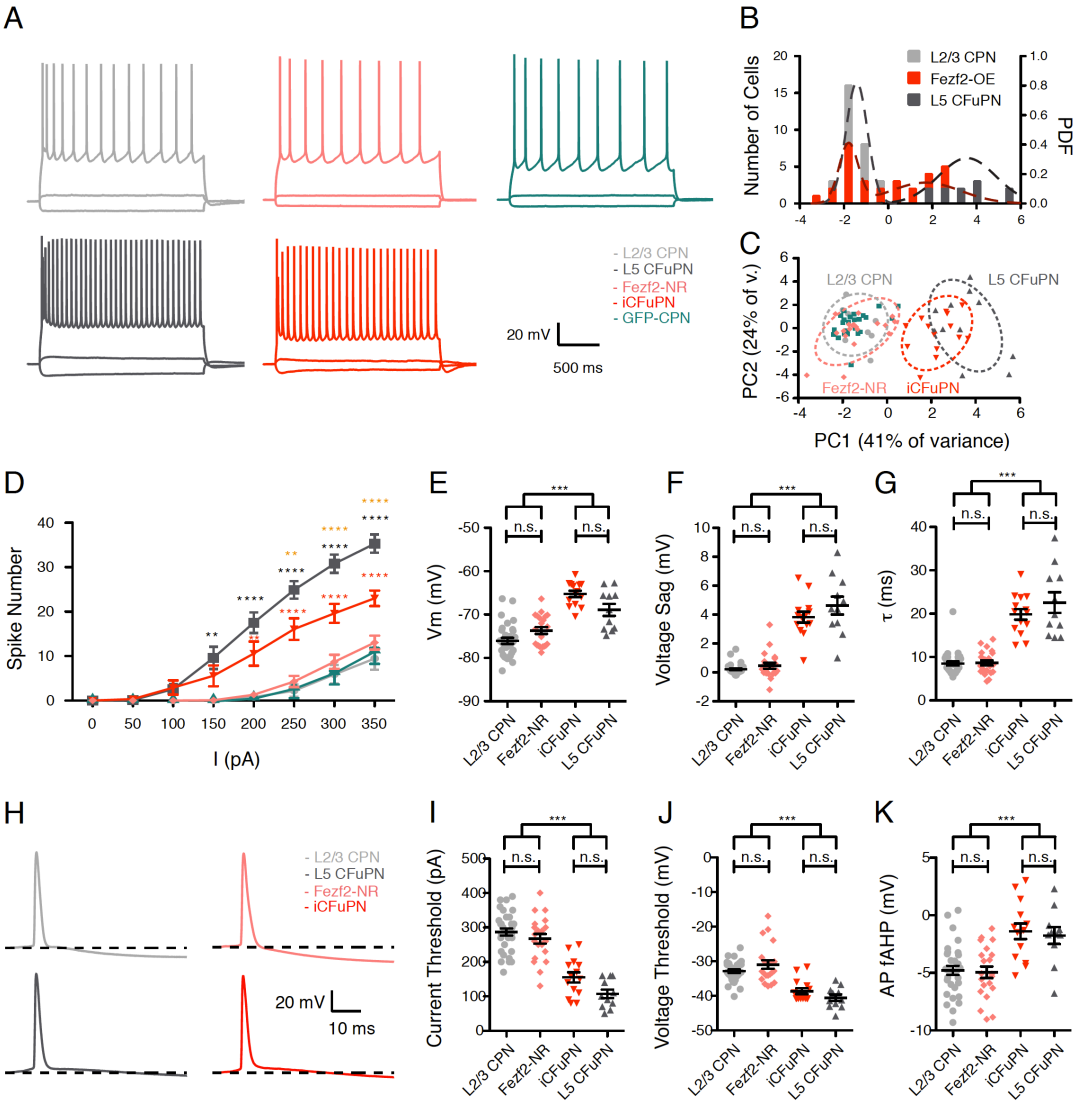

Figure 4.3 (Continued)

Figure 4.4. Electrophysiological properties of upper-layer PNs and classification of iCFuPNs vs. Fezf2-NR PNs

(A) Comparisons of electrophysiological properties of L2/3 CPNs, GFP-CPNs and Fezf2-overexpressing PNs. In the following order: current threshold, resting potential, voltage threshold for action potential at threshold current, amplitude of action potential, fAHP (fast after-hyperpolarization), half-width of action potential, action potential rise time, action potential decay time, voltage sag, membrane time constant (tau), input resistance and membrane capacitance. No significant differences were found between endogenous L2/3 CPNs and GFP-CPNs; consequently these populations were pooled for Figure. 4.3 and associated text. The values for the complete Fezf2-overexpressing population (before algorithmic classification) are also presented. Comparison of means: ** $p<0.01$; *** $p<0.001$; not significant if not indicated. Comparison of variance: † $p<0.05$; †††† $p<0.0001$; not significant if not indicated.

(B) Heatmap of Pearson product-moment correlation coefficients between factors shown in Table 4.1. Abbreviations: Cm, capacitance; Vm, resting potential; fAHP, action potential fast afterhyperpolarization; Vsag, voltage sag; tau, membrane time constant; Rm, membrane resistance; APRise, action potential rising time; APhw, action potential half-width; APDecay, action potential decay; VThr, action potential voltage threshold, CThr, current threshold; APAmp, action potential amplitude. (C) Loading plot for the PCA on electrophysiological parameters in Figure 4.3C. Abbreviations are as in B. Also see Table 4.2. (D-E) Characteristics of the logistic-regression-based classifier algorithm used to classify Fezf2-overexpressing cells as iCFuPNS or Fezf2-NR on the basis of their electrophysiological properties. (D) Flowchart of the algorithm-building strategy: The

classifier was trained using 60% of control cell data (GFP-CPNs and endogenous L2/3 CPNs vs. L5 CFuPNs) with a new random selection for each run, tested on the remaining 40% of control cell data, and then applied to classify Fezf2-overexpressing cells. (E) Performance metrics of the algorithm over 1000 test runs on validation dataset. Histogram of Accuracy, the fraction of correct predictions. Histogram of Recall, the fraction of true positive samples that are classified as positive (i.e., 1 – false negative rate). Histogram of Precision, the fraction of classified-as-positive samples that are true positives (i.e., 1 – false positive rate). Histogram of F-score, a weighted average of the precision and recall (best performance is 1 and worst is 0). (F) Histogram of the fraction of Fezf2-overexpressing cells classified as reprogrammed over 1000 classification runs. (G) Final probability of classifying each individual Fezf2 cell as reprogrammed.

Figure 4.4 (Continued)

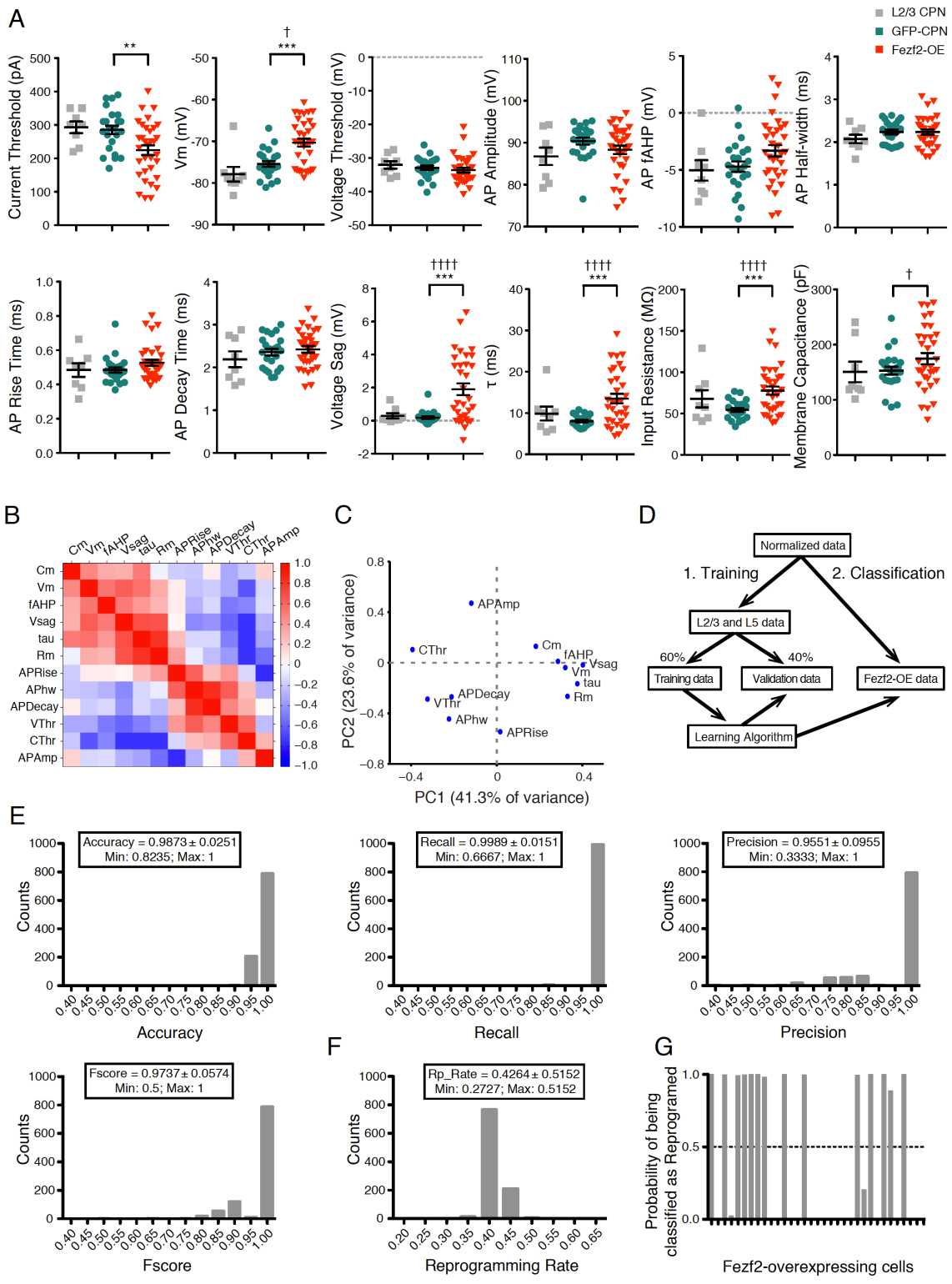

Figure 4.4 (Continued)

Table 4.1. Electrophysiological properties of cortical PNs

Electrophysiological properties of L2/3 CPN , L5 CFuPN, iCFuPN and Fezf2-NR neurons

Parameter	ANOVA p value	L2/3 CPN	L5 CFuPN	iCFuPN	Fezf2-NR
Current Threshold (pA)	< 0.0001	283.64±10.60 [a,d]	107.27±13.20	-155.00±15.38	267.14±14.32 [b,d]
Resting Potential (mV)	< 0.0001	-76.01±0.69 [a,d]	-68.93±1.44	-65.26±0.76	-73.71±0.81 [a]
AP Voltage Threshold (mV)	< 0.0001	-32.70±0.56 [a,d]	-40.54±0.97	-35.49±0.87	-32.19±0.99 [b,d]
AP Amplitude (mV)	0.676	88.31±1.44	-86.89±3.94	86.74±1.78	87.13±2.00
AP fAHP (mV)	< 0.0001	-4.93±0.42 [a,e]	1.76±0.76	1.39±0.70	-4.96±0.51 [b,f]
AP Half-width (ms)	0.0058	2.20±0.05 [f]	1.76±0.13	2.12±0.10	2.28±0.07 [e]
AP Rising Time (ms)	0.5554	0.51±0.03	0.51±0.04	0.53±0.03	0.53±0.02
AP Decay Time (ms)	0.0014	2.31±0.07 [e]	1.66±0.18	2.22±0.11	2.43±0.09 [d]
Voltage Sag (mV)	< 0.0001	0.20±0.07 [a,d]	4.62±0.65	3.82±0.38	0.46±0.21 [a,d]
Membrane Time Constant (ms)	< 0.0001	8.47±0.47 [a,d]	22.56±2.50	19.85±1.28	8.66±0.61 [a,d]
Resistance (MΩ)	< 0.0001	60.64±4.21 [a,d]	127.08±19.51	98.23±7.56	66.97±5.21 [c,e]
Capacitance (pF)	0.0002	149.15±7.56 [b]	190.55±14.86	212.97±15.67	138.79±10.40 [b,f]

Dunn's Multiple Comparison Test:

vs. iCFuPN: [a] $p<0.001$; [b] $p<0.01$; [c] $p<0.05$

vs. L5 CFuPN: [d] $p<0.001$; [e] $p<0.01$; [f] $p<0.05$

Table of electrophysiological parameters for control CPNs (combining endogenous L2/3 CPNs and GFP-CPNs, as parameters for these groups were not different), endogenous L5 CFuPNs, and algorithmically identified iCFuPNs and Fezf2-nonreprogrammed neurons.

Table 4.2. Electrophysiological profiling of cortical projection neurons

Eigenvectors of PCA on 12 electrophysiological properties

	PC1	PC2	PC3	PC4	PC5
Fraction Variance	0.413	0.236	0.112	0.065	0.055
Variable					
CThr	**-0.3937**[a]	0.1044	0.0413	-0.1805	0.1319
Vm	**0.3204**[b]	-0.0385	0.2875	-0.3756	0.1780
VThr	**-0.3236**[b]	-0.2870	0.0301	-0.2373	0.3822
APamp	-0.1189	0.4707	0.2411	0.2697	-0.2384
APhw	-0.2229[c]	-0.4445	0.2594	0.1678	-0.2135
fAHP	0.2861[b]	0.0114	0.2066	-0.5548	-0.5775
Apr	0.0163	-0.5458	-0.0610	-0.1918	0.0362
Apd	-0.2112[c]	-0.2691	0.5207	0.2342	-0.3296
Vsag	**0.4027**[a]	-0.0171	-0.0427	-0.0332	0.0530
tau	**0.3769**[a]	-0.1665	0.1567	0.3632	0.1818
Rm	**0.3308**[b]	-0.2658	-0.2500	0.3668	-0.1094
Cm	0.1827	0.1303	0.6187	0.0459	0.4594

Significance of factor loading on overall variation along PC1: [a] $p<0.001$; [b] $p<0.01$; [c] $p<0.05$

Table of eigenvectors for the principal component analysis of electrophysiological parameters in cortical PNs (Figure 4.3C). Fraction of variance explained for each of the first 5 principal components is indicated, along with p values for significance of factor loading on total variation along PC1, calculated as correlation of gene expression to the sample score (Yamamoto et al., 2014). Important variables (absolute values over 0.32) on PC1 are bolded.

while 19/33 were classified as CPNs, (~58%; Fezf2-NR)(Figure 4.4F-G). After classification, iCFuPNs and Fezf2-NR PNs showed a clear separation in Vm, Vsag, Tau, CThr, voltage threshold (VThr), and fast after-hyperpolarization (fAHP) (Figures 4.3D-K and Table 4.1). This ratio is consistent with our previously reported efficiency of molecular reprogramming (Rouaux and Arlotta, 2013) and in line with our single cell gene expression analysis.

Altogether, the data indicate that individual iCFuPNs shift their molecular signature and their intrinsic electrophysiological properties to resemble those of L5 CFuPNs.

iCFuPNs are more inhibited than parental L2/3 CPNs

Whether individual PNs subtypes can differentially affect afferent synaptic input from local INs is still debated. Our reprogramming model generates sparse populations of CFuPNs within an ectopic L2/3 location, and thus can be used to examine whether PN subclass identity affects local inhibitory synaptic input at the level of individual cells, independent of laminar context.

We first assessed the inhibitory network targeting GFP-CPNs, endogenous L5 CFuPNs, and Fezf2-OE PNs using electrophysiological recordings of miniature inhibitory postsynaptic currents (mIPSCs) at P22-P26 (Figures 4.5A-G). Consistent with previous literature (Lee et al., 2014), we found that L5 CFuPNs exhibited more frequent inhibitory events than GFP-CPNs (L5 CFuPNs 4.02±0.64 Hz; GFP-CPNs 2.56±0.21 Hz). The average mIPSC frequency in Fezf2-OE cells (3.56±0.25 Hz) was similar to L5 CFuPNs, and higher than GFP-CPNs (Figures 4.5B-C), suggesting increased inhibitory

Figure 4.5. iCFuPNs receive increased inhibition

(A-G) mIPSC events demonstrate inhibition in iCFuPNs similar to L5 CFuPNs and higher than L2/3 CPNs. GFP-CPN n=30, Fezf2-OE n=33, L5 CFuPN n=16. Error bars: mean ± SEM. (A) Representative mIPSCs traces. (B) Average mIPSC frequency and (C) cumulative inter-event interval (IEI) from all cells. (D) Average mIPSC amplitude and (E) cumulative amplitude from all cells. (F) Average mIPSC weighted decay (τ_w) and (G) cumulative τ_w from all cells. (H-M) Increased inhibition is specific to iCFuPNs within Fezf2-OE brains. (H) Representative responses to hyperpolarizing current steps (-100 to -500 pA), mIPSC traces and image reconstruction. GFP-CPNs n=12, Fezf2-NR n=15, iCFuPN n=6; from 5 Fezf2-OE and 3 GFP-OE brains. Dotted lines: pial surface. (I) iCFuPNs were identified by Vsag higher than the maximal GFP-CPN Vsag value. (J) mIPSC frequency is increased in iCFuPNs compared to Fezf2-NR and GFP-CPNs. (K) mIPSCs amplitude remains constant between all three groups. (L) Comparison of average mIPSC frequency in iCFuPNs and Fezf2-NR cells from the same brains (connected pairs) shows that increased inhibition is specific to iCFuPNs. (M) Fezf2-OE cells increase their apical tuft width regardless of their reprogrammed state.

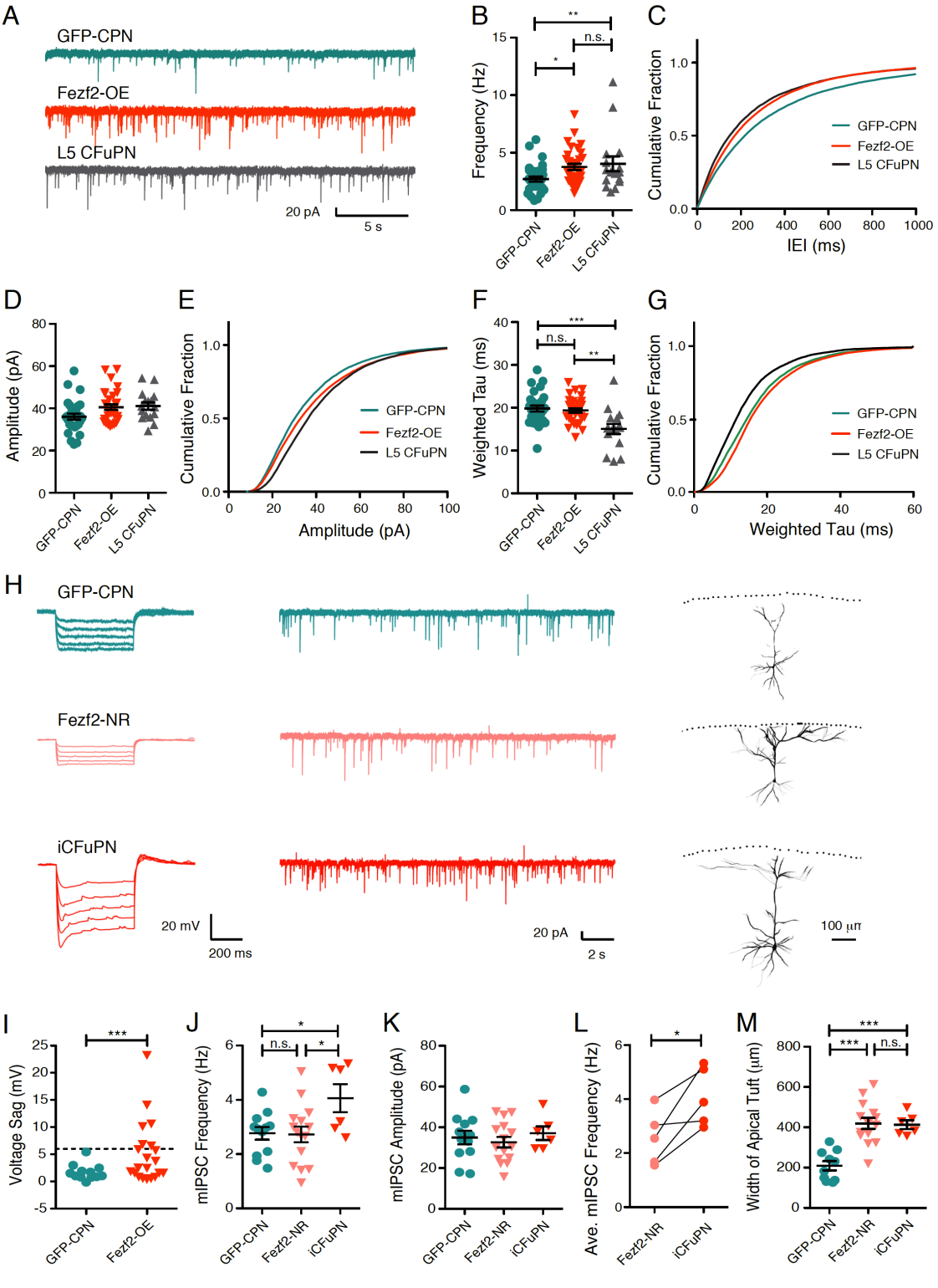

Figure 4.5 (Continued)

input onto iCFuPNs, but the mean amplitude of inhibitory events was similar between all groups (all comparisons: $p>0.05$) (Figures 4.5D-E).

This increase in inhibition could reflect multiple possible causes. To exclude the possibility of a change in intrinsic sensitivity of iCFuPNs to GABA, we first examined the subunit composition of $GABA_A$ receptors using electrophysiological and molecular analyses. mIPSCs originate mainly from perisomatic synapses (Soltesz et al., 1995), which are enriched for α1-containing $GABA_A$ (GABRA1) receptors (Hensch, 2005; Klausberger et al., 2002). GABRA1 produces mIPSCs with faster decay kinetics (Picton and Fisher, 2007). We found that the decay time constant (weighted τ_w) of mIPSCs was slower in GFP-CPNs than in L5 CFuPNs (19.81±3.74 ms, 15.04±4.77 ms, respectively, $p<0.001$), and this property remained unchanged upon Fezf2 overexpression (19.37±2.92 ms) (Figures 4.5F and 4.5G). Differential changes in mIPSC kinetics following benzodiazepine exposure can also reveal differences in the stoichiometry of GABA receptors and changes in synapse location (Kilman et al., 2002; Nusser et al., 1998). Therefore, we recorded mIPSCs before and after application of the GABRA1 agonist Zolpidem, which prolongs the opening of GABRA1+ receptors (Crestani et al., 2000). We did not detect any significant difference in Zolpidem-induced changes in mIPSC amplitude, decay kinetics, or charge transfer (Figures 4.6A-B), indicating that the density of GABRA1+ receptors is unchanged between iCFuPNs and CPNs.

Finally, we performed single-cell quantitative RT-PCR on P15 iCFuPNs and GFP-CPNs for all 10 GABA receptors known to be expressed in the cerebral cortex (Wisden et al., 1992) (Figures 4.6C-F). We found no significant differences in either the proportion of RNA-positive cells or the mean expression level among RNA-positive cells

Figure 4.6. GABA receptor subunit expression is unchanged in induced CFuPNs

(A-B) Pharmacological analysis with GABRA1 benzodiazepine agonist Zolpidem shows that iCFuPN are not intrinsically more sensitive to inhibition. GFP-CPN n= 14, Fezf2-overexpressing n= 14. Error bars: mean ± SEM. (A) Representative averaged mIPSC traces of sample GFP-CPN and Fezf2-overexpressing neurons before and after Zolpidem application. (B) Fold changes of mIPSC amplitude, decay weighted tau and charge transfer after Zolpidem application. No significant difference in any parameter between GFP-CPN and Fezf2-overexpressing neurons was detected.

(C-F) Single-cell qPCR analysis of GABA receptor expression in iCFuPNs. GFP-CPN n=46, iCFuPN n=53.

(C-D) Confirmation of reprogramming to iCFuPN identity. (C) Principal component analysis (PCA) of mRNA expression of molecular markers defining CPN and CuFPN identities. CPNs were preselected based on Satb2 expression, while iCFuPNs were preselected for expression of Er81 and/or CryM. PCA shows that iCuFPNs (red) distribute differently from control GFP-CPNs (green) along PC2. Histogram of PC2 distribution is fit to Gaussian curves (R^2: iCFuPN = 0.836, GFP-CPN = 0.692).

(D) PCA loading plot showing the contribution of individual genes to the first and second PCA axes; distance from the origin along each axis corresponds to strength of contribution to that axis. PC2 shows opposite contributions of CPN (green) and CFuPN (red) marker genes. Also see Table 4.3.

(E-F) Single-cell gene expression analysis for all GABA receptors expressed in the murine cerebral cortex. (E) Proportion of single cells that expressed GABA receptor mRNA at any level (in percent). No gene showed statistically different percent positivity

between the two groups. (F) Gene expression level of GABA receptors among mRNA-positive cells. No gene showed statistically different mean expression between the two groups. Error bars: mean ± SEM.

(G) Additional examples of reconstructions from cells used for recordings in Figure 4.5 H-M.

Figure 4.6 (Continued)

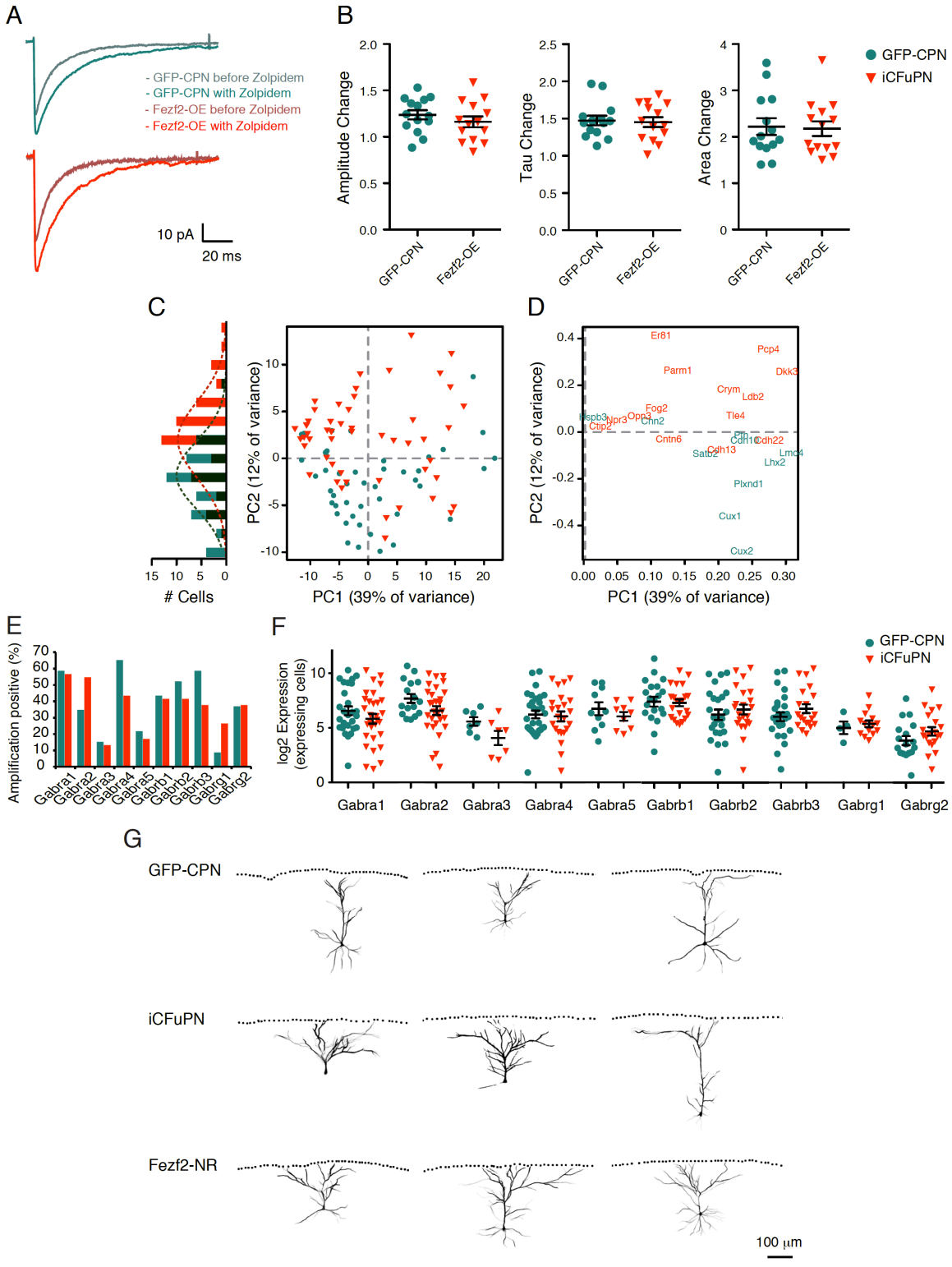

Figure 4.6 (Continued)

Table 4.3. Molecular verification of induced CFuPN identity for single-cell analysis of GABA receptor expression

Table of eigenvectors for the principal component analysis of marker gene expression in single GFP-CPN and iCFuPN (Figures 4.6C, D), sorted by loading onto PC2 in order to highlight opposite contributions of Er81/Pcp4 (CFuPN markers) and Cux1/Cux2 (CPN markers). Fraction of variance explained for each of the first 5 principal components is indicated, along with p values for significance of factor loading on total variation along PC2, calculated as correlation of gene expression to the sample score (Yamamoto et al., 2014). Important variables (absolute values over 0.32) on PC2 are bolded

Table 4.3 (Continued)

Eigenvectors of PCA on single-cell gene expression of marker genes in induced CFuPNs and callosal PNs used for GABA receptor expression

	PC1	PC2	PC3	PC4	PC5
Fraction variance	39.1%	11.8%	7.02%	5.01%	4.55%
Gene					
Er81	0.116	**0.413**[a]	-0.379	0.020	-0.003
Pcp4	0.274	**0.353**[b]	0.045	0.095	0.372
Parm1	0.138	0.264[a]	-0.038	-0.110	-0.115
Dkk3	0.301	0.258[c]	0.025	-0.057	-0.049
Crym	0.215	0.183	0.435	0.165	0.298
Ldb2	0.251	0.151	0.261	-0.203	-0.032
Fog2	0.108	0.102[c]	-0.200	-0.242	-0.253
Tle4	0.227	0.071	-0.304	-0.155	0.010
Opn3	0.083	0.066	0.027	0.095	-0.006
Hspb3	0.011	0.061	-0.326	0.461	-0.272
Npr3	0.049	0.048[c]	0.006	0.049	0.066
Chn2	0.102	0.046	-0.097	0.015	-0.030
Ctip2	0.025	0.022[c]	0.003	0.018	0.045
Ptn	0.236	-0.019	-0.298	-0.049	0.173
Cntn6	0.125	-0.031	0.118	0.248	0.223
Cdh22	0.272	-0.036	-0.026	0.632	-0.175
Cdh10	0.237	-0.037	0.150	-0.177	-0.285
Cdh13	0.201	-0.078	0.267	-0.090	-0.317
Lmo4	0.307	-0.093	0.198	-0.050	-0.113
Satb2	0.179	-0.093[c]	0.126	0.072	-0.239
Lhx2	0.283	-0.132	-0.200	-0.102	-0.065
Plxnd1	0.242	-0.223[b]	-0.128	-0.215	0.019
Cux1	0.217	**-0.360**[a]	-0.188	-0.094	0.493
Cux2	0.234	**-0.509**[a]	-0.040	0.151	-0.023

Significance of factor loading on overall variation along PC2: [a] $p<0.0001$; [b] $p<0.001$; [c] $p<0.05$.

for any receptor (Figure 4.6E-F). Together, these results indicate that the increased inhibition of iCFuPNs is not due to a stoichiometric change in $GABA_A$ receptor subunits.

Another possible explanation for the observed increased inhibition onto iCFuPNs cells is a nonspecific homeostatic change in the upper cortical circuit. We therefore compared the frequency of inhibition in iCFuPNs and Fezf2-NR cells within the same brains (Figures 4.5H-M). iCFuPNs showed increased mIPSC frequency across animals (Figure 4.5J) and this difference was also apparent between iCFuPNs and Fezf2-NR neurons from the same brain (Figure 4.5L), confirming that the increase of inhibition is a result of cell-specific IN-iCFuPN interactions and not of a global change in the local circuit.

We next considered that the observed increase in inhibition could be due to inhibitory input onto distinct regions of PNs (e.g., cell soma, axonal hillock, or dendritic arbor). CFuPNs differ from CPNs in cell morphology, including larger somas (Larkman and Mason, 1990) and broader apical dendrite tuft arborization (Oswald et al., 2013).

To assess changes in dendritic morphology, we filled cells with biocytin after recording to enable tracing and reconstruction, and measured the width of the arborization of the apical tuft (Figures 4.5H and 4.6G). In Fezf2-OE cells, tuft width was increased regardless of the reprogramming state of the neuron (in mm: GFP-CPN 209.3±23.29; Fezf2-NR 419.3±27.86; iCFuPN 413.1±21.79) (Figures 4.5H, 4.5M and 4.6G). As this increase did not correlate with reprogramming of electrophysiological properties, we conclude that it is unlikely to be the source of the difference in inhibition. Notably, this result also suggests that Fezf2 overexpression can induce specific neuronal traits (i.e., dendritic morphology), even in the absence of a global identity change.

As mIPSCs are primarily caused by perisomatic inputs (Soltesz et al., 1995), we next analyzed changes in the cell soma. Confocal image stacks of GFP expression in Fezf2-OE and GFP-CPNs were used for 3D reconstruction and rendering, and iCFuPNs were identified by immunostaining for the CFuPN marker CryM (Arlotta et al., 2005; Rouaux and Arlotta, 2013). We found that the soma height and maximum width of iCFuPNs ($GFP^+/CryM^+$) were significantly larger than those of GFP-CPNs (soma height in mm: GFP-CPN 16.02±0.68; iCFuPN 19.89±0.53. Soma maximum width in mm: GFP-CPN 13.27±0.56; iCFuPN 14.62±0.31. Height/width ratio: GFP-CPN 1.219 ± 0.034; iCFuPN 1.371 ± 0.042) (Figures 4.7C-F). This difference is consistent with previous demonstrations of larger soma and greater height/width ratio in CFuPNs compared to L2/3 CPNs (Larkman and Mason, 1990). Importantly, while the height/width ratio of iCFuPN matched that previously reported for endogenous CFuPN (Larkman and Mason, 1990), the absolute dimensions of the cells were smaller, suggesting that the increased inhibition observed in iCFuPN cannot be explained by soma-size changes alone.

iCFuPNs receive increased perisomatic PV+ input

We next considered that increased inhibition onto PNs could be a result of an increase in the total number of INs surrounding and synapsing with iCFuPNs or an increase in the number of inhibitory synapses from individual INs.

We have previously demonstrated that when an entire class of PNs is substituted with another, the lamination of INs is affected (Lodato et al., 2011). We therefore investigated if our electroporation-based model, which instead causes focal reprogramming of a small proportion of CPNs, results in a local change in the

Figure 4.7. Focal reprogramming does not alter gross PV-cell lamination

(A) Laminar distribution of PV interneurons assessed by immunostaining for GFP and Parvalbumin (PV) in brains that were electroporated with Cdk5r-Fezf2-IRES-eGFP (n = 4) does not show an increase in PV interneurons in the upper layers of electroporated hemispheres compared to the contralateral hemisphere.

(B) Total number of PV interneurons per column is unchanged between electroporated and contralateral hemispheres. Error bars: mean ± SEM.

(C) Representative 3D reconstructions and renderings of GFP-CPNs and iCFuPNs used for soma height, width, and ratio analysis. CPN showed more variability in soma size, exhibiting both large (top row) and smaller soma (bottom row) (also see panel D-E).

(D-F) iCFuPNs increase their soma size and elongation compared to GFP-CPNs. (D) Soma height. (E) Soma maximum width. (F) Height/width ratio. Error bars: mean ± SEM. GFP-CPN n=23, iCFuPN n=26.

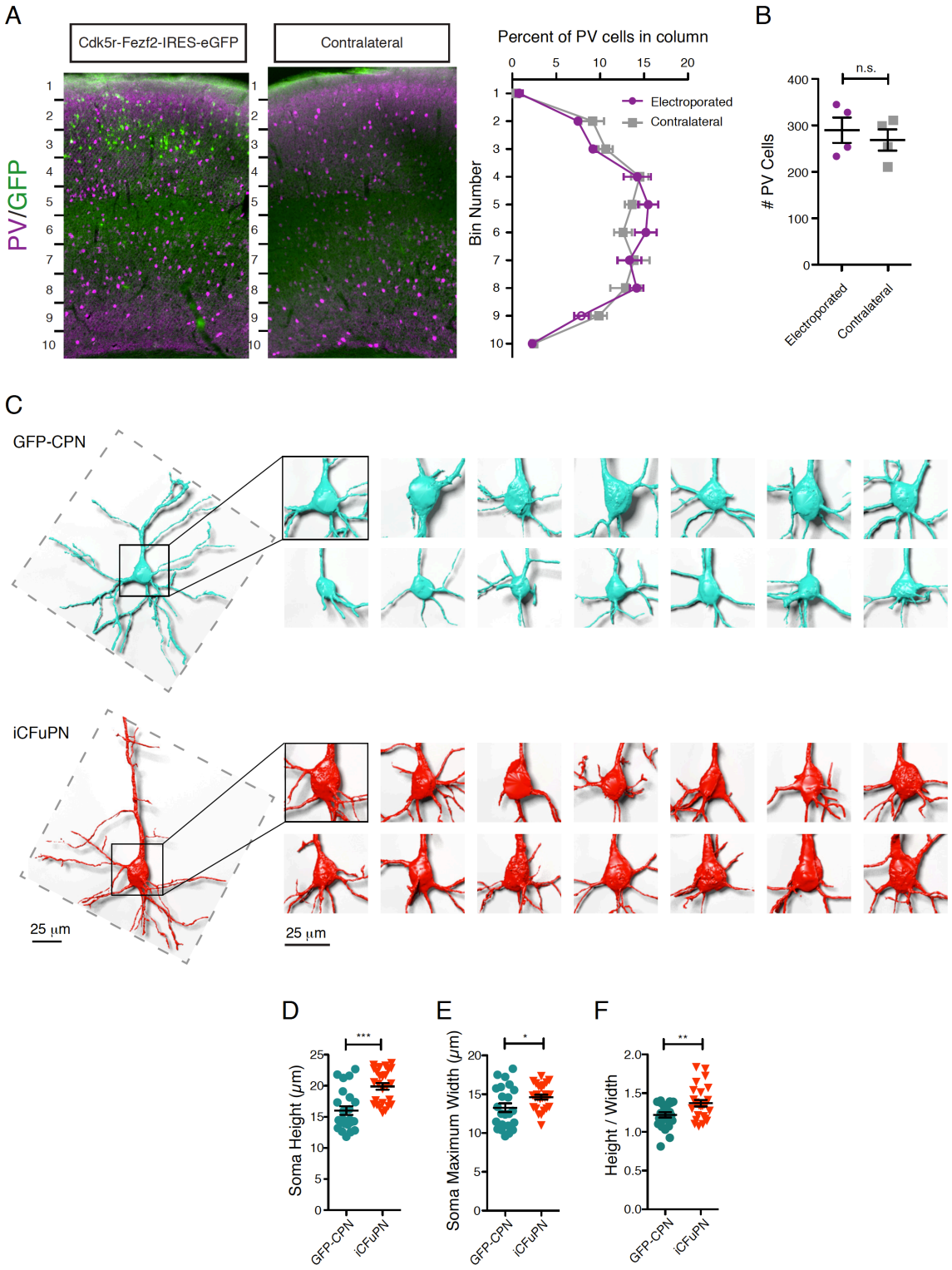

Figure 4.7 (Continued)

distribution of INs. Given that mIPSCs are primarily caused by perisomatic inputs, we concentrated on PV+ INs due to their preferential location within the deep layers of the cortex and the perisomatic nature of their synapses (Soltesz et al., 1995). The distribution of PV+ INs was quantified in GFP^+ regions of Fezf2-OE cortices and compared to the contralateral non-electroporated hemisphere (P28; n=4). We did not observe a significant change in PV+ IN lamination (Figure 4.7A-B), thus excluding the possibility that the increased inhibition is caused by a higher concentration of INs around the electroporated cells.

Next, we examined whether the increased inhibition of iCFuPNs was due to a higher density of PV+ GABAergic synapses onto these neurons. We quantified PV+ puncta density on the cell soma of iCFuPNs ($GFP^+/CryM^+$), L5 CFuPNs ($CryM^+$) and GFP-CPNs at P28 (Figure 4.8A). iCFuPNs acquired a PV+ puncta density equivalent to L5 CFuPNs, and higher than GFP-CPNs (in puncta/mm^2: L5 CFuPN 0.25±0.003; GFP-CPN 0.20±0.003; iCFuPN 0.25±0.004; iCFuPN vs. GFP-CPN $p<0.0001$, iCFuPN vs. L5 CFuPN $p=0.3056$) (Figure 4.8C), suggesting that their increased inhibition may reflect an increase in PV+ synaptic contacts.

To functionally test differences in PV+ IN input to iCFuPNs, we overexpressed Fezf2 in transgenic mice in which PV-Cre induction of ChR2 channelrhodopsin allows optogenetic stimulation of PV+ INs (see Chapter 2).

We measured the minimal light-evoked response (min-$IPSC_{PV}$), which likely reflects a single PV+ IN firing event, in L2/3 CPNs, L5 CFuPNs, and Fezf2-OE neurons via whole-cell voltage-clamp recording of PNs during optogenetic wide-field stimulation of PV+ INs (Figures 4.8D and 4.8E). There was no significant difference in min-$IPSC_{PV}$

Figure 4.8. iCFuPNs receive greater PV+ IN input

(A-C) iCFuPNs have increased PV+ puncta density. GFP-CPNs n=100, iCFuPNs n=200, L5 CFuPNs n=80. Error bars: mean ± SEM. (A) Representative immunofluorescence images for GFP, CryM and PV at P28. (B) iCFuPNs have greater soma size and (C) PV+ puncta density. (D-G) Optogenetic excitation of PV+ INs in reprogrammed cortices shows two patterns of response in Fezf2-OE neurons, resembling L2/3 CPNs and L5 CFuPNs, respectively. L2/3 CPNs n=21, Fezf2-OE cells n=21, L5 CFuPNs n=18. (D) Representative max-$IPSC_{PV}$ (main) and min-$IPSC_{PV}$ (inset) light-evoked response traces. (E) Amplitude of min-$IPSC_{PV}$ responses. (F) Amplitude of max-$IPSC_{PV}$ responses. (G) Fits of max-$IPSC_{PV}$ response data to single (L2/3 CPNs and L5 CFuPNs) or mixed (Fezf2-OE) Gaussian curves: Fezf2-OE cells show bimodal distribution (R^2: L2/3 CPN = 0.499, L5 CFuPN = 0.596, Fezf2-OE = 0.740).

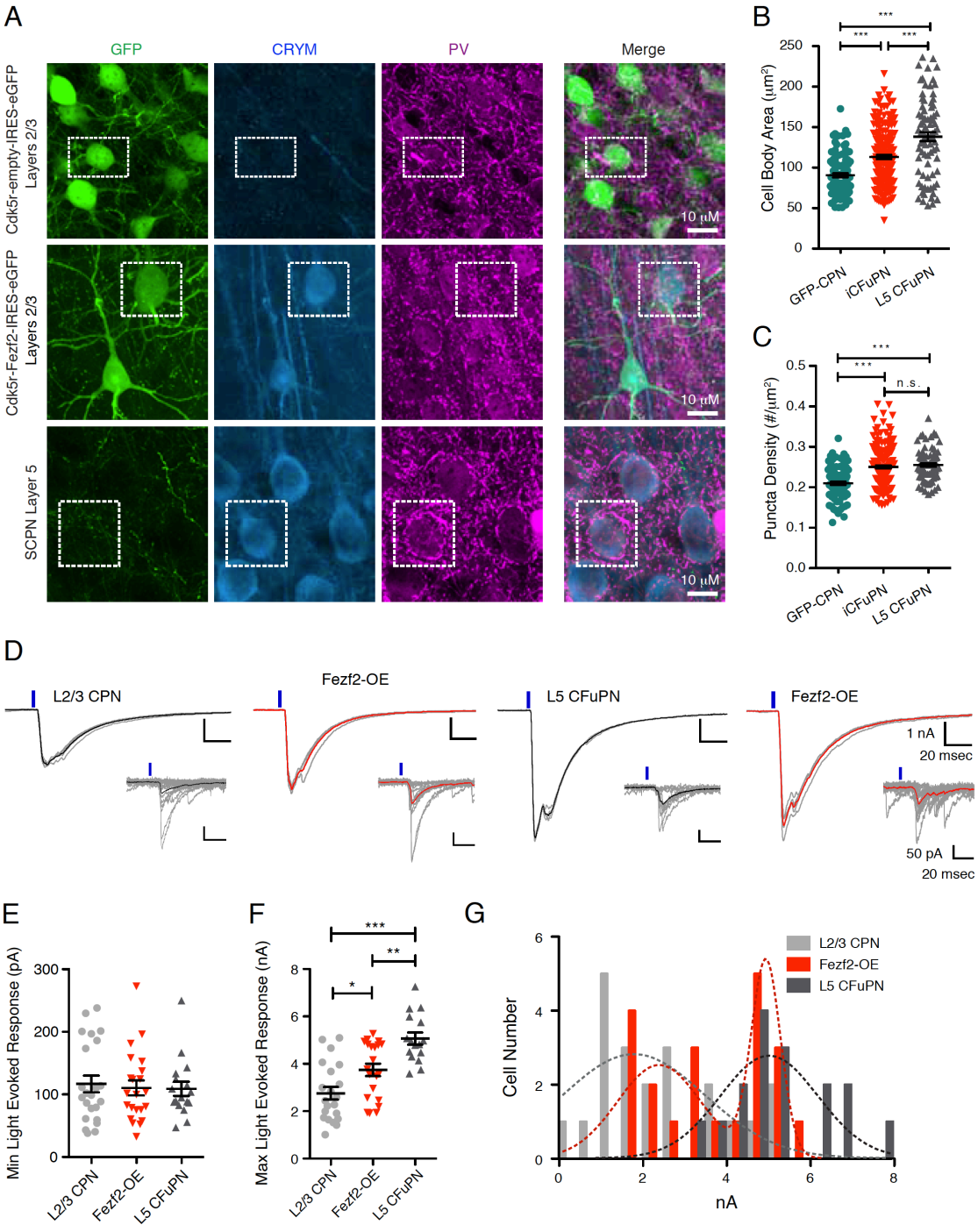

Figure 4.8 (Continued)

among these cells (all comparisons: $p>0.05$) (Figure 4.8E), suggesting that synapses between single PV^+ INs and PNs have a similar physiological strength in all groups.

To assess the total number of PV synapses, we measured the maximal optogenetically-driven IPSC (max-$IPSC_{PV}$, Figure 4.8D and 4.8F), the plateau response to increasing light intensity. The average max-$IPSC_{PV}$ of endogenous L2/3 CPNs was significantly smaller than that of L5 CFuPNs (L2/3 2756 ± 268.3 pA; L5 5067 ± 254.8 pA; $p<0.0001$) (Figure 4.8F), consistent with L5 CFuPNs receiving more PV synapses than L2/3 CPNs.

As a population, Fezf2-OE neurons showed an intermediate max-$IPSC_{PV}$ (3740 ± 260.0 pA). However, fitting the data to a mixed Gaussian distribution showed a bimodal max-$IPSC_{PV}$ response in Fezf2-OE cells (LRT, $p=0.0011$): 42% of the population had a mean response similar to L5 CFuPNs (4893.7 pA), whereas 58% had a mean response similar to L2/3 CPNs (2917.3 pA) (Figure 4.8G), consistent with our measurements of reprogramming efficiency.

Altogether, our data indicate that iCFuPNs acquire increased numbers of PV+ IN inputs to resemble L5 CFuPNs, regardless of their ectopic location. This effect is specific, as endogenous L2/3 CPNs intermingled with iCFuPNs appropriately receive fewer inputs. We conclude that altering PN class-specific identity is sufficient to instruct a change in inhibitory synapses from PV+ INs and to change the local inhibitory circuitry.

Discussion

Proper balance between excitatory and inhibitory neurons in the neocortex is essential for correct development and function (Rossignol, 2011). Inhibition mediated by

PV+ fast spiking INs is particularly interesting: perisomatic feed-forward inhibition ensures temporal precision of signal transduction in PNs (Pouille and Scanziani, 2001), and fast spiking INs can control the direction of activity flow in the local circuit (Xiang et al., 1998).

Reprogramming the identity of neurons within the CNS has attracted attention due to its potential therapeutic application (Amamoto and Arlotta, 2014). Here, we used our previously established reprogramming model, in which one class of cortical PNs is converted into another, as a tool to investigate the role of PN class-specific identity in the establishment of the inhibitory microcircuitry.

We show that iCFuPNs can reprogram their molecular, morphological and electrophysiological traits to resemble CFuPNs. Notably, iCFuPNs showed a Vsag equivalent to L5 CFuPNs and larger than L2/3 CPNs, consistent with previous observations that Vsag is larger in L5 PNs than L2/3 neurons (Mason and Larkman, 1990). This is interesting in light of the fact that Vsag is a characteristic of hyperpolarization-activated (Ih) current, which is important in regulating neuronal excitability, spike timing precision and network rhythmic activities (Luthi and McCormick, 1998). This suggests that iCFuPNs share functional properties with L5 CFuPNs.

We then used this reprogramming model to investigate the contribution of PN identity to the formation of PN-IN microcircuitry. It was recently shown that individual INs preferentially synapse onto specific subtypes of PNs (Lee et al., 2014; Otsuka and Kawaguchi, 2009). However, the question of whether IN microcircuits provide different inputs to different subtypes of PNs on a cell-by-cell basis is still debated. Examining

whether this bias also exists for PNs in ectopic locations will help resolve whether this effect is an intrinsic property of the individual PN or a consequence of some element of the normal laminar context.

Here we targeted and reprogrammed a subset of upper-layer CPNs, generating ectopic iCFuPNs in L2/3 scattered among L2/3 CPNs. These iCFuPNs were recognized and innervated by PV+ INs as L5 CFuPNs, distinct from closely-adjacent CPNs. This leads to the conclusion that target selection by INs occurs at the single neuron level, and provides evidence that PNs can, at least in part, guide the establishment of their afferent inhibitory synapses. This supports the theory that INs may be able to selectively modulate only certain PNs even if they are physically intermingled (Krook-Magnuson et al., 2012; Lee et al., 2014; Varga et al., 2010).

Together, the data indicate that circuit wiring among PN and IN partners in the neocortex is at least partly controlled by the identity of the PN, and that these decisions are made in a single-neuron-to-neuron manner. In addition, the work suggests that direct neuronal reprogramming is a tool to investigate the mechanisms that shape the local neocortical microcircuit, and to inform future studies on circuit plasticity in the central nervous system.

Chapter 5

Sex-Specific Effects of Early Life Stress on Prefrontal Parvalbumin Inhibition and Anxiety Behaviors

Author contribution:

Zhanlei Ye, Kimberly Schaefer, Hanna Sophie Knobloch-Bollmann, Hopi Hoekstra, Takao K Hensch

Z.Y. and T.K.H designed the experiments. Z.Y. performed and analyzed most experiments. H.S.K. performed *BDNF* qPCR. K.S. assisted Z.Y. for behavior experiments. H.H. supervised the study on peromyscus. T.K.H. supervised the project.

Summary

In humans, females show greater risk to develop anxiety disorders compared with males. Emerging evidence suggests gene-sex-early life experience interaction in the development of anxiety disorders. However, the mechanisms underlying sex differences are not fully understood. Here, in biparental *Peromyscus Polionotus* (PO) and lab mice C57BL/6J, we found that female mice experiencing early life stress (ELS) exhibited increased anxiety and impaired parvalbumin (PV) inhibition in the medial prefrontal cortex (mPFC). The sex-specific effect of ELS on anxiety behaviors may be mediated by differential expression of *BDNF* in females and males after ELS. Similar sex-dependent expression pattern of *BDNF* was also observed in BDNF Val/Met animals, among which females showed increased anxiety, but not males. Taken together, our data show that ELS

causes increased anxiety and impaired prefrontal inhibition in female animals across species and ELS paradigms. Our results highlight the key role of prefrontal PV+ neurons in gene-sex-environment interaction in anxiety disorders.

Introduction

Epidemiological data in humans show significant differences between females and males in the incidence of psychiatric disorders. In particular, emotional disorders, including post-traumatic stress disorder (PTSD) (Kessler et al., 1995), panic disorder, generalized anxiety, and major depressive disorder (Eaton et al., 2012; Somers et al., 2006), are more prevalent in females (see review (Cover et al., 2014)). Prior anxiety disorders beginning early in life might explain to a great part the higher female risk for major depression (Breslau et al., 1995), highlighting the importance of understanding the mechanisms underlying sex differences in anxiety disorders.

Emerging evidence points to neurodevelopmental origins of psychiatric disorders, including anxiety disorders (see review (Leonardo and Hen, 2008)). The Virginia twin study confirmed the sex differences in emotional disorders (Eaves et al., 1997), suggesting a gene-sex-environment interaction in developing anxiety disorders in females. Indeed, females are more susceptible to affective disorders in adolescence and throughout adulthood, especially if they have experienced early life stress (ELS) (see review (Bale and Epperson, 2015)). However, the majority of animal studies on ELS either combined both sexes or focused on males only (Molet et al., 2014), which failed to reveal the mechanisms of the increased risk for anxiety in females.

The extent of environmental impacts on neuronal circuits is limited by the plasticity of the brain. Neuronal circuits controlling perception and behaviors are radically shaped by experiences during critical periods of brain development. Parvalbumin (PV) expressing interneurons have been shown to be pivotal for critical period plasticity (Hensch, 2004, 2005). And PV+ neurons are particularly vulnerable to genetic and environmental insults associated with psychiatric disorders (Gogolla et al., 2009; Lewis et al., 2012; Marin, 2012). In humans, ELS has been linked to negative behavioral consequences and compromised structure and function of the prefrontal cortex (PFC) (Pechtel and Pizzagalli, 2011). And the PFC is strongly implicated in the stress response (Arnsten, 2009, 2015) and anxiety behaviors (Calhoon and Tye, 2015). However, how PV inhibition in the PFC is affected by ELS, and whether the effects are sex-dependent, remain unclear.

In this study, we investigated the behavioral and neurological consequences of ELS in both female and male mice. We show that adult females experiencing ELS exhibited anxiety-like behaviors, in company with impairment in PV inhibition in the medial PFC (mPFC).

Results

Increased anxiety in adult females after ELS in biparental, monogamous *Peromyscus polionotus* and C57BL6/J

The *Peromyscus polionotus* (PO) is reported to be monogamous and provides biparental care to pups (Bedford and Hoekstra, 2015). Given their behaviors and social structures, we first wanted to mimic ELS in humans by performing parental separation

during postnatal day (P) 2-P14 (Millstein and Holmes, 2007) in POs (Figure 5.1A). 8 litters (average liter size = 3.57±0.57(SEM)) were randomly selected for parental separation during postnatal (P) 2 to P14 for 2 hours per day at a random time during the light cycle. Age-matched control animals were randomly selected from the breeding colony.

To assess the effects of ELS, we performed behavior tests in 6-month old adults. In the open field test, ELS females exhibited a trend of heightened locomotion (total distance traveled in 30min 27825 ± 4313 cm, N=13) compared to control (CTL) females (total distance 17815 ± 3789 cm, N=9, p=0.0974, Figures 5.1B, C). When normalized to each individual's locomotion, ELS females showed significantly reduced center duration (0.5725 ± 0.09850) in comparison with CTL females (1.000 ± 0.1504, p=0.0218, Figures 5.1B, C), suggesting increased anxiety level in ELS females.

The similar behavioral pattern was also present in a more complicated apparatus with compartments, the 3-chamber apparatus. ELS females showed significantly higher activity (Figures 5.2A, B). The average velocity of ELS females (23.87 ± 1.480 cm/sec) was significantly greater than that of CTL females (16.29 ± 1.064 cm/sec, p=0.0030, Figure 5.2B). Although no change in the preference for mouse over object was detected, the total time spent in the proximity of target mouse and object was reduced in ELS females (CTL 491.6 ± 22.47 sec, ELS 416.3 ± 20.22 sec, p=0.0243, Figure 5.2C). Decreased time spent engaging in interaction with novel mouse/object would indicate anxiogenic behavior, as we observed a significant negative correlation between the interaction time and velocity in the 3-chamber test (beta=-5.902 ± 2.771, F(1,20)=4.536, p=0.0465, Figure 5.2D). The normalized center duration in the open field test was also

Figure 5.1. Increased anxiety in adult females after ELS in biparental, monogamous *Peromyscus polionotus* and C57Bl6/J

(A-C) Increased anxiety in females after ELS in *Peromyscus polionotus* (PO). (A) Time table of experimental design. Parental separation was performed during postnatal day (P) 2 to 14; behavioral analysis was performed after 6 month. (B) Sample traces of control (CTL) and early life stress (ELS) females' tracking in the open field (OF) test. Blue box indicates the center of the arena. (C) Distance traveled and Duration in the center normalized by animals' locomotion in the OF tests. (F CTL n=9, F ELS n=13, M CTL n=7, and M ELS n=12)

(D-F) Increased anxiety in females after ELS in C57BL6/J. (D) Time table of experimental design. Fragmented care was performed during P2 to 9; behavioral analysis was performed after P60. (E) Duration in the center normalized by animals' locomotion in the OF tests in female and male animals. (Female CC n=10, FC n=6; male CC n=6, FC n=13.) (F) Open arm preference normalized to the mean of CC animals in the elevated plus maze (EPM) test in female and male animals. (Female CC n=8, FC n=6; male CC n=8, FC n=8.)

Error bars represent SEM. 2 tailed t-tests in C,E and F. * $p<0.05$, ** $p<0.01$

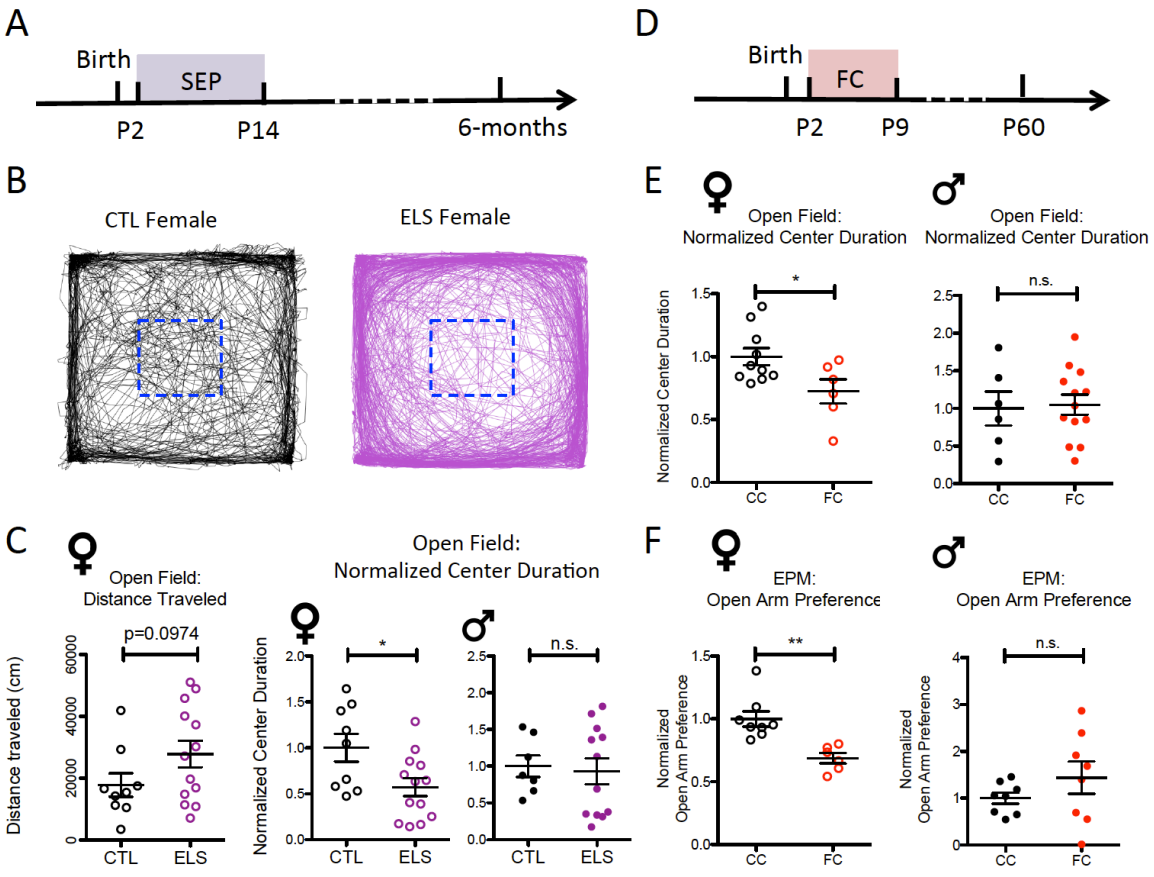

Figure 5.1 (Continued)

Figure 5.2. Hyperactivity and reduced social interaction in ELS females of the biparental, monogamous *Peromyscus polionotus*

(A) Sample traces of CTL and ELS females' tracking during exploration of 3-Chamber test. (B) Average velocity and (C) Time spent in the area close to target mouse or object (MnO Time) in the 3-Chamber tests. (D) Linear correlation of MnO time with velocity in 3-Chamber test ($R^2=0.1927$, beta=-5.902 ± 2.771, $F(1,20)=4.536$, $p=0.0465$); average velocity in the OF test and average velocity in the 3-Chamber test ($R^2=0.1522$, beta=0.5366 ± 0.2832, $F(1,20)=3.590$, $p=0.0727$); and normalized center duration in the OF test and average velocity in the 3-Chamber test ($R^2=0.1903$, beta=-0.03277 ± 0.01512, $F(1,20)=4.700$, $p=0.0424$). (E) Linear correlation of average PV intensity in the mPFC with velocity in the 3-Chamber test ($R^2=0.2217$, beta=-0.5814 ± 0.2436, $F(1,20)=5.697$, $p=0.0270$)

Solid lines: linear prediction; dotted lines: 95% confidence interval. Error bars represent SEM. Female CTL n=9, female ELS n=13, male CTL n=7, and male ELS n=12. 2 tailed t-tests in C; 2-way ANOVA in B followed with Bonferroni post-test. * $p<0.05$, ** $p<0.01$

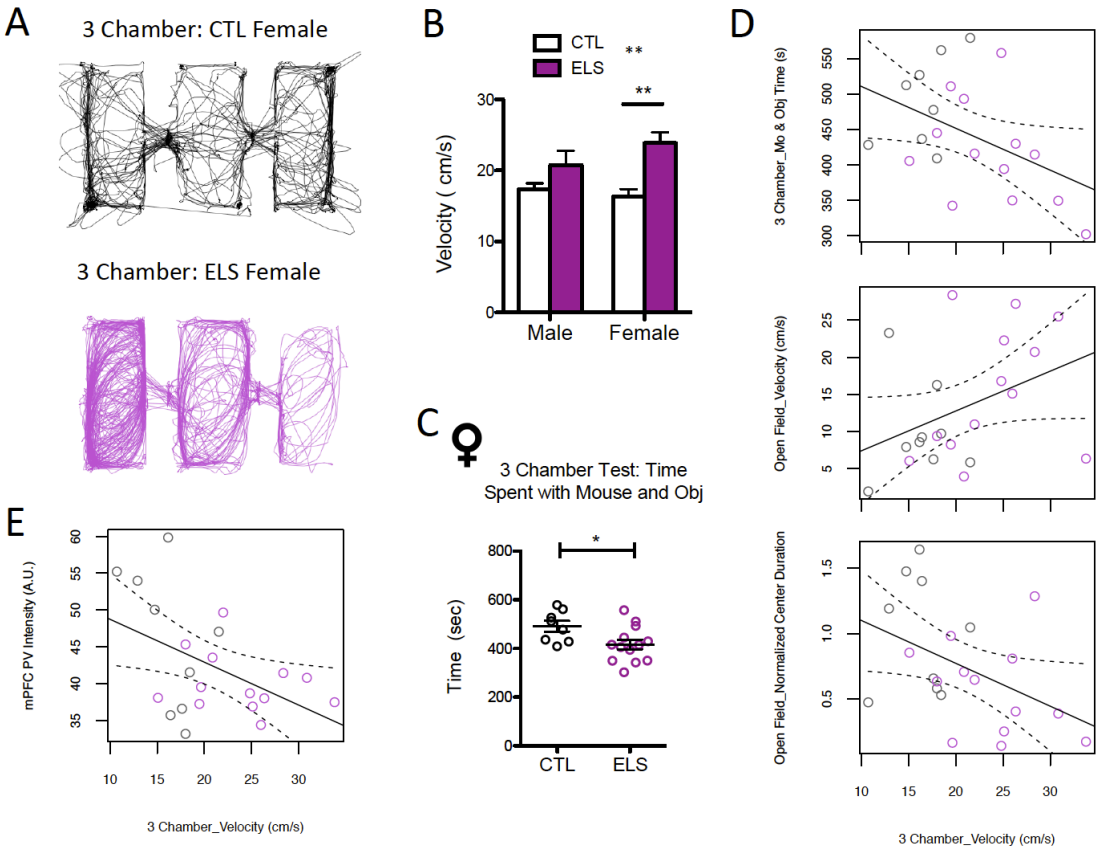

Figure 5.2 (Continued)

significantly negatively correlated with the velocity in the 3-chamber test (beta=-0.03277 ± 0.01512, F(1,20)=4.700, p=0.0424, Figure 5.2D), indicating that the behavioral phenotype of hyperactivity and increased anxiety in ELS females were consistent across different behavioral paradigms.

We did not observe significant changes in ELS males in normalized center duration in the open field test (Figure 5.1C) or overall activity in 3-chamber test (Figure 5.2B), suggesting that anxiety behaviors in PO males were not affected by parental separation during P2-P14.

To validate our finding in POs and also introduce ELS to lab mice, we adapted the model of fragmented care (FC) during P2-9 with limited bedding materials (Ivy et al., 2008) (Figure 5.1D). FC paradigm has been shown to robustly disrupt parental behaviors of dams (Heun-Johnson and Levitt, 2016; Ivy et al., 2008; Molet et al., 2016), and alter emotional behaviors in adolescence male rat (Molet et al., 2016). Recently, it was shown that FC causes accelerated maturation of fear conditioning behaviors in male mice (Bath et al., 2016). However, it remains unclear how female mice are affected by FC, and whether there are sex-specific effects of FC in lab mice.

When tested after P60, FC females showed significantly less center during in the open field (OF) test (F-CC 1.000 ± 0.06823, F-FC 0.7247 ± 0.09651, p=0.0317, Figure 5.1E), and significantly lower preference for the open arm in the elevated plus maze (EPM) test (F-CC 1.000 ± 0.06116, F-FC 0.6867 ± 0.04095, p=0.0020, Figure 5.1F), in comparison with females receiving control care (CC). However, no significant differences were observed in FC males when compared with CC males (OF: M-CC 1.000 ± 0.2254, M-FC 1.050 ± 0.1324, p=0.8432; EPM: M-CC 1.000 ± 0.1189, M-FC 1.439 ±

0.3437, p=0.2474, Figures 5.1E, F). No significant change in locomotion was detected in females or males after FC (Figure 5.3). Consistent with our results in POs, we found that ELS (using FC paradigm) during P2-P9 resulted in increased anxiety in females but not males in C57BL6/J mice.

In summary, our results indicate that ELS by disrupting parental care during early postnatal weeks causes increased anxiety in adult females across species.

Selective impairment of PV network in the mPFC of ELS females

The medial PFC (mPFC) in mice is highly involved in emotion regulation (Calhoon and Tye, 2015; Riga et al., 2014). Given the role of PV+ interneurons in regulating plasticity and behaviors, we therefore aimed to examine how PV inhibition in the mouse mPFC was affected by ELS.

In POs, the average PV intensity in the mPFC was significantly lower in ELS females (CTL 45.94 ± 3.188 A.U., ELS 38.76 ± 1.259 A.U., p=0.0281, Figures 5.4A, B). The average PV intensity in the M1 area was not significantly different between CTL and ELS females (Figures 5.4B, 5.5A), suggesting that the decrease in PV expression in females was selective to the mPFC after ELS. Notably, in female POs, PV intensity in the mPFC was positively correlated with their normalized center duration in the open field test (beta=7.232 ± 3.301, F(1,20)=4.801, p=0.0404, Figure 5.4E), and negatively correlated with animals' average velocity in the 3-chamber test (beta=-0.5814 ± 0.2436, F(1,20)=5.697, p=0.0270, Figure 5.2E), suggesting the involvement of mPFC PV inhibition in regulating anxiety behaviors in females. We did not observe significant differences in PV intensity in the mPFC of male POs after ELS (CTL 41.86 ± 1.381

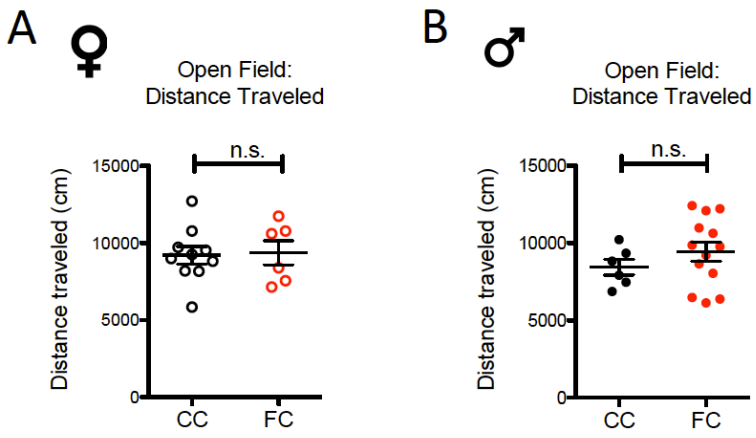

Figure 5.3. No difference in locomotion in ELS females and males of C57BL/6J

(A) Distance traveled in 30min open field test in females (B) Distance traveled in 30min open field test in males. (Female CC n=10, FC n=6; male CC n=6, FC n=13.) 2-tailed t-test. $p>0.05$

Figure 5.4. Selective Impairment of PV network in the mPFC of ELS females

(A) Example images of PV staining in the mPFC of CTL and ELS female POs. L1-L5: layer 1 – layer 5 of the mPFC. Scale bar: 100 μm (B) Average intensity of PV staining in female POs' mPFC, M1 and male POs' mPFC. (F CTL n=9, F ELS n=13, M CTL n=7, and M ELS n=12.)

(C) Example images of PV staining in the mPFC of CC and FC C57 females. Scale bar: 100 μm (D) Average intensity of PV staining in the mPFC and M1 of FC C57 animals. (Female CC n=5 animals, FC n=5 animals)

(E) Linear correlation of average PV intensity in the mPFC of POs with normalized center duration in the OF test. Female POs: $R^2=0.1936$, beta=7.232 ± 3.301, $F(1,20)=4.801$, $p=0.0405$. Male POs: $R^2=0.009654$, beta=-1.228 ± 3.016, $F(1,17)=0.1657$, $p=0.6890$. Solid lines: linear prediction; dotted lines: 95% confidence interval. Error bars represent SEM.

2 tailed t-tests in B and D. * $p<0.05$, ** $p<0.01$

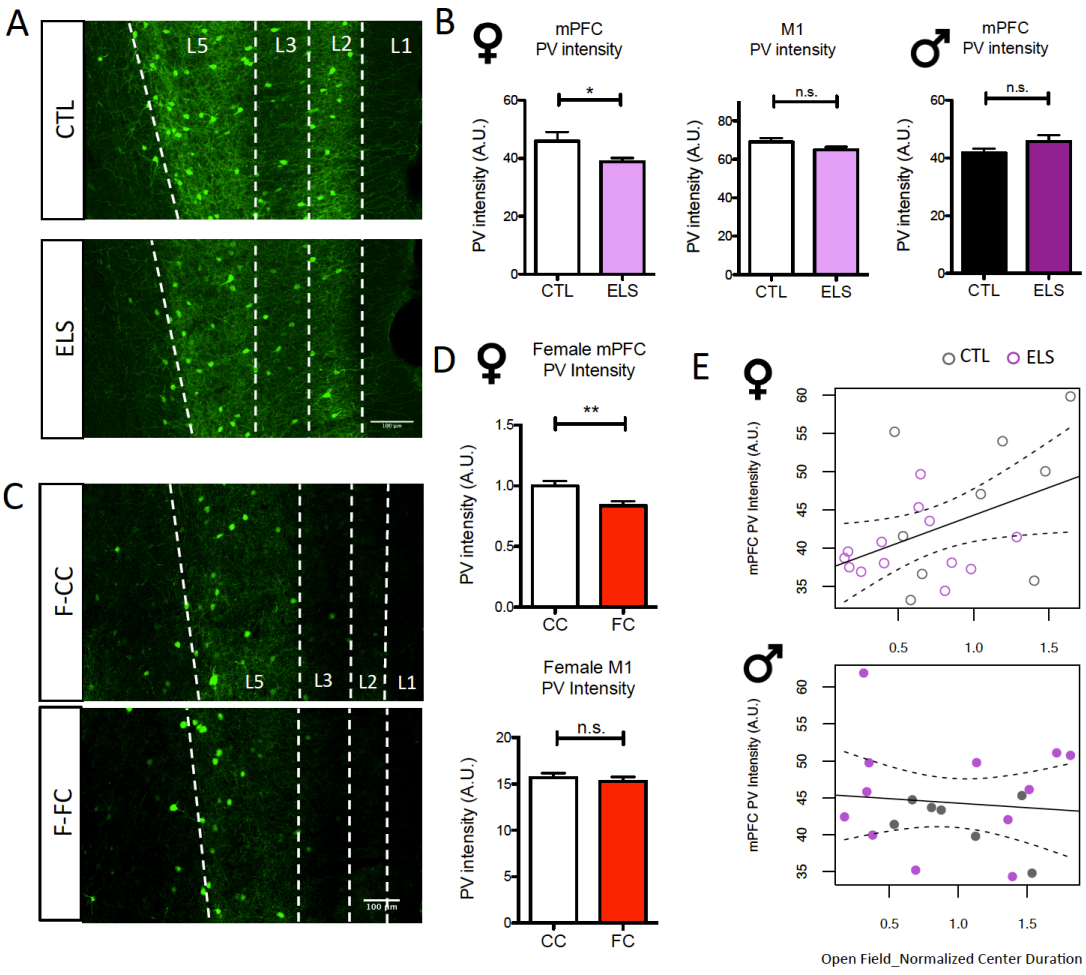

Figure 5.4 (Continued)

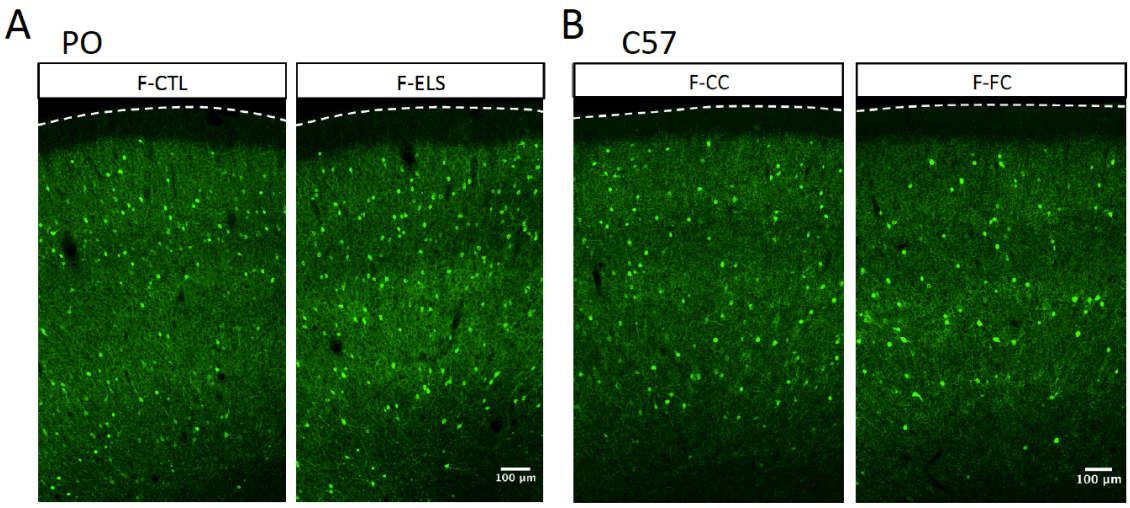

Figure 5.5. No differences in PV intensity in the primary motor cortex of females after ELS

(A) Example images of PV staining in M1 area in female POs. Quantification in Figure 5.4B (B) Example images of PV staining in M1 area in female C57s. Quantification in Figure 5.4D. Scale bar: 100 µm

A.U., ELS 45.76 ± 2.215 A.U., p=0.2269, Figure 5.4B). Nor did we detect a significant correlation of PV intensity and anxiety behavior in male POs (beta=-1.228 ± 3.016, F(1,17)=0.1657, p=0.6890, Figure 5.4E).

We again examined the PV+ interneurons in the mPFC in CC and FC C57 females. The average PV intensity in layer 5 (L5) of the mPFC was significantly reduced in FC females compared with CC females (F-CC 1.000 ± 0.04040 A.U., F-FC 0.8375 ± 0.03719 A.U., Figures 5.4C, D). The average PV intensity in the M1 area was not significantly different between CC and FC females (Figures 5.4D, 5.5B). Similar to our findings in POs, FC selectively reduced PV intensity in the mPFC of female mice.

Reduced inhibition onto Type A L5 pyramidal neurons after FC in females

Consistent with the anatomical changes in Figure 5.4, the frequency of miniature inhibitory post-synaptic currents (mIPSCs) was significantly reduced in mPFC L5 pyramidal neurons (F-CC 1.219 ± 0.1281 Hz, F-FC 0.8487 ± 0.09087 Hz, p=0.0215, Figure 5.8C), suggesting a reduced number of inhibitory synaptic inputs onto L5 pyramidal neurons in the mPFC of FC females.

L5 pyramidal neurons can be divided into 2 subtypes (A and B) based on the existence of voltage sag (Vsag) (Lee et al., 2014). Type A neurons which project to subcortical regions have prominent Vsag and more PV inputs; while Type B neurons which send callosal projecting axons have small or no Vsag, and fewer PV inputs. Pooling all neurons from CC and FC female animals, the histogram of Vsag exhibited a double-peak distribution (Figure 5.6A). The cut-off was set at 5mV to distinguish the 2 populations. The distributions of the two types of neurons were not significantly different

Figure 5.6. Reduced inhibition onto Type A L5 pyramidal neurons after FC in female mPFC

(A) Histogram of voltage sag (Vsag) in all neurons from female CC and FC animals. Red line: fitted density plot. (B) Percentage of Type A and Type B neurons in female CC and FC animals recorded. (Type A: CC n=16 cells from 3 animals, FC n=16 from 3 animals; Type B: CC n=17 from 3 animals, FC n=15 from 3 animals. Fisher's exact test: p=1.000) (C-E) Type A neurons and (F-H) Type B neurons respectively. From top to bottom: (C), (F), sample traces of membrane voltage response to -200pA current injection, showing the size of Vsag, with scale bar: 200msec, 10mV; (D), (G), sample traces of mIPSCs, with scale bar: 1sec, 20pA; (E), (H), cumulative plot of inter-event intervals (IEI) and average frequency (insert) of mIPSCs from CC and FC females. Error bars represent SEM. K-S test for comparison of cumulative plots; 2-tailed t-test for comparison of frequency. * $p<0.05$, **** $p<0.0001$

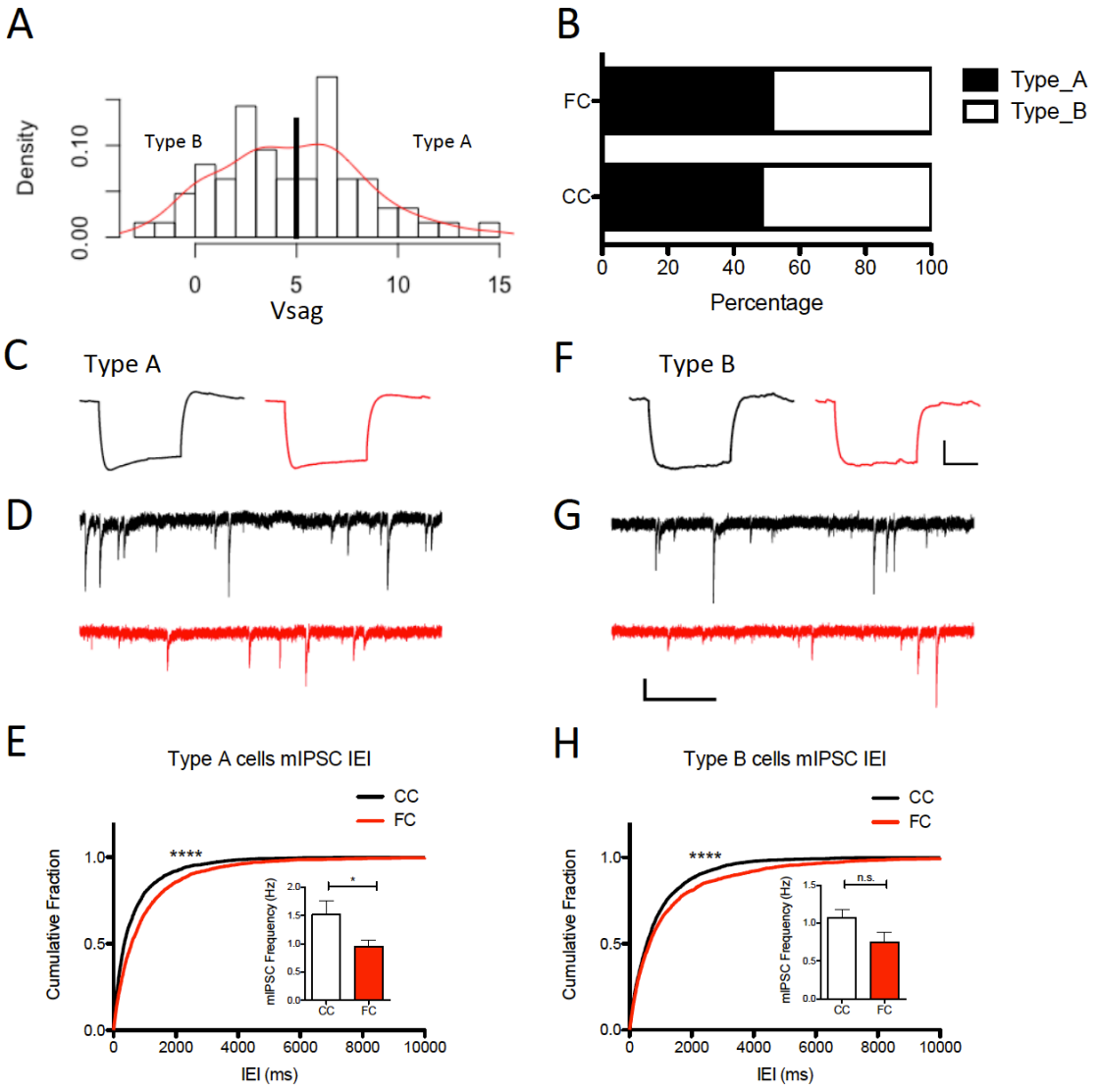

Figure 5.6 (Continued)

in CC and FC female animals (Type A neuron percentage: F-CC 48.48%, F-FC 51.61%, Fisher's exact test p=1.000, Figure 5.6B). This indicated that the difference we observed in the frequency of mIPSCs between FC and CC females (Figure 5.8C) was not due to sampling bias in the subtypes of pyramidal neurons. Consistent with previous studies, we observed a higher frequency of mIPSCs in Type A neurons (2-way ANOVA, p=0.044). FC had a significant effect in reducing the frequency of mIPSCs across cell types (p=0.0057), but the effects on type A pyramidal neurons were more prominent (Figures 5.6C-H).

$GABA_A$ receptors containing α1 subunits (GABRA1) are preferentially enriched at somatic synapses innervated by PV+ neurons (Freund and Katona, 2007; Klausberger et al., 2002). Inhibitory currents carried by α1 subunits containing receptors have faster decay (Goldstein et al., 2002; Vicini et al., 2001). We, therefore, analyzed the decay time of mIPSCs recorded from female CC and FC animals (Figures 5.7, 5.8D). The average decay time was significantly greater in FC females in both Type A and Type B L5 pyramidal neurons (Type A, CC 6.104 ± 0.3814 msec , FC 7.700 ± 0.3285 msec, p=0.0036; Type B, CC 6.667 ± 0.5125 msec, FC 8.136 ± 0.3470 msec, p=0.0280. Figure 5.7). mRNA expression level of *GABRA1* was also significantly reduced in the frontal cortex of FC females (Figure 5.8E)

We did not observe changes in the amplitude or rise time of mIPSCs after FC in either type of L5 pyramidal neurons in females (Figures 5.8 A, B).

Figure 5.7. Increased mIPSC decay time after FC in female mPFC

(A) Sample traces of average mIPSCs from Type A L5 pyramidal neurons, normalized to the average amplitude. Scale bar: 10msec. (B) Cumulative plot of decay time and average decay time (insert) of mIPSCs from Type A L5 neurons in female CC and FC animals. (C) Sample traces of average mIPSCs from Type B L5 pyramidal neurons, normalized to the average amplitude. Scale bar: 10msec. (D) Cumulative plot of decay time and average decay time (insert) of mIPSCs from Type B L5 neurons in female CC and FC animals. Type A, CC n=16 cells from 3 animals, FC n=16 from 3 animals; Type B, CC n=17 from 3 animals, FC n=15 from 3 animals. Error bars represent SEM. K-S test for comparison of cumulative plots; 2-tailed t-test for comparison of frequency. * $p<0.05$, ** $p<0.01$, **** $p<0.0001$

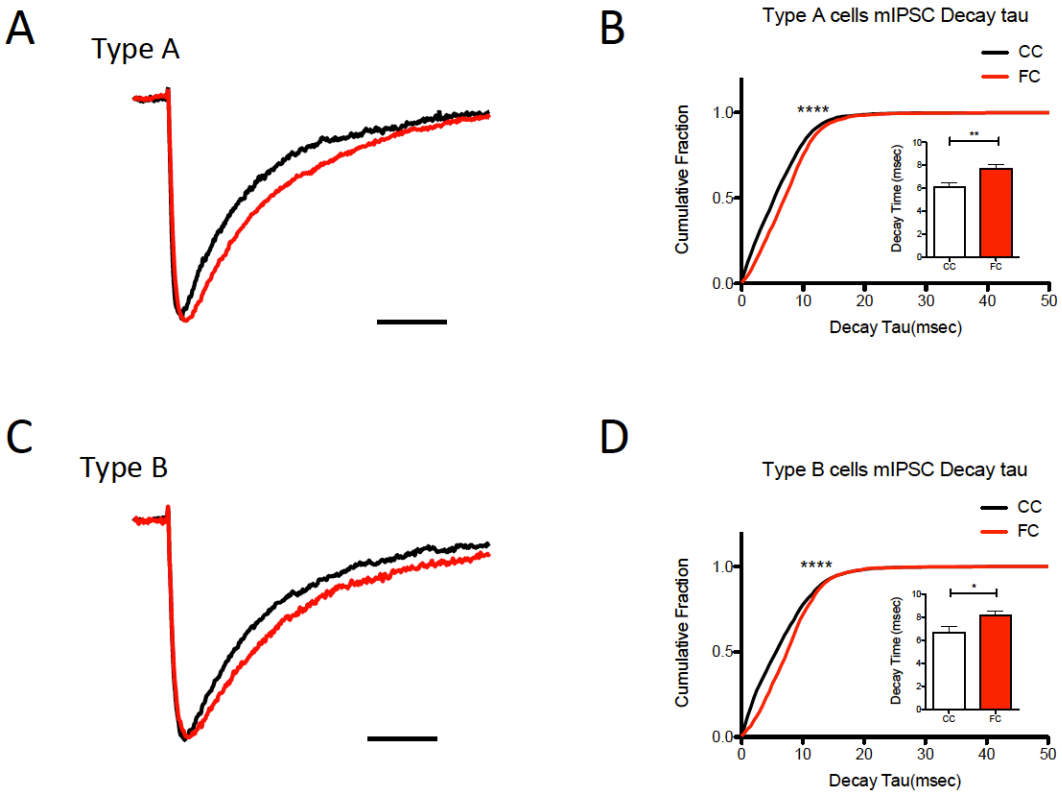

Figure 5.7 (Continued)

Figure 5.8. Changes in mIPSC amplitude, rise time, decay time, frequency, and *GABRA1* expression in female FC mPFC

(A) mIPSC Amplitude and (B) Rise time in female mPFC L5 pyramidal neurons.(C) mIPSC frequency in pooled female mPFC L5 pyramidal neurons (D) mIPSC decay time in pooled female mPFC L5 pyramidal neurons. (E) Relative expression level of *GABRA1* in the frontal cortex of female animals (N=3). Type A, CC n=16 cells from 3 animals, FC n=16 from 3 animals; Type B, CC n=17 from 3 animals, FC n=15 from 3 animals. Error bars represent SEM. 2-way ANOVA, followed by Bonferroni multiple comparisons in (A-B). 2-tailed t-test in (C-E). * $p<0.05$, ** $p<0.01$. No statistical differences were detected if not indicated

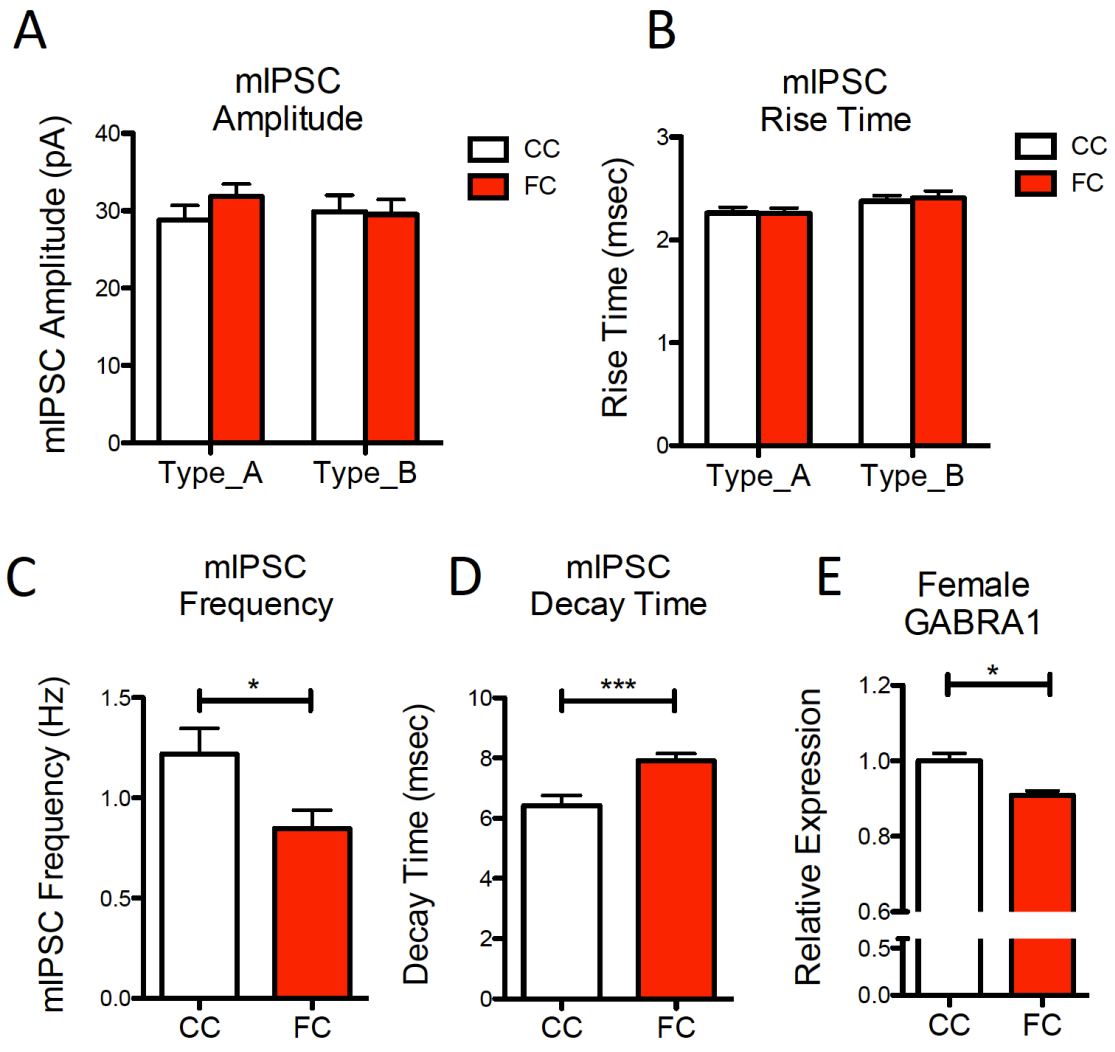

Figure 5.8 (Continued)

Increased inhibition onto Type B L5 pyramidal neurons after FC in males

We also examined inhibition in the male mPFC by measuring mIPSCs. Using the same criterion to distinguish Type A and Type B L5 pyramidal neurons, we found no significant difference in the distribution of subtypes between CC and FC males (Type A neuron percentage: M-CC 46.88%, M-FC 41.38%, Fisher's exact test: p=0.7974, Figures 5.9A, B). We observed an increased frequency of mIPSCs only in Type B L5 pyramidal neurons in FC males, but not in Type A neurons (Figures 5.9C-H). There were no significant changes in the amplitude, rise time or decay time of mIPSCs after FC in either type of mPFC L5 pyramidal neurons in males (Figures 5.10A-C). And the expression levels of $GABA_A$ receptor α1 subunits in the frontal cortex of FC males did not differ from that of CC males (Figure 5.10D).

Differential expression of *BDNF* may underlie the effects of ELS

To probing the potential mechanisms underlying the sex-specific effects of ELS, we examined the expression level of brain-derived neurotrophic factor (BDNF). BNDF is well known for positively regulating the maturation of PV+ interneurons (Huang et al., 1999). And BDNF has been shown to affect stress response and anxiety-like behaviors (Govindarajan et al., 2006; Lakshminarasimhan and Chattarji, 2012). Interestingly, we found that *BDNF* mRNA was significantly down-regulated in FC females (Figure 5.11A), but significantly up-regulated in FC males (Figure 5.11A)

In humans, BDNF Val66Met (Val/Met) is a common polymorphism with allele (Met) frequency ranging from 25-32% in Caucasian populations to 40-50% in Asian populations (Verhagen et al., 2010). A single nucleotide substitution from guanine (G) to

Figure 5.9. Increased inhibition onto Type B L5 pyramidal neurons after FC in male mPFC

(A) Histogram of voltage sag (Vsag) in all neurons from male CC and FC animals. Red line: fitted density plot. (B) Percentage of Type A and Type B neurons in male CC and FC animals recorded. (Type A: CC n=15 cells from 3 animals, FC n=12 from 3 animals; Type B: CC n=17 from 3 animals, FC n=17 from 3 animals. Fisher's exact test: p=0.7974) (C-E) Type A neurons and (F-H) Type B neurons respectively. From top to bottom: (C), (F), sample traces of membrane voltage response to -200pA current injection, showing the size of Vsag, with scale bar: 200msec, 10mV; (D), (G), sample traces of mIPSCs, with scale bar: 1sec, 20pA; (E), (H), cumulative plot of inter-event intervals (IEI) and average frequency (insert) of mIPSCs from CC and FC males. Error bars represent SEM. K-S test for comparison of cumulative plots; 2-tailed t-test for comparison of frequency. * $p<0.05$, **** $p<0.0001$

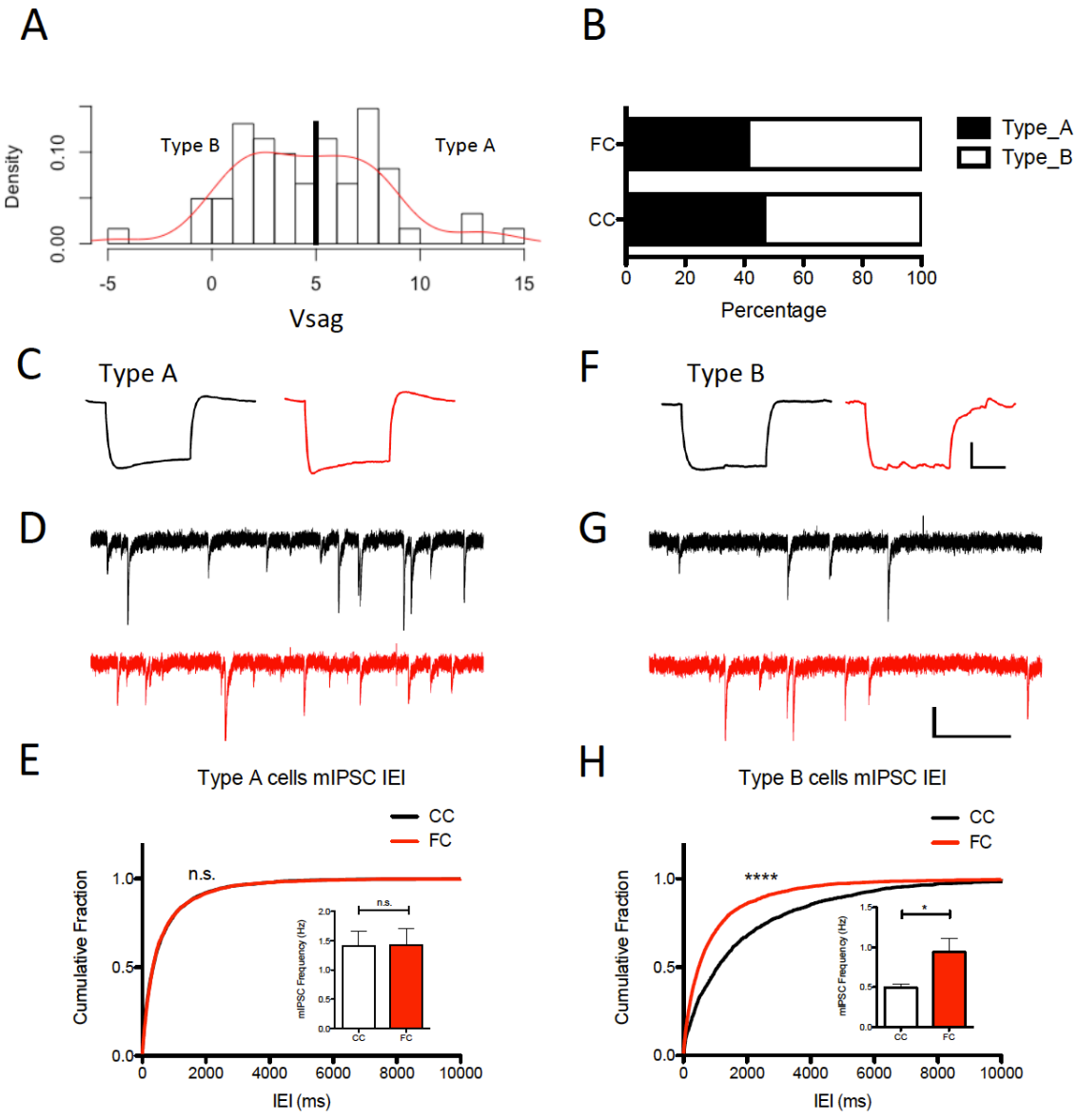

Figure 5.9 (Continued)

Figure 5.10. No change in mIPSC amplitude, rise time, decay time, or *GABRA1* expression in male FC mPFC

(A) mIPSC Amplitude, (B) Rise time and (C) Decay time from male CC and FC mPFC. (D) Relative expression level of *GABRA1* in the frontal cortex of male animals (N=3). Type A, CC n=15 cells from 3 animals, FC n=12 from 3 animals; Type B, CC n=17 from 3 animals, FC n=17 from 3 animal. Error bars represent SEM. 2-way ANOVA in (A), (B) & (C). 2-tailed t-test in (D). No statistical differences were detected. $p>0.05$

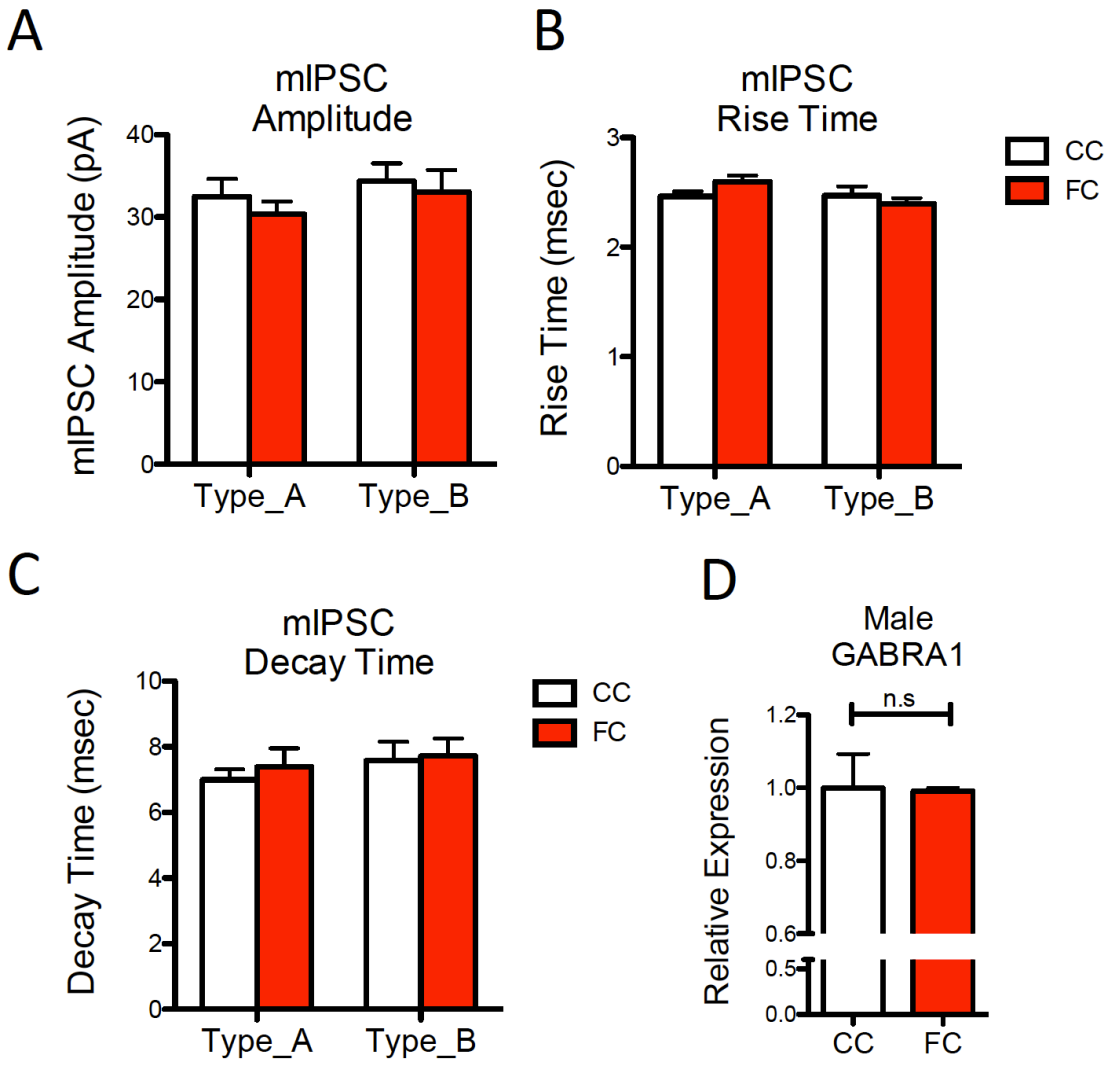

Figure 5.10 (Continued)

Figure 5.11. BDNF Val/Met mimics the effects of fragmented care

(A) Expression of *BDNF* mRNA in the frontal cortex of female and male animals comparing CC and FC. (N=3) (B) Expression of *BDNF* mRNA in the frontal cortex of BDNF Val/Met female and male animals. (N=3) (C) Sample traces of Val/Val and Val/Met females' tracking in the open field test. Red boxes indicate the center of the arena. (D) Distance traveled in 30min open field test in female and male BDNF Val/Met animals. (E) Duration in the center normalized by animals' locomotion in the OF test in female and male animals. (Female Val/Val n=10, Val/Met n=10; male Val/Val n=6, Val/Met n=12.) (F) Sample traces of Val/Val and Val/Met females' tracking in the elevated plus maze (EPM) test. (G) Open arm preference normalized to the mean of Val/Val animals in the EPM test in female and male animals. (Female Val/Val n=8, Val/Met n=8; male Val/Val n=8, Val/Met n=7.) Error bars represent SEM. 2 tailed t-tests in A, B, E and F; * $p<0.05$, ** $p<0.01$.

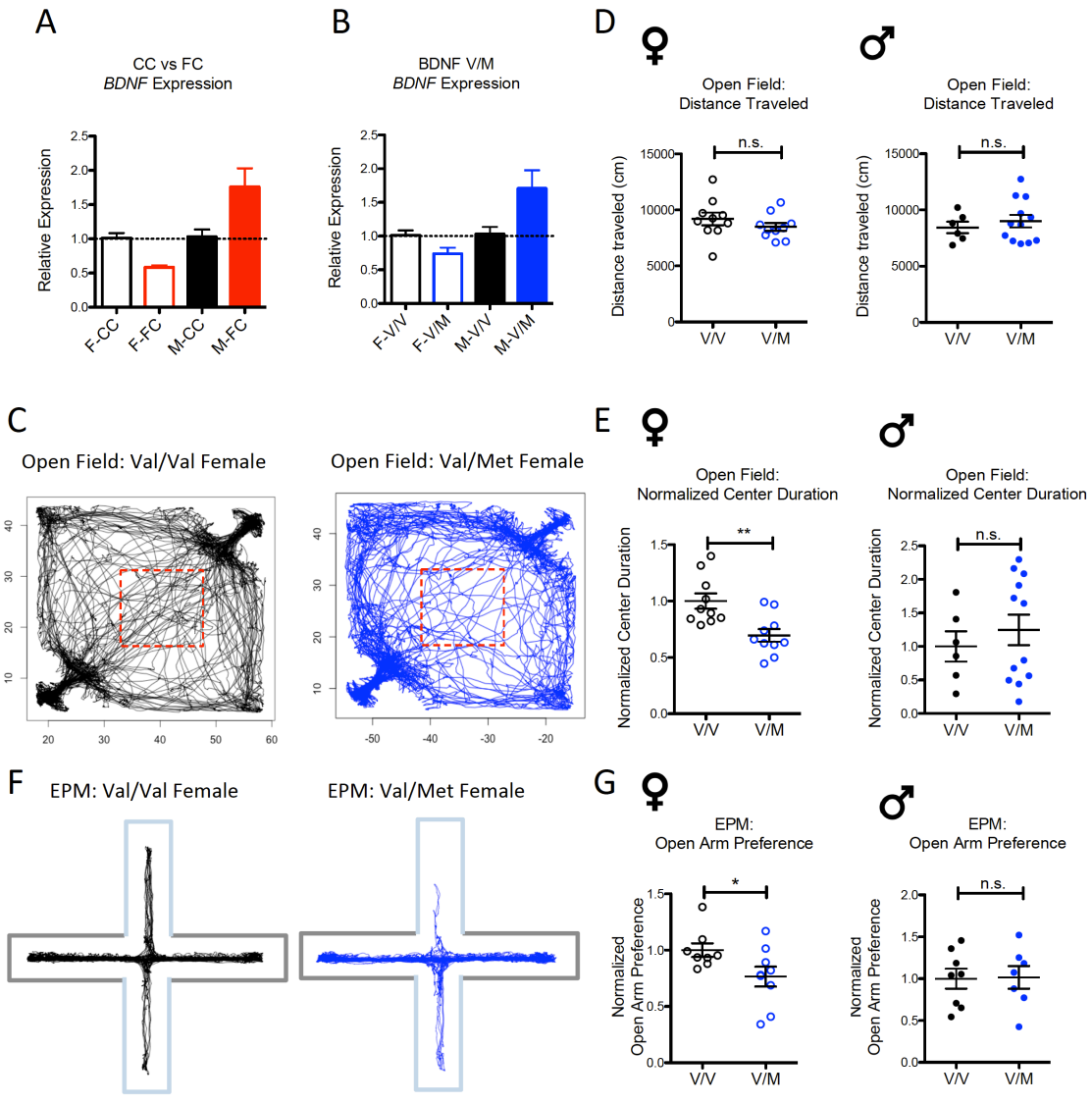

Figure 5.11 (Continued)

adenine (A) causes a change in an amino acid from valine (Val) to methionine (Met) in the pro-domain of BDNF protein. The Met allele affects cellular traffic and activity-dependent release of BNDF (Egan et al., 2003). When introduced to mice, BDNF Met/Met male animals show reduced BDNF expression and elevated anxiety behaviors in the open field test and the elevated plus maze (Chen et al., 2006). To our surprise, BDNF Val/Met (heterozygous) animals raised in normal conditions showed sex-specific regulation on the expression level of *BDNF* in the frontal cortex (Figure 5.11B). *BDNF* mRNA was reduced in Val/Met females (compared to Val/Val females), but increased in Val/Met males (compared to Val/Val males).

Given the similarity of *BDNF* expression pattern to FC animals, we wanted to test whether BDNF Val/Met animals mimic the sex-specific pattern of anxiety behaviors. Val/Met females showed significantly less center-during in the open field (OF) test (F-V/V 1.000 ± 0.06823, F-V/M 0.6957 ± 0.05672, p= 0.0030, Figure 5.11C, E), and significantly lower preference for the open arm in the elevated plus maze (EPM) test (F-V/V 1.000 ± 0.06116, F-V/M 0.7653 ± 0.08790, p=0.0020, Figures 5.11F, G), in comparison with Val/Val females. However, no significant differences were observed in Val/Met males when compared with Val/Val males (OF: M-V/V 1.000 ± 0.2254, M-V/M 1.248 ± 0.2273, p=0.5029; EPM: M-V/V 1.000 ± 0.1189, M-V/M 1.016 ± 0.1353, p=0.9320, Figures 5.11E, G). Our results on BDNF Val/Met male were consistent with the previously published study in male mice(Chen et al., 2006). No significant change in locomotion was detected in female or male BDNF Val/Met animals after FC (Figures 5.11D).

Taken together, our data suggested that the differences in anxiety-like behavior in females and males might be caused by differential expression of *BDNF* after FC.

Differential modulation of PV inhibition in female and male mPFC after Enriched Environment

To test whether sex differences in PV inhibition we observed was specific to sex (female only) or experience (adversity only), we decided to adapt the model of enriched environment (EE) to expose male and female animals to "positive" experiences. EE using Marlau cage(Fares et al., 2013) has been shown in multiple studies to have profound beneficial effects (see review (Nithianantharajah and Hannan, 2006)), including promoting BDNF expression (Fares et al., 2013) and the maturation of PV+ neurons (Greifzu et al., 2014) . However, whether PV inhibition in the mPFC will be differentially modulated in males and females after EE remains unknown.

Here, we confirmed that EE significantly increased the PV+ cell density and intensity in L5 of the mPFC in male animals (PV density: CTL 134.5 ± 8.549/mm^2, EE 186.6 ± 10.01/mm^2, p=0.0027; PV intensity: CTL 0.8197 ± 0.04665 A.U., EE 1.267 ± 0.03969 A.U., p<0.0001, Figures 5.12C, D). To our surprise, there was no significant difference between control and EE females (Figures 5.12A, B). Consistent with the anatomical data, we observed a significant increase in mIPSC frequency in mPFC L5 pyramidal neurons only in males (M-CTL, 0.9211 ± 0.1431 Hz, M-EE, 1.654 ± 0.1590 Hz, p=0.0011, Figures 5.12 G, H), but not in females (F-CTL 1.219 ± 0.1281, F-EE 1.131 ± 0.1307, p=0.6333, Figures 5.12 E, F), suggesting that mPFC PV inhibition was affected by EE in a sex-dependent manner.

Figure 5.12. Increased PV inhibition in male mPFC after enriched environment

(A) Example images of PV staining in the mPFC of CTL and EE female C57s. L1-5: layer 1 – layer 5 of mPFC. Scale bar: 100 μm (B) Density of PV+ cells and average intensity of PV staining in L5 mPFC of female C57 EE animals compared with C57 CTL animals.

(C) Example images of PV staining in the mPFC of CTL and EE male C57s. Scale bar: 100 μm (D) Density of PV+ cells and average intensity of PV staining in L5 mPFC of male animals. Average PV intensity was normalized to the average of CTL female animals. N=3 animals for each group in (A-D).

(E) Example mIPSC traces from EE females. Scale bar: 1 sec, 20pA. (F) Frequency, amplitude, rise time and decay time of mIPSCs comparing female CTL and EE animals.

(G) Example mIPSC traces from EE males. Scale bar: 1 sec, 20pA. (F) Frequency, amplitude, rise time and decay time of mIPSCs comparing male CTL and EE animals. Female CTL n=33 cells from 3 animals, female EE n=36 cells from 3 animals; male CTL n=32 cells from 3 animals, male EE n=33 cells from 2 animals. Error bars represent SEM. 2-tailed t-test, **$p<0.01$, ****$p<0.0001$. $p>0.05$ if not indicated.

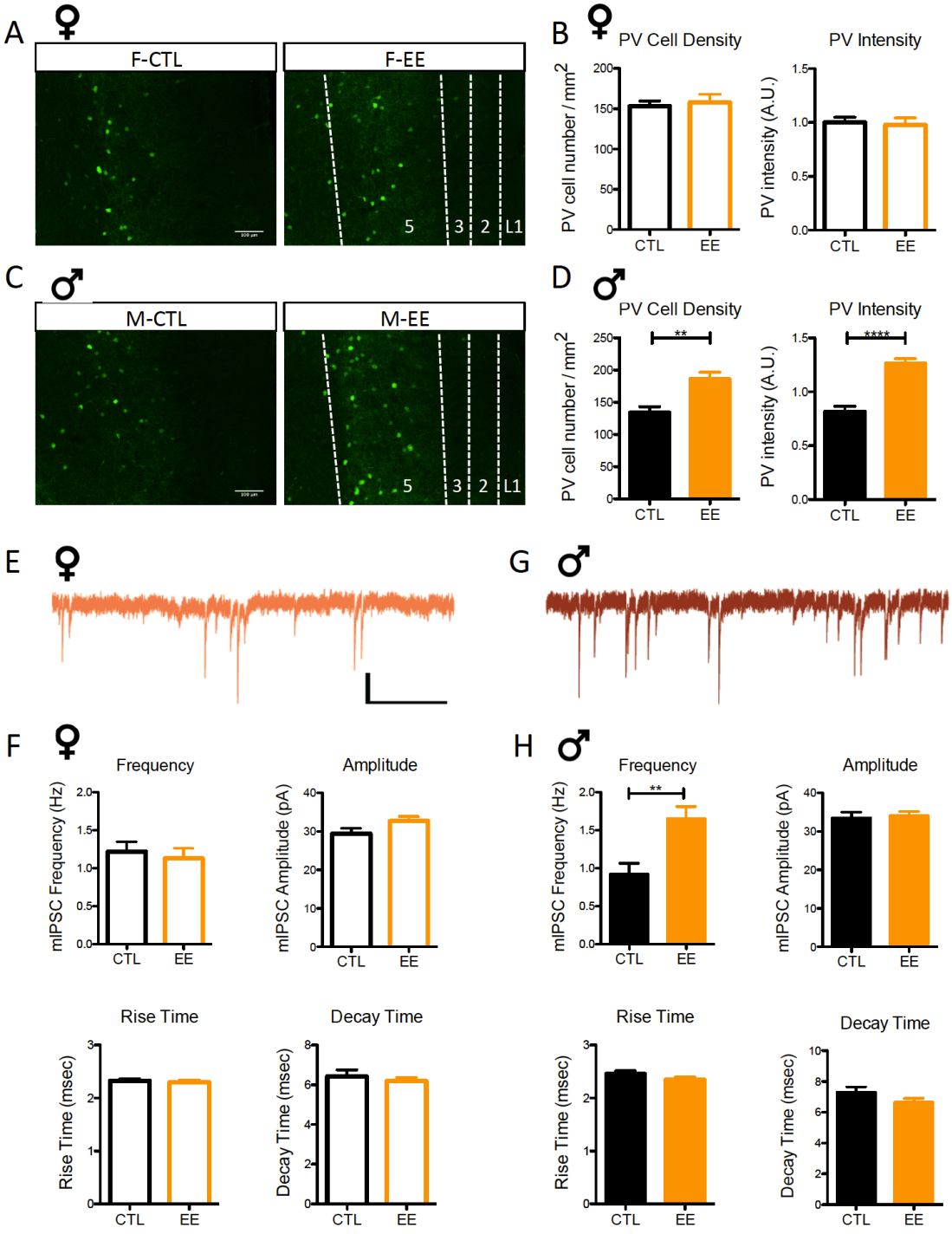

Figure 5.12 (Continued)

Taken together, our results indicat that there exist profound sex-dependent effects by early life experiences in mPFC PV inhibition.

Discussion

In this study, we established models for studying the impact of ELS in both C57BL/6J lab mice and monogamous, biparental wild mice POs. Based on anatomical and physiological results, we discovered sex-specific effects of disrupted parental care on PV+ interneurons in the mPFC, and their potential involvement in regulating anxiety behaviors in females. We also provided a potential mechanism, differential expression of *BDNF*, to explain the sex differences after ELS.

Why are females more affected in anxiety behaviors after ELS? Pups receiving more licking/grooming during the first postnatal week are less stressed and show increased expression of BDNF in the hippocampus (Liu et al., 2000; Liu et al., 1997; Weaver et al., 2004). Therefore, one possibility is biased caregiving (pup-licking) towards male offsprings in mice (Moore, 1995; Moore and Morelli, 1979). It is possible that such bias will be increased when parental care is limited, e.g., in ELS models. Ethologically, the fitness of males is crucial for reproduction in polygamous animals. To test this hypothesis, one would need to perform analysis conditioning on the amount/quality of care individual pup received during early life. However, it is unlikely that sex-specific effects of ELS were caused by differences in maternal care female and male pups received. The sex differences in anogenital licking-grooming (Moore, 1995) appear only toward the second postnatal week (Meaney, 2001), which is later than our FC window during P2-P9. Before P7, the differences in licking/grooming received between

male and female pups were still debatable (Champagne et al., 2003; Kosten and Nielsen, 2014). Furthermore, female mice reared by low pup-licking mothers exhibited anxiety-like behaviors, but not males (Pedersen et al., 2011). Indeed, our results on BDNF Val/Met animals (Figure 5.11) also suggested intrinsic differences between females and males that could lead to differential regulation of gene expression hence behaviors.

We did not rule out that males were not susceptible at all to ELS. We have been focusing our study on internalized behaviors only. But human studies also showed that men had a higher risk for attention deficit hyperactivity disorder (ADHD), substance abuse, autism and schizophrenia (see review (Cover et al., 2014)). We found that *BDNF* expression was increased in males after ELS (Figure 5.11). Overexpression of *BDNF* is known to accelerate the maturation of inhibition and thus cause precocious critical period plasticity (Huang et al., 1999) for ocular dominance in the primary visual cortex. The effects of BDNF could influence beyond visual cortex, implicating mistiming of plasticity during the cascade of critical periods (Hensch, 2005). In fact, overexpression of *BDNF* in BDNF transgenic animals has been linked to abnormal working memory and cognitive functions (Cunha et al., 2009; Papaleo et al., 2011). FC males showed pre-maturation of hippocampal PV+ neurons (Bath et al., 2016). And we also observed increased inhibition onto Type B L5 pyramidal neurons in the male FC mPFC (Figure 5.9). Therefore, it is possible that other aspects males' behaviors, e.g., externalized behaviors, could be altered by FC. Here, we did not found changes in anxiety behaviors in males after ELS, suggesting different brain circuits or etiology between internalized and externalized disorders.

It has been shown that BDNF Met/Met male animals exhibited similar anxiety-like behavior as heterozygous BDNF +/- animals (Chen et al., 2006). Our results on FC females and BDNF Val/Met females further strengthened the hypothesis that decreased *BDNF* level would increase anxiety level in both females and males. According to our findings, BDNF could also serve as a biomarker for anxiety behaviors after ELS. Besides, human studies indicate a strong interaction between stressful life events and BDNF Val/Met polymorphism (Hosang et al., 2014). BDNF Met allele was statistically linked with resilient phenotype to the childhood adversity and adolescence anxiety (Chen et al., 2015; Cruz-Fuentes et al., 2014). However, how BDNF polymorphism modulates the sensitive to ELS is yet to be studied.

The mPFC in mice plays an important role in regulating anxiety behaviors (Calhoon and Tye, 2015; Riga et al., 2014). In humans, Amygdala-mPFC anatomy is linked to negative affect (Holmes et al., 2012). Optogenetic study in mice showed that mPFC-Amygdala projections are involved in anxiety-related behavior (Vialou et al., 2014). At the meantime, our data suggested that inhibition onto Type A pyramidal neurons, which send subcortical projections, was particularly affected in females after ELS (Figures 5.6, 5.7). Type A pyramidal neurons also express Dopamine receptor D2 (D2R) (Gee et al., 2012). And photostimulation of DA projection from ventral tegmental area (VTA) to the mPFC evokes anxiety-like behavior (Gunaydin et al., 2014). However, it has not been directly tested how prefrontal PV inhibition modulated mPFC-Amygdala or mPFC-VTA connection.

We found that in male ELS mPFC, inhibition onto callosal projection Type B neurons was increased. Autistic model BTBR mice, which show repetitive behaviors

such as increased marble burying (McFarlane et al., 2008), are known to have no corpus callosum (Kim et al., 2016; Wahlsten et al., 2003). The axonal targets of callosal projection pyramidal neurons include contralateral cortex and striatum (Molyneaux et al., 2007). Human and animal studies suggest compulsive repetitive behaviors may arise from abnormalities in corticostriatal circuits (Burguiere et al., 2015). For example, optogenetic stimulation of axon terminals from lateral orbitofrontal cortex to striatum alleviates compulsive grooming behaviors in animals with SAPAP3 deletion (Burguiere et al., 2013). Social deficits are one of the characteristic symptoms in autistic spectrum disorders in humans. Abnormal social behaviors in autistic model Shank3B-/- mice are coupled with striatal dysfunction. And Shank3 is highly expressed in striatum (Peca et al., 2011). 5-HT hypofunction is associated with aggression in humans (reviewed by (Seo et al., 2008)). Aggressive behaviors in rats are associated with increased DA in nucleus accumbens, and decreased 5-HT in the mPFC (van Erp and Miczek, 2000). 5-HT selectively excites (or biphasically inhibits-excites) callosal projection neurons in L5 of the mPFC (Avesar and Gulledge, 2012). It is possible that decreased activity of Type B neurons, due to increased inhibition, may result in aggressive behaviors in ELS males.

Adult re-introduction of Shank3 rescues social interaction deficit and repetitive grooming behavior in Shank3B-/- animals, but not anxiety (Mei et al., 2016). This suggests that anxiety behavior is probably not directly mediated by corticostriatal circuits, but rather subcortical circuits. The failure to correct anxiety behavior in adult Shank3-/- animals also proposes a potential critical period for correcting anxiety. Indeed, previous work from our lab has identity a critical period in early adolescence (P15-P25) in mice for acoustic preference, which is mediated by anxiolytic effects of music (Yang et al.,

2012). Recent study showed that this critical period could be affected by factors that altered the maturation of PV+ interneurons in the mPFC, such as Otx2 (Chapter 6). It will be of great interest to study how this critical period is changed in ELS females, and when will be a potential intervention time window to correct anxiety behaviors in ELS females.

Lastly, this study revealed profound sex differences in PV inhibition in the mouse mPFC. Our results also confirmed that PV+ interneurons could be affected in commonly existing polymorphisms (BDNF Val/Met, Figure 5.11); and they were sensitive to environmental impacts, both positive (EE, Figure 5.12) and negative (ELS, Figures 5.1-10). But the direction and magnitude of change were experience- and sex-dependent. Nevertheless, our results pointed out mPFC PV+ interneuron as the key to the gene-sex-environment interactions in psychiatric disorders.

Chapter 6

Parvalbumin Interneurons Regulate Critical Period Plasticity in the Mouse Medial Prefrontal Cortex

Author contribution

Zhanlei Ye, Henry Hing Cheong Lee, Clémence Bernard, Takao K Hensch

Z.Y. performed developmental study in C57 animals, and critical period mappings. H.H.L. performed c-fos staining, ABR and EEG recording. C.B. generated Otx2AA mouse, and performed immunohistochemistry in Otx2AA study. T.K.H supervised the project.

Summary

The maturation of parvalbumin (PV)+ interneurons is pivotal in controlling the onset of critical period plasticity in primary sensory cortices. Whether PV+ neurons are essential for similar processes in the prefrontal cortex (PFC) remains untested. Our lab has previously mapped a critical period for acoustic preference in mice, which involves the medial PFC (mPFC). Here, we mapped the development of PV+ neurons in the mouse mPFC, which matches the critical period window for acoustic preference. In a mouse model that the binding of Otx2 homeoprotein and perineuronal net (PNN) was affected by a genetic point mutation, we found that critical period plasticity across brain regions was altered similarly. We also found that disrupting PV-PV inhibition resulted in enhanced gamma oscillation and adult plasticity in the mPFC, which can be suppressed

by a metabotropic glutamate receptor (mGluR) type 2/3 agonist. Taken together, our data show that PV+ interneurons play a key role in controlling critical period plasticity in the mouse mPFC, which might be regulated via similar mechanisms as primary sensory cortices. Our findings can provide insights into potential interventions for early life stress (ELS).

Introduction

During postnatal brain development, distinct critical periods (CPs) across different modalities must be well orchestrated. For example, CPs for sensory processing typically arise before more complex, highly integrated cognitive functions (Hensch, 2005). Our lab has previously identified a CP window for the formation of acoustic preference in mice (Yang et al., 2012). Between postnatal day (P) 15 to P25 (but not in adults), passive exposure to music can shift mice's innate bias for silent to music (Yang et al., 2012). The medial prefrontal cortex (mPFC) was indicated to be important for music preference (Yang et al., 2012). Interestingly, Parvalbumin (PV) + cells emerge in cortical regions just ahead of their respective CP onset (Le Magueresse and Monyer, 2013). However, whether PV+ neurons are essential for CP onset in the mPFC remains untested.

Our lab has previously shown that the non-cell autonomous Otx2 homeoprotein is essential for PV+ cell maturation in primary visual cortex (V1) and consequently responsible for regulating CP timing for ocular dominance plasticity therein (Beurdeley et al., 2012; Sugiyama et al., 2008). While Otx2 protein has also been found in other cortical regions (Spatazza et al., 2013), a similar developmental role for Otx2 in other

modalities beyond V1 remains unknown. Indeed, an *Otx2* polymorphism has been related to bipolar disorder (Sabunciyan et al., 2007), suggesting that a more global role for Otx2 is likely. Here, we directly address this question by genetic disruption of a pivotal aspect of postnatal Otx2 signaling.

Plasticity in V1 is controlled by the experience-dependent transfer of Otx2 produced outside the cortex (Beurdeley et al., 2012; Sugiyama et al., 2008). Binding to the perineuronal net (PNN) – an extracellular matrix structure enriched in glycosaminoglycans (GAG) that tightly enwrap PV+ cells as they mature – is a crucial step (Bernard and Prochiantz, 2016; Beurdeley et al., 2012; Miyata et al., 2012; Pizzorusso et al., 2002). Thus, cortical infusion of exogenous Otx2 protein just after eye opening (but before normal CP onset) accelerates PV+ cell maturation in V1 and prematurely triggers plasticity in mice, while CP onset is delayed by extracellular blockade of Otx2 protein (Sugiyama et al., 2008). Conversely, PNN removal or reducing Otx2 levels in adulthood reopens a new window of plasticity (Beurdeley et al., 2012; Pizzorusso et al., 2002; Spatazza et al., 2013). Of therapeutic relevance (Hubel and Wiesel, 1970; Sanke, 1988), the latter manipulations successfully restore vision to amblyopic mice (Beurdeley et al., 2012; Spatazza et al., 2013).

Our lab previously identified a short arginine-rich sugar-binding motif within Otx2 that interacts specifically with disulfated chondroitin sulfate GAG side chains in the PNN (Beurdeley et al., 2012). Here, we constructed a knock-in mouse bearing point mutations in this motif. This allowed us first to determine whether the short peptide sequence is intrinsically needed for PNN-mediated PV+ cell-specific Otx2 localization. Second, we could then test whether this Otx2 mutation would have a global impact

beyond the visual system by analyzing its effect across modalities. Indeed, we found altered PV+ cell maturation and delayed CP timing not only for amblyopic effects in V1 (paper accepted), but also for tonotopic map plasticity and acoustic preference behavior in primary auditory (A1) and the medial prefrontal cortex (mPFC), respectively. Our mouse model thus reveals a global role for Otx2 in regulating CP timing throughout the cortex and confirms the importance of GAG binding in localizing non-cell autonomous Otx2 to PV+ cells.

Previously in Chapter 5, we have shown that early life stress (ELS) impairs PV network and reduces the expression of $GABA_A$ receptors α1 in the female mPFC. It has been established that α1 subunit controls the onset of critical period plasticity during normal development (Fagiolini et al., 2004). Importantly, PV+ cells are critical circuit component generating oscillatory activities at gamma range (30-80Hz) (Cardin et al., 2009; Sohal et al., 2009), a phenomenon associated with memory, learning and plasticity (Lisman, 2010; Traub et al., 1998; Yamamoto et al., 2014). Here, using a genetic approach to specifically delete α1 subunit the from PV+ cells (PV-α1 KO), we found that changing PV-PV inhibition alone leads to enhanced gamma power and CP plasticity in adults. The changes in PV-α1 KO animals could be reversed by metabotropic glutamate receptor type 2/3 (mGluR 2/3) agonist LY379268, indicating a potential therapeutic target for psychiatric disorders and ELS.

Results

Development of PV+ neurons in the mPFC matches the critical period for acoustic preference

To test whether PV+ neurons are involved in CP in the mPFC, we first decided to map the development of PV+ interneurons in the mouse mPFC using PV staining as an approximation for PV inhibition. We performed immunostaining of PV on brain samples collected from P14, P21, P28, P35, P45, and P70 female and male C57BL6/J animals. The mPFC is believed to have a late development (Flechsig Of Leipsic, 1901; Giedd and Rapoport, 2010) given its involvement in higher cognitive functions. Here, we found that PV signal was barely detectable in P14 samples (Figures 6.1A, B). There was a fast increase in the density of PV+ neurons between P14 and P21, the latter of which is the weaning age of lab mice (Figures 6.1A-C), in both females and males. The density of PV+ neurons reached a plateau at P35 (Figure 6.1C), and the average PV intensity peaked around P35-P45 (Figure 6.1D). The maturation time course of PV+ neurons in the mPFC matches the CP for acoustic preference (P15-P25) (Yang et al., 2012), suggesting that PV+ neurons may play a role in controlling the onset of CP in the mPFC, similar to primary sensory cortices.

Comparing age-matched females and males, we found that females in generals had a significantly higher density of PV+ neurons (2-way ANOVA, $p<0.0001$, Figure 6.1C) and greater PV intensity (2-way ANOVA, $p<0.0001$, Figure 6.1D). Interestingly, there was also a significant interaction between sex and age in PV intensity (Figure 6.1D). Females showed a significant peak in PV intensity at P35. But in males, the average PV intensity was higher in P45, suggesting delayed PV maturation mPFC in males (Figure 6.1D).

Figure 6.1. Developmental trajectories of mPFC PV+ neurons in female and male C57BL/6J mice

(A) Example images of PV staining in the mPFC of female C57 animals at various ages. Scale bar: 100 μm (B) Example images of PV staining in the mPFC of male C57 animals at various ages. Scale bar: 100 μm. (C) Density of PV+ cells and (D) Average intensity of PV staining in L5 mPFC of female and male C57 mice across ages. N=3 animals for each group. Average PV intensity was normalized to the average of P70 female animals. Error bars represent SEM. 2-way ANOVA, followed by Bonferroni multiple comparisons in (C-F). * $p<0.05$, *** $p<0.001$. No statistical differences were detected if not indicated.

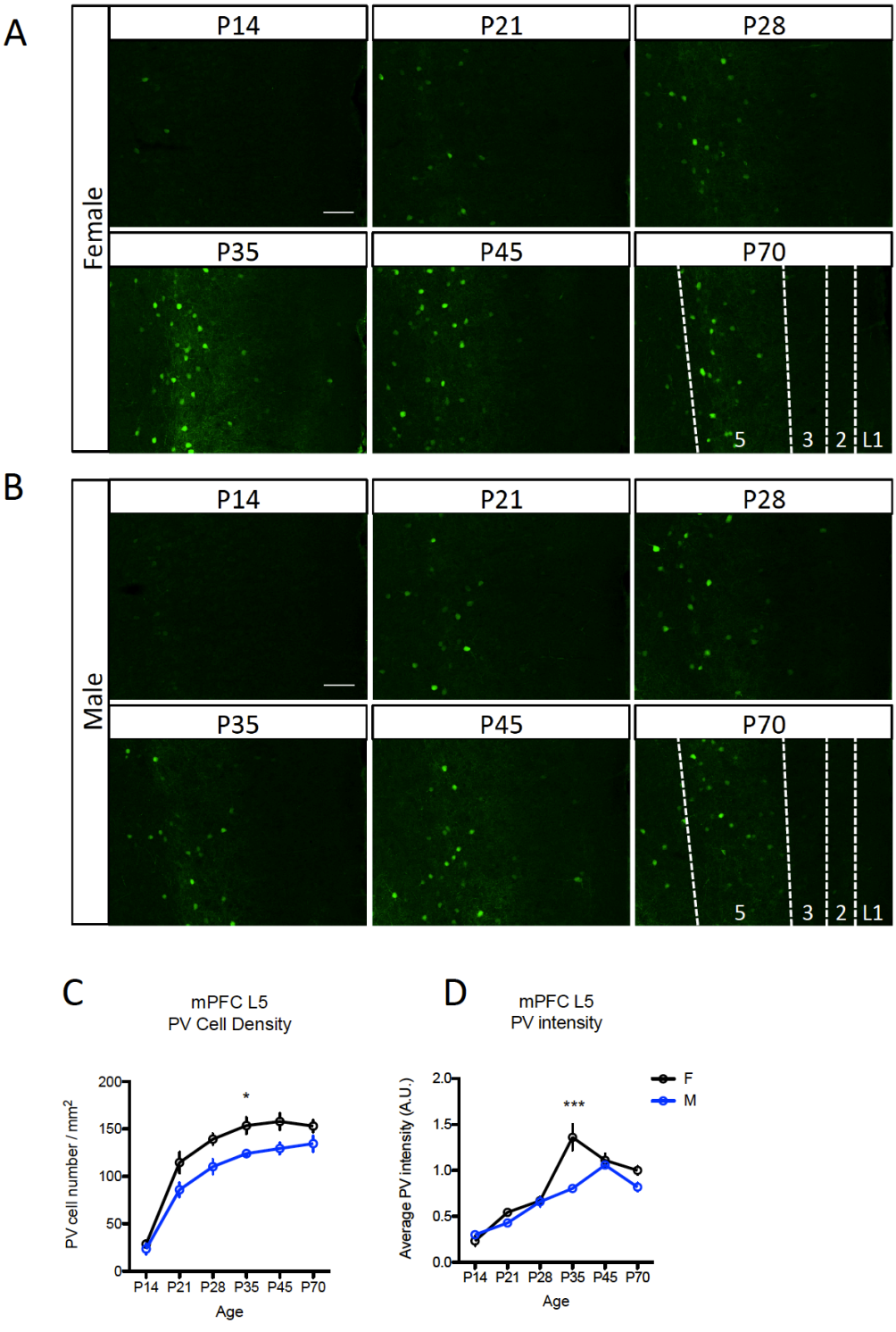

Figure 6.1 (Continued)

Genetic Otx2 mis-localization delays critical period plasticity across brain regions

Delayed auditory plasticity in Otx2$^{+/AA}$ mouse A1 and mPFC

An arginine-rich GAG-binding motif spans the junction between the N-terminal and homeodomain in Otx2 (Figure 6.2A). This motif can be weakened through an R36A and K37A double mutation (RK to AA) that reduces affinity for GAGs (Beurdeley et al., 2012), which led us to construct an Otx2-AA knock-in mouse line (both heterozygous *Otx2*$^{+/AA}$ and homozygous *Otx2*$^{AA/AA}$ mice) (Bernard et al., 2014). Previous study from our lab had revealed a gene dosage-dependent impairment of retinal structure (Bernard et al., 2014), as confirmed here by loss of visual acuity only in the Otx2-AA homozygous mutants. We, therefore, focused on the Otx2-AA heterozygous animals.

Lee et al. found that in V1, Otx2 failed to accumulate dramatically in PNN-bearing cells (positive for WFA, *Wisteria Floribunda Agglutinin* staining), during juvenile development up to P100, but instead significantly increased accumulation of Otx2 protein in non-PNN-bearing cells (negative for WFA) of *Otx2*$^{+/AA}$ mice. *Otx2*$^{+/AA}$ mice showed normal baseline acuity but delayed visual plasticity (paper accepted).

We next examined whether Otx2 RK to AA mutation might also affect the timing of other CP events (Spatazza et al., 2013). In mice, optimal auditory processing involves thalamocortical refinement in the days following hearing onset. During a brief 3-day window starting from P12, passive tone-rearing can modify response strength and topography in A1(Barkat et al., 2011). Given the earlier emergence of PV+ cells in A1, it has been hypothesized that they also play a role in auditory CP plasticity (Takesian and Hensch, 2013). In fact, Otx2 accumulates in PV+ cells of A1 similar to V1 (Spatazza et al., 2013). Immunohistochemical analysis in *Otx2*$^{+/AA}$ mice also revealed a delayed PV+

Figure 6.2. Delayed auditory plasticity in *Otx2*$^{+/AA}$ mice

(A) A GAG-binding motif is found between the N-terminal (Nter) and the homeodomain of Otx2. The 'RK' doublet is mutated to 'AA' in the resulting AA mutant. (B) Representative images of Otx2, PV and WFA staining in primary auditory cortex (A1) layer 4 (L4) at P20 (scale bar: 100 μm). (C,D) Staining intensity of Otx2, PV and WFA (C, N=4-7 mice per group) and number of Otx2+ cells (D, N=5-8 mice per group) in A1 L4 at P20. (E) Illustration of thalamocortical brain slice preparation to study auditory plasticity (representative traces from a WT slice, scale bar: 100msec, 0.05ΔF/F). (F) Normalized (norm.) maximal ΔF/F across L4 loci in response to different ventral medial geniculate body (MGBv) stimulus sites for WT (N=13, $p<0.0001$ for stimulus location, 2-way ANOVA) and *Otx2*$^{+/AA}$ (N=18, $p=0.0986$ for stimulus location) mice exposed to a 7-kHz tone between P16-20. (G-H) Topographic slope calculated from location of maximal $\Delta F/F$ across L4 loci in response to different MGBv stimulus sites 1-6. (All values: mean ± SEM; t-test; *$p < 0.05$, **$p < 0.01$).

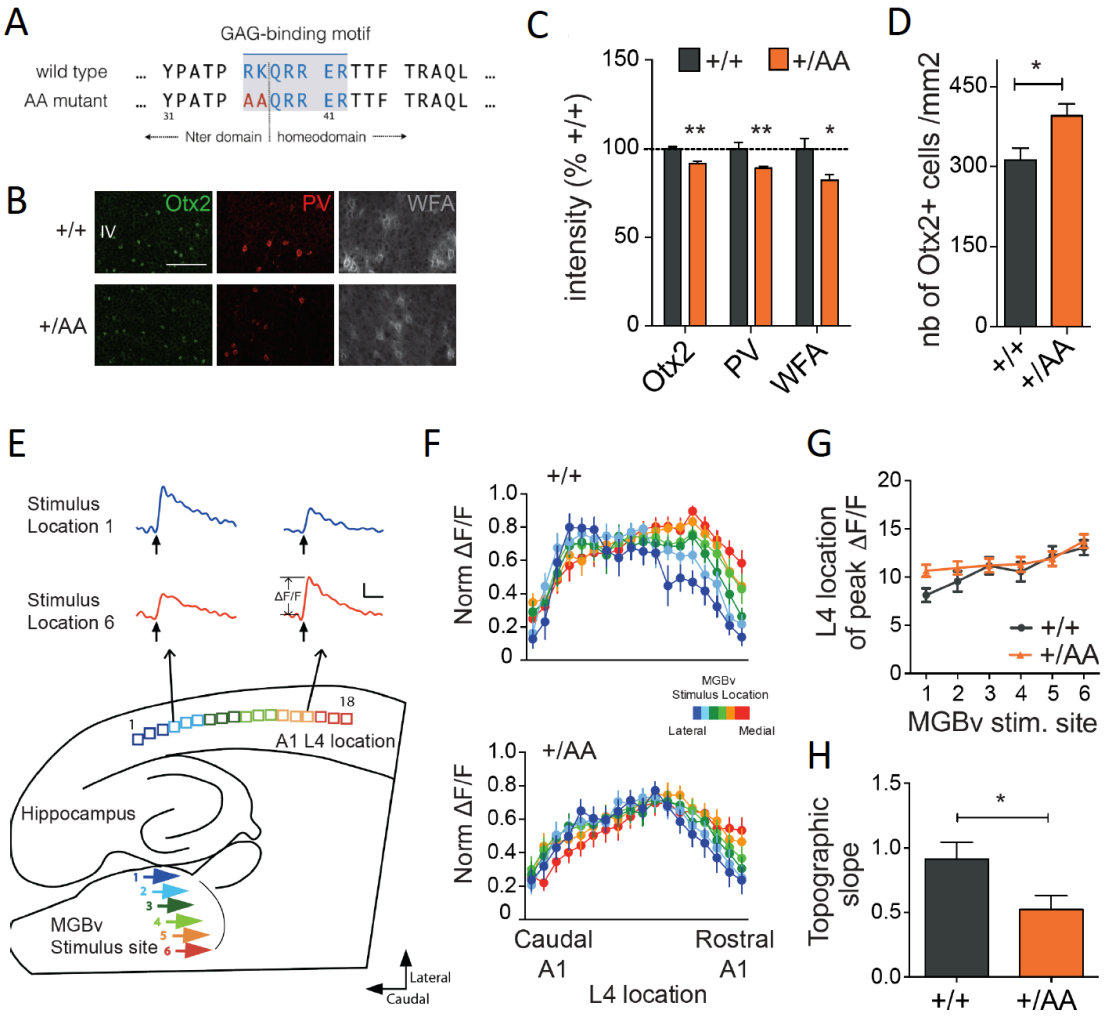

Figure 6.2 (Continued)

cell maturation and Otx2 protein mis-localization at P20 after the typical auditory CP (Figures 6.2B-D).

Since *Otx2*$^{+/AA}$ mice exhibited normal auditory thresholds as measured by auditory brainstem response (ABR; Figure 6.3), we pursued further functional analysis. Using voltage-sensitive dye imaging in an acute thalamocortical brain slice preparation (Barkat et al., 2011), we found that late passive tone-rearing from P16-20 altered the topography in A1 of *Otx2*$^{+/AA}$ mice, at an age when WT littermates were no longer plastic (Barkat et al., 2011) (Figures 6.2E-H). Thus, targeted accumulation of Otx2 in PV+ cells also plays a role in regulating CP timing in A1.

Sequentially after this basic tonotopic plasticity, exposure to more complex acoustic stimuli (such as music) can shape lasting preference behaviors in mice. During a ten-day window starting at P15 (but not in adulthood), the mouse's innate bias for silent shelter can be shifted in favor of music, revealing CP plasticity for this complex behavior (Yang et al., 2012). Neurons in the mPFC concurrently develop a biased responsiveness in favor of the acquired music preference (Yang et al., 2012). Immunohistochemistry again revealed a delayed PV+ cell maturation and broadly dispersed Otx2 protein in the mPFC of *Otx2*$^{+/AA}$ mice at P60 (Figures 6.4A-C), suggesting a potential delay in this higher cognitive CP.

Using a nesting paradigm requiring no training and free of confounding olfactory, visual or tactile cues (Figure 6.4D), we found that music exposure for two weeks at P60 successfully reversed the innate preference for silent shelter only in *Otx2*$^{+/AA}$ mice (Figure 6.4E). Changes in preference behavior are related to other limbic functions of the mPFC circuits (Garvert et al., 2015; Yang et al., 2012). Here too, we found the delayed

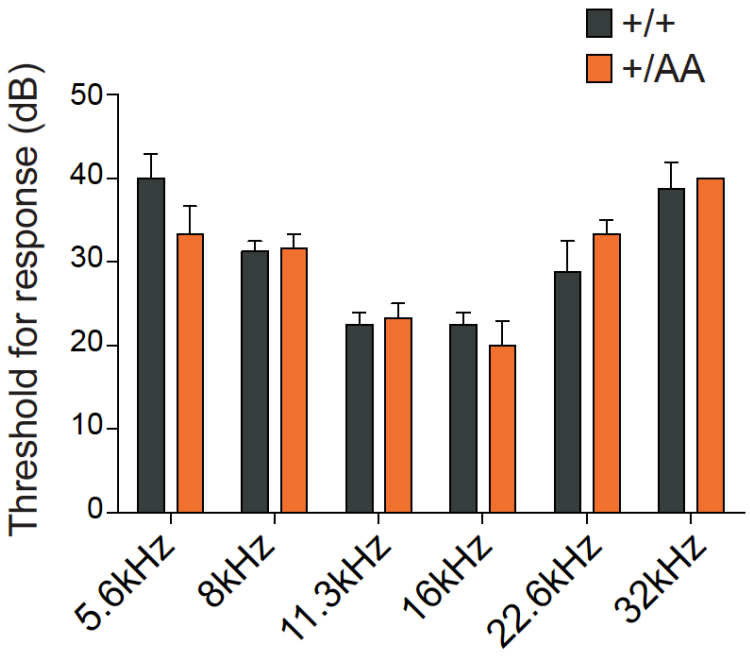

Figure 6.3. Normal auditory response in *Otx2*$^{+/AA}$ mice

Threshold for auditory brain stem response (ABR) across hearing frequency (N=4 per group). (All values: mean ± SEM, t-test; *p<0.05, **p < 0.01, ***p < 0.001).

Figure 6.4. Altered experience-dependent acoustic preference in adult *Otx2*$^{+/AA}$ mice

(A) Representative images of Otx2, PV and WFA immunostaining in the medial prefrontal cortex (mPFC) L5 at P60 (scale bar: 100 µm). (B, C) Staining intensity of Otx2 and PV (B, N=4 mice per group) and number of Otx2+ and WFA+ cells (C, N=4-5 mice per group) in L5 of the infra- and pre-limbic regions of mPFC at P60. (D) Typical traces of activity of a mouse inside the arena at the start (first 30 min) and at the end (last 30min of the 3h experiment) of the acoustic preference behavior assay. (E) Adult (P60) mice were passively exposed to music for 2 weeks and tested for acoustic preference. Cumulative frequency distribution of WT (N=7) and *Otx2*$^{+/AA}$ mice (N=16) before (initial) and after (post-music) two-week music exposure. (All values: mean ± SEM; t-test; *$p < 0.05$, ***$p < 0.001$).

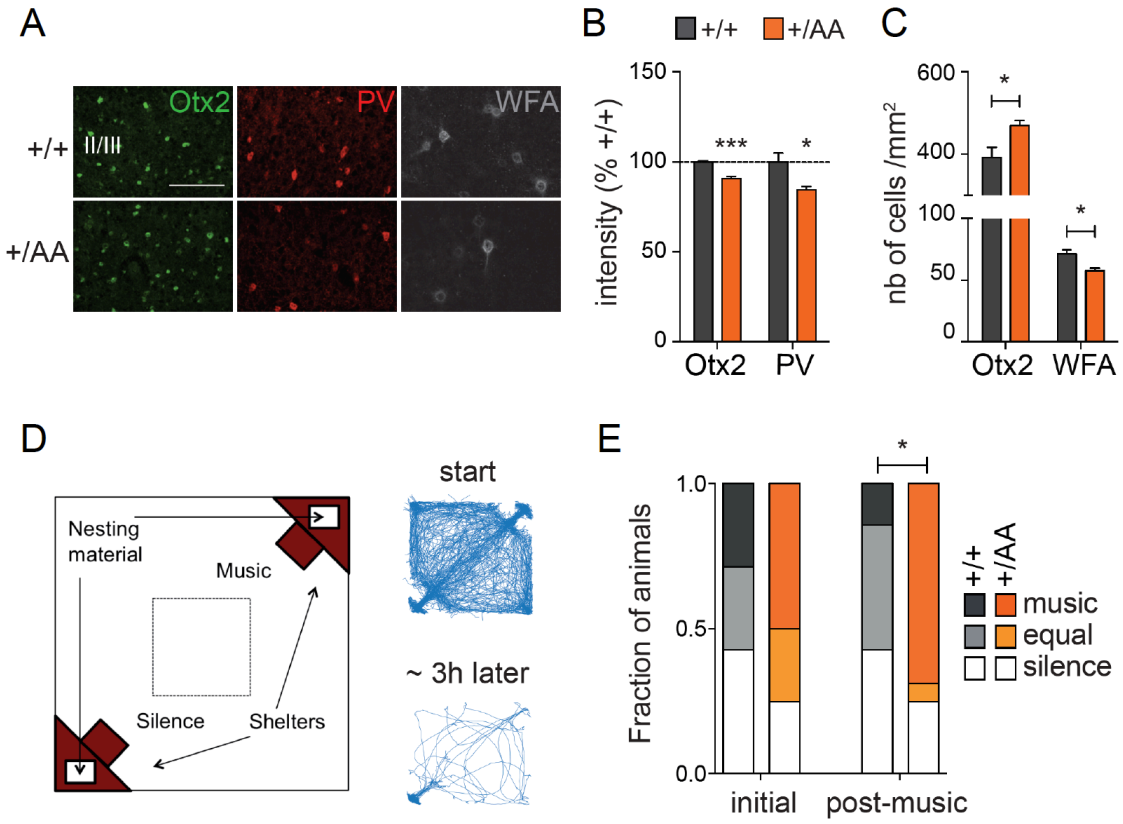

Figure 6.4 (Continued)

acquisition of a music preference in adulthood was linked to anxiolysis. The duration and number of center crossings during the first 30-minute exploratory phase in the open field were increased after music exposure (Figures 6.5A-C). The *Otx2*$^{+/AA}$ mice showed increased c-Fos activity in mPFC upon music exposure at P60 compared to WT mice (Figures 6.5D-F, Figure 6.6), which was seen only if the mice were exposed to music (Figures 6.7A-C). In addition, the percentage of Otx2+ cells co-stained with c-Fos was also increased in *Otx2*$^{+/AA}$ mice only after music exposure (Figure 6.5G, Figure 6.7D), suggesting mis-localization of Otx2 leads to activation of neuronal circuits beyond normal CP. Thus, the same *Otx2*$^{+/AA}$ mice carry a delayed CP plasticity across multiple brain regions.

BDNF Val/Met females show critical period plasticity in adult

Brain-derived neurotrophic factor (BDNF) is considered a common pathway to regulate CP plasticity in V1 (Hensch and Bilimoria, 2012). Previously in Chapter 5, we have shown that BDNF Val/Met females show reduced *BDNF* expression level, while BDNF Val/Met males show increased *BDNF* expression (Figure 5.11). The phenotype in BDNF Val/Met animals mimics the effects of early life stress (ELS), which impaired PV networks in females.

Using the same music preference paradigm, we found that music exposure for two weeks starting from P60 successfully reversed the innate preference for silence only in BDNF Val/Met female mice (Figures 6.8C-D), but not in BDNF Val/Val female mice (Figures 6.8A-B), or BDNF Val/Met male mice (Figures 6.8E-F). Our finding showed

Figure 6.5. Anxiolysis and recruitment of mPFC circuits following music exposure in *Otx2*$^{+/AA}$ mice

(A-C) Open field behavior in the first 30 minutes reflecting exploratory anxiety are compared before (Pre) and after (Post) two-week exposure of *Otx2*$^{+/AA}$ mice to music. Several parameters are compared: (A) duration of time spent at the center of the open field, (B) total distance traveled in the field, and (C) number of times crossing the center of the open field. All data are normalized to WT littermates conditions (N=17 mice per genotype).

(D-G) Immunofluorescence staining of Otx2 and c-Fos in the mPFC reveals circuit activation after 1h of music exposure. (D) Representative images of Otx2 and c-Fos staining in the mPFC at P60 (scale bar: 100 μm, cortical layers I-V are labeled). c-Fos signal intensity between genotypes is compared under several parameters: (E) cumulative frequency plot, (inset) mean intensity (arbitrary unit, a.u.), (F) percentage of high intensity c-Fos+ cells. (G) Percentage of Otx2+ cells co-localized with c-Fos staining (indicated by arrowheads in (D)) (N=5 mice per genotype) (All values: mean ± SEM; t-test in A-C and F-G, K-S test in E; *$p<0.05$, ***$p<0.001$).

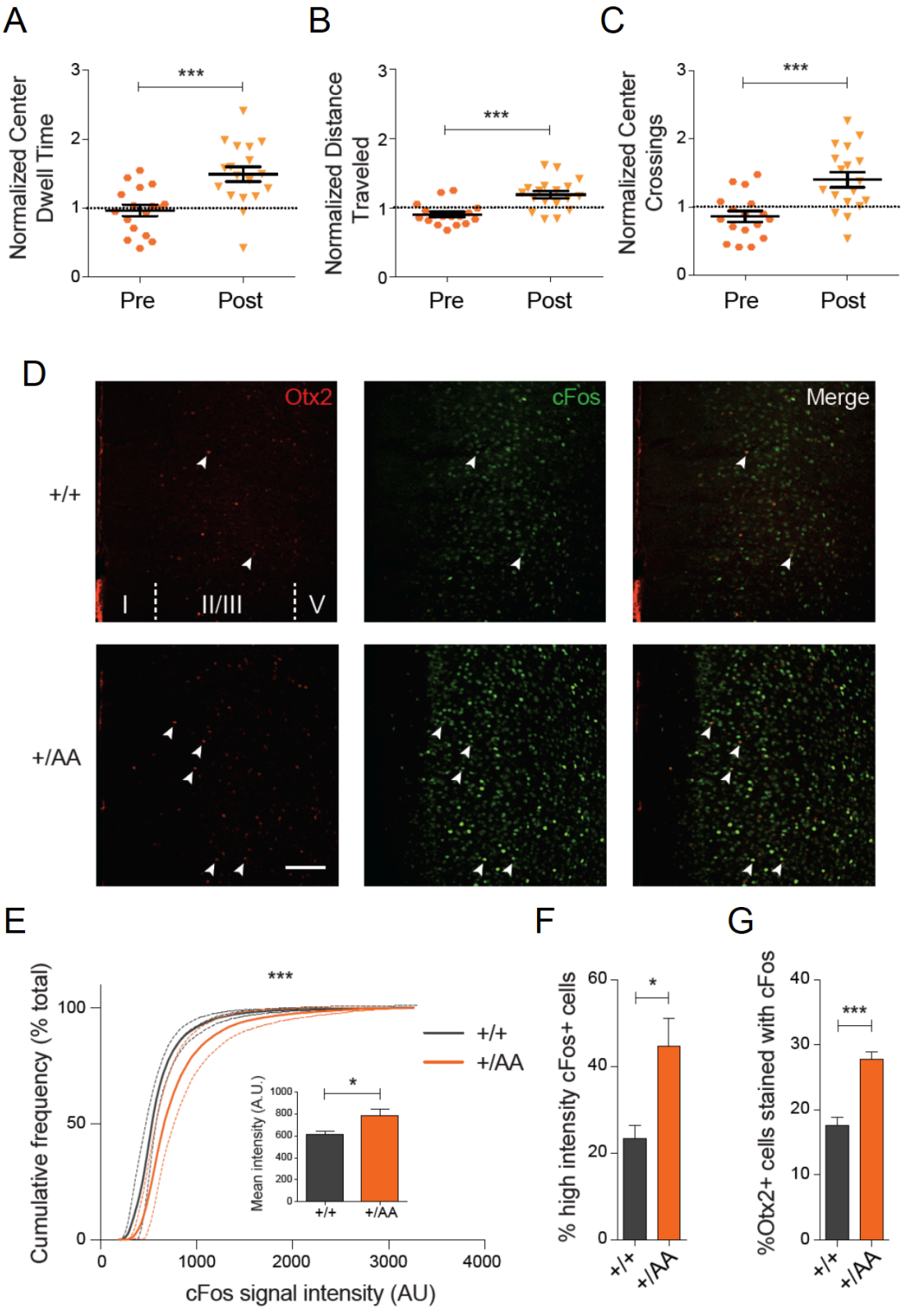

Figure 6.5 (Continued)

Figure 6.6. Quantification of c-Fos immunostaining in the mPFC after 1h music exposure, comparing WT and *Otx2*$^{+/AA}$ mice at P60

(A) Minimum and (B) Maximum c-Fos intensity (arbitrary unit, a.u.). (C) Total number of c-Fos+ cells. (E-F) c-Fos intensity value (a.u.) at (D) 25% percentile, (E) 75% percentile and (F) median of the cumulative frequency plot as shown in (E) (N=5 mice per group). (All values: mean±SEM, t-test; n.s.= not significant; *p<0.05).

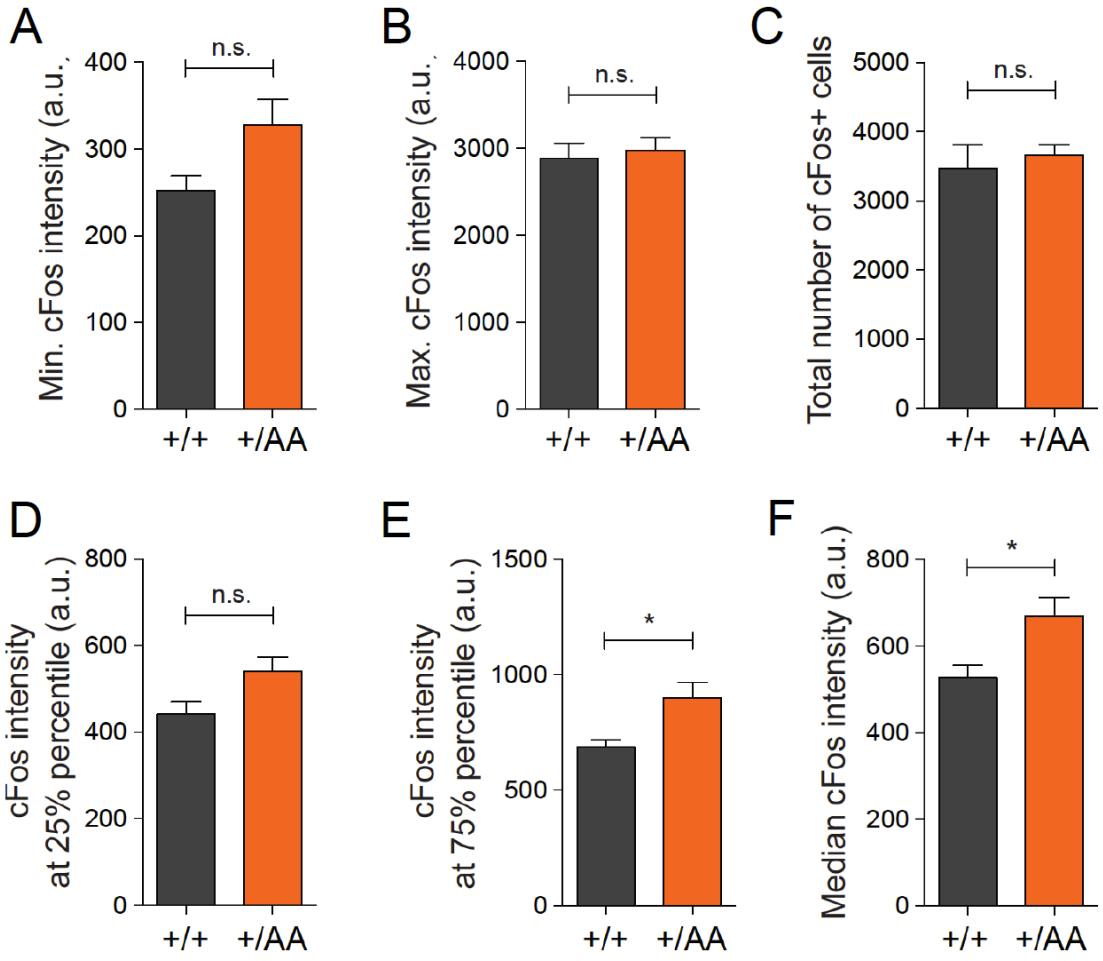

Figure 6.6 (Continued)

Figure 6.7. Immunofluorescence staining of Otx2 and c-Fos in the mPFC reveals circuit activation after 1h of music exposure compared to 'no music' control in *Otx2*$^{+/AA}$ mice

(A) Representative images of Otx2 and c-Fos staining in mPFC at P60 (scale bar: 100 μm, cortical layers I-V are labeled). c-Fos signal intensity between genotypes is compared under several parameters: (B) cumulative frequency plot, (inset) mean intensity (arbitrary unit, a.u.), (C) total number of c-Fos+ cells. (D) Percentage of Otx2+ cells co-localized with c-Fos staining (indicated by arrow heads in (A)) (N=2-3 mice per group) (All values: mean ± SEM; t-test in C-D, K-S test in B; *$p<0.05$, ***$p<0.001$).

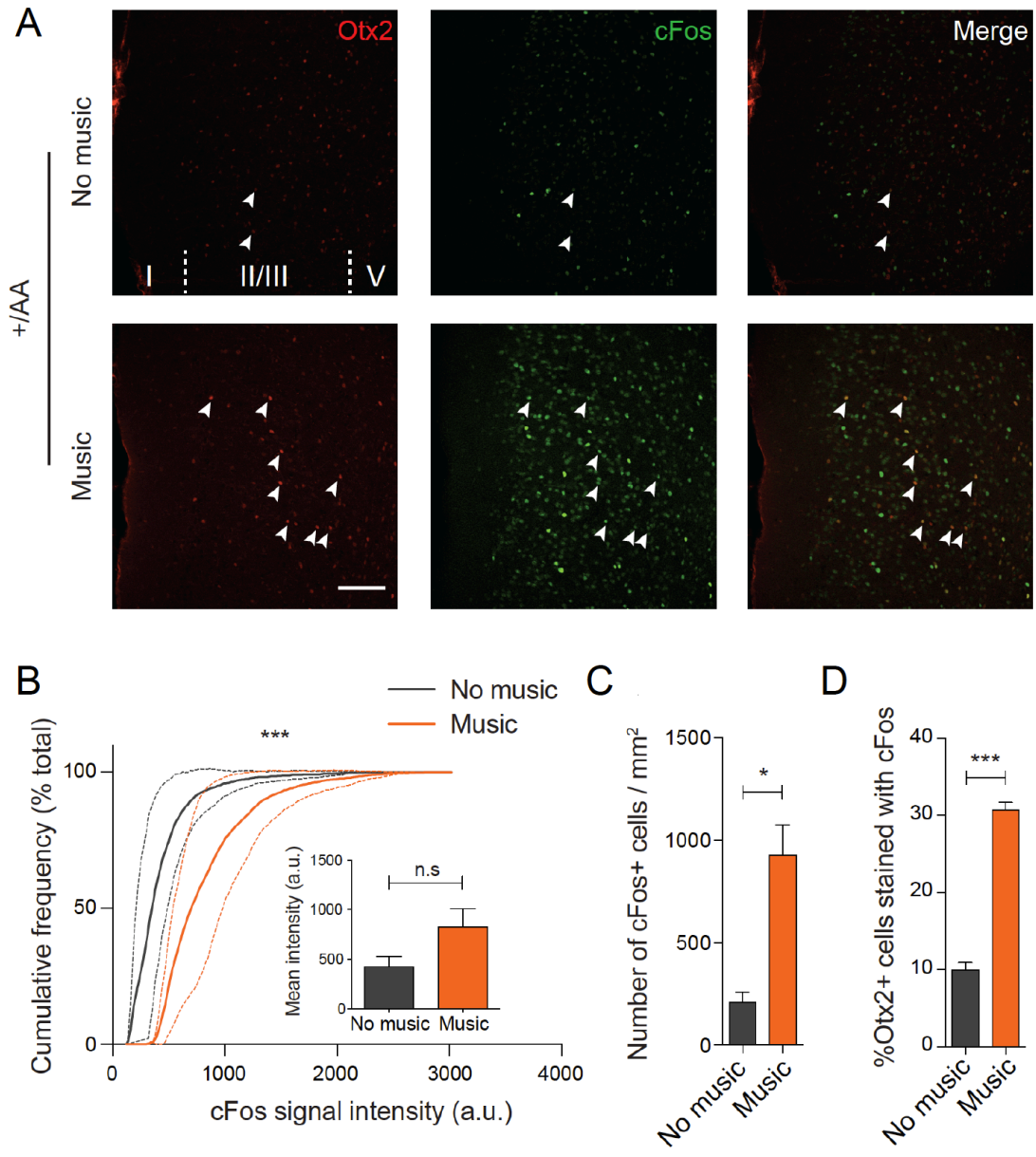

Figure 6.7 (Continued)

Figure 6.8. Altered experience-dependent acoustic preference in adult BDNF Val/Met female mice

(A,C,E) Representative traces showing the last 30min of motion activities inside the arena of (A) Female Val/Val, (C) Female Val/Met and (E) Male Val/Met animals. The location for silence and music chambers inside the arena are indicated.

(B,D,F) Cumulative distribution of music preference and comparison of pre- and post-music preference in (B) Female Val/Val, (D) Female Val/Met and (F) Male Val/Met animals. F-V/V n=8, F-V/M n=8, M V/M n=12. Log-rank test and paired t-test in (B,D,F). *$p<0.05$

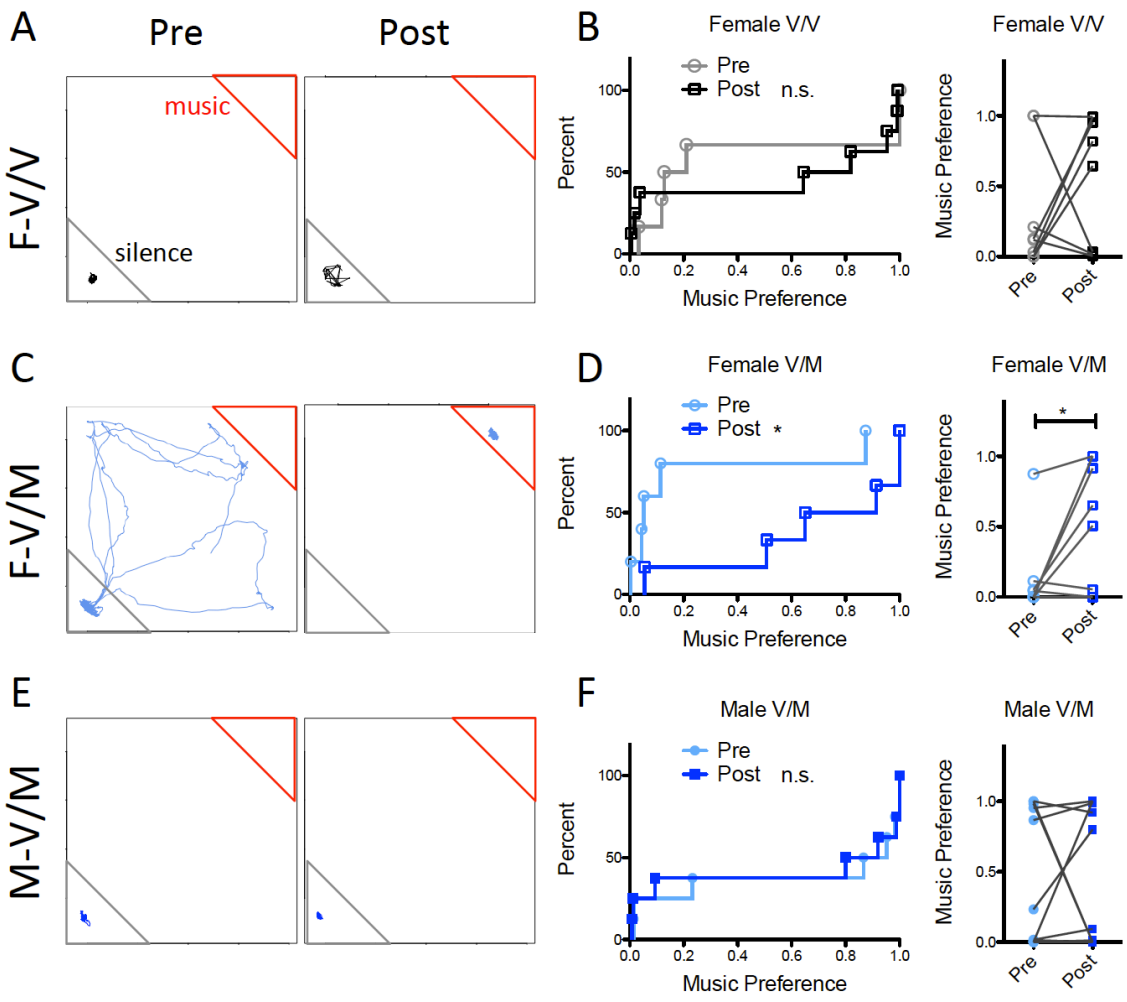

Figure 6.8 (Continued)

that reducing *BDNF* in adult resulted in plasticity for acoustic preference in the mPFC, suggesting that ELS female might also show similar plasticity in adulthood.

mGluR2/3 agonist LY379268 blocks adult cortical plasticity in PV-a1 knockout animals by suppressing gamma oscillation

Mature PV+ neurons mainly inhibit one another (Pfeffer et al., 2013). And α1 subunit-containing $GABA_A$ receptors are preferentially targeted by PV+ neurons (Freund and Katona, 2007; Klausberger et al., 2002). We wanted to test the function of PV-PV inhibition in critical period plasticity using a genetic approach to specifically delete α1 subunit the from PV+ cells (PV-α1 KO, Figure 6.9A).

PV+ cells are also known to generate oscillatory activities particularly in the gamma frequency range (30-80Hz)(Cardin et al., 2009; Wulff et al., 2009). Therefore, we used electroencephalogram (EEG) to record global oscillatory activities in awake, behaving mice. Strikingly, the power of gamma oscillations (30-80Hz) was selectively enhanced in PV-α1 KO mice across brain regions (Figures 6.9B, C). In WT mice, music exposure in adulthood did not alter this innate preference for the silence shelter (Figures 6.9F, G). However, a significant amount of PV-α1 KO mice preferred to reside in the music chamber after music exposure in adulthood (Figures 6.9F, G), suggesting an enhanced level of plasticity in the prefrontal region in PV-α1 KO mice.

We speculated that the enhanced gamma power in PV-α1 KO mice was due to an enhanced E/I balance in PV+ cells because their recurrent inhibition was selectively reduced (Figure 6.9A). We, therefore, attempted to rescue PV-α1 KO mice by reducing excitatory input onto PV cells. It has been previously shown that mGluR2/3 agonists

Figure 6.9. mGluR2/3 agonist LY379268 blocks adult cortical plasticity in PV-a1 knockout animals by suppressing gamma oscillation

(A) Working model of PING (pyramidal-interneuron gamma) mechanism showing an impaired inhibition onto PV+ cells (red) due to selective ablation of $GABA_AR$-α1 subunits in PV+ cells but not in pyramidal cells in PV-α1 KO mice. mGluR2/3 agonist LY379268 reduces excitatory input onto PV+ cells (grey). (B) Sample EEG traces of WT, KO and KO treated with LY379268 are shown (top). Scale bars=0.5V, 0.5s. Power spectra in gamma frequency range (30-80Hz) of these three conditions are shown (bottom). N=4WT, 7KO mice. Error bars=SEM. (C) Quantified gamma power compared to WT in three cortical regions: prefrontal cortex (PFC), somato-sensory cortex (SSC) and visual cortex (VC). Data=mean±SEM. N=4WT, 4KO mice in each brain region. (D), Quantification of gamma power in PV-α1 KO mice before (baseline) and after LY379268 treatment (N=7 KO mice).

(E) Experimental paradigm studying prefrontal cortex plasticity. (F) Representative traces showing the last 30min of motion activities inside the arena. The location for silence and music chambers inside the arena are indicated. (G) The preference for silence or music chamber in different experimental conditions is summarized. N=7WT, 9KO mice.

*p<0.05, **p<0.01, ***p<0.001, n.s.=not significant. Unpaired t-test in C; paired t-test in D. Chi-square test in G.

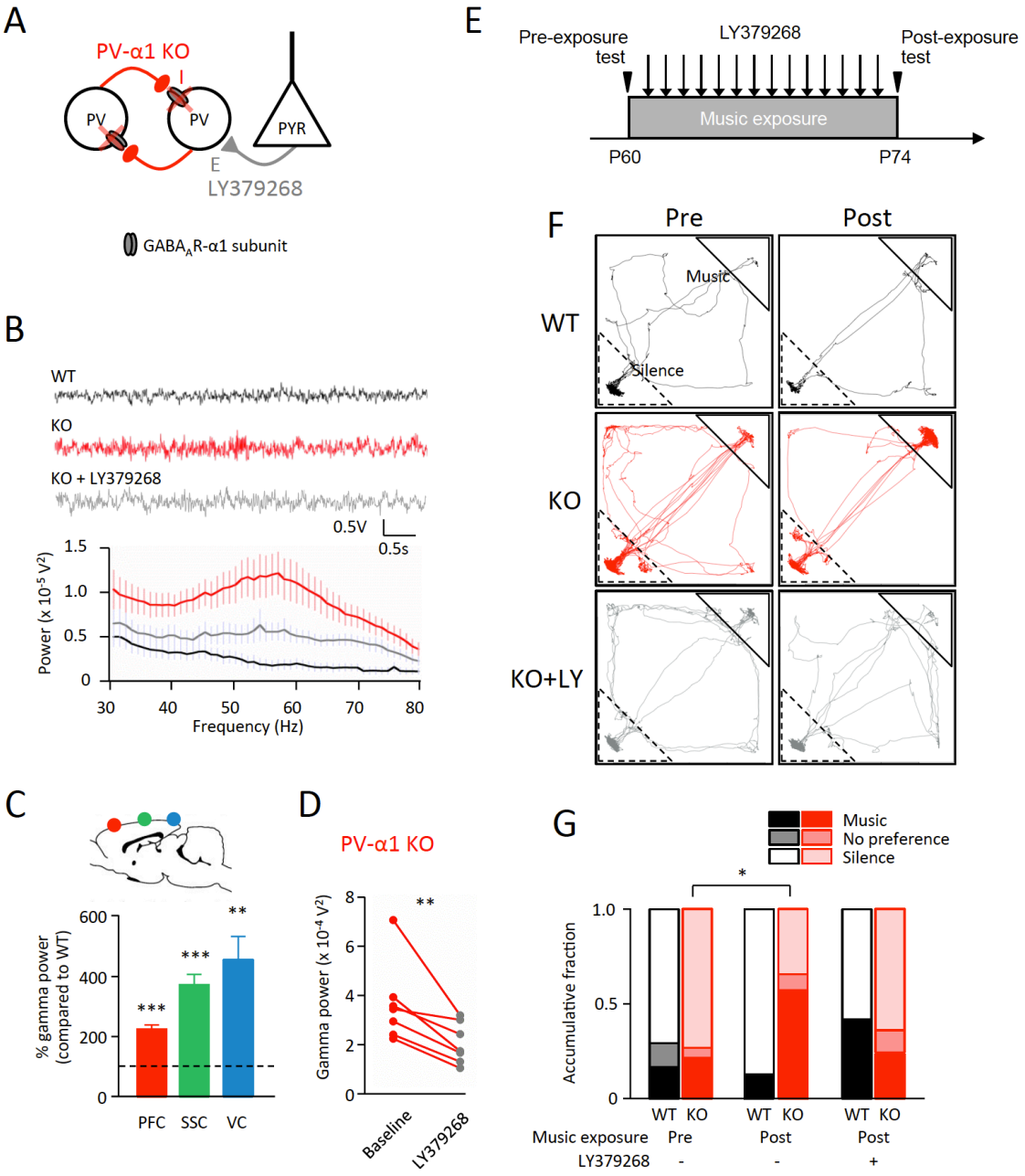

Figure 6.9 (Continued)

suppress cortical excitation (Renger et al., 2002). It has also been shown that the mGluR2/3 agonist LY379268 blocked pharmacologically-induced gamma oscillations (Jones et al., 2012). Our results revealed that LY379268 treatment successfully reduced gamma power in PV-α1 KO mice to that of WT levels (Figure 6.9B, D). Furthermore, daily injection of LY379268 during music exposure successfully rescued this KO mice phenotype (Figures 6.9 E-G).

Discussion

Here, we showed that the maturation time course of PV+ neurons in the mPFC matches the critical period for acoustic preference. We further showed that animals exhibit abnormal adult plasticity when they have impaired PV functions (*Otx2*$^{+/AA}$, BDNF Val/Met, PV-α1 KO) in the mPFC. Our data support the interpretation that PV+ neurons regulate the critical period plasticity in the mPFC.

We provide genetic evidence that disrupting the essential GAG-binding motif within endogenous Otx2 alone leads to its mis-localization and attenuates its accumulation in PV+ cells. Our lab previously proposed a two-threshold model in which Otx2 controls the opening and closure of a CP through a positive feedback loop (Prochiantz and Di Nardo, 2015; Spatazza et al., 2013). In brief, a nascent PNN surrounding PV+ cells attracts Otx2, which in turn promotes further maturation of the PNN. Our analysis of the Otx2-AA mice supports this model and extends it across multiple brain regions. Attenuated accumulation (~20% decrease) of Otx2 protein in PV+ cells of V1 (data not published), A1 and mPFC is sufficient to delay PNN and PV expression and alter CP timing. Recent work indicates that PV+ cell-intrinsic *Clock*

signaling contributes to CP timing (Kobayashi et al., 2015), suggesting that once internalized, Otx2 must interact with these mechanisms to fine-tune CP timing.

Our genetic model further reveals that non-cell autonomous Otx2 regulates plasticity more broadly across cortical modalities. In *Otx2*$^{+/AA}$ mice, PV+ cell maturation was delayed throughout the neocortex and ectopic windows of cortical plasticity arose in occipital (data not published), parietal and frontal areas, including A1 and mPFC. This is consistent with a global source of Otx2 coordinating CP timing across brain regions. Work from our lab previously identified the choroid plexus as one such central Otx2 source (Spatazza et al., 2013). Whether misaligned CP trajectories across brain regions give rise to cognitive consequences will be of great interest. For example, Otx2 signaling may orchestrate complex behaviors reflecting the interplay of multiple sequential CP, such as language (Werker and Hensch, 2015) and many mental disorders (Meredith et al., 2012).

Disrupted Otx2 signaling and its consequences may, in fact, be a hallmark of psychiatric and intellectual disorders (Gogolla et al., 2009; Le Magueresse and Monyer, 2013; Maeda, 2015). Multisensory integration in the insular cortex is compromised along with PV+ circuits and their PNNs in mouse models of autism spectrum disorders (Gogolla et al., 2014). PNN density is low in the amygdala, entorhinal and prefrontal cortices of schizophrenia patients (Berretta et al., 2015; Mauney et al., 2013; Pantazopoulos et al., 2010) and high in the motor cortex of patients with Rett Syndrome (Belichenko et al., 1997). Weakened PV+ circuits in the mPFC cause deficits in social behavior (Yizhar et al., 2011) and behavioral aspects of schizophrenia in both mouse models (Brown et al., 2015) and patients (Akbarian et al., 1995; Brown et al., 2015;

Glausier et al., 2014; Hashimoto et al., 2003). Gene expression in the choroid plexus is altered in major depressive disorders (Turner et al., 2014), and deficits in circadian genes (Roybal et al., 2007) as well as *Otx2* polymorphisms (Sabunciyan et al., 2007) are associated with bipolar disorders.

Our data also suggest that ELS females could show abnormal adult critical period plasticity in the mPFC. Firstly, expression of α1 subunit in the frontal cortex is reduced in ELS females. α1 subunit is known to regulate the onset of critical period plasticity during normal development in V1 (Fagiolini et al., 2004). Here we showed that deletion of α1 subunit specifically in PV+ cells also resulted in adult critical period plasticity (Figure 6.9). Secondly, adult BDNF Val/Met females show similar *BDNF* expression level and anxiety behavior as adult ELS females. Our data here showed that BDNF Val/Met females exhibit plasticity for acoustic preference in adulthood (Figure 6.8). Lastly, ELS females showed impaired PV network in the mPFC.

Our data also provide potential therapeutic targets for ELS. mGluR2 has been implicated in stress susceptibility. mGluR2-KO animals showed a higher susceptibility to chronic unpredictable stress in adulthood (Nasca et al., 2015). We showed that an mGluR2 agonist was able to suppress abnormal adult plasticity (Figure 6.9). Furthermore, extending CP plasticity in the mPFC of *Otx2*$^{+/AA}$ mice enabled music to reduce anxiety in adulthood (Figure 6.5). Potential beneficial effects of judiciously manipulated brain plasticity paired with behavioral therapies(Yinger and Gooding, 2014) may then be promising avenues for psychiatric disorders.

Chapter 7

Discussion

Critical period plasticity is regulated by local inhibition, especially PV+ fast spiking interneurons. The goal of this thesis is to probe intrinsic, extrinsic and environmental impacts on the local inhibition in the neocortex. My work here led to two major conclusions. First, local excitation/inhibition (E/I) balance is sensitive to PV+ neuron cell-intrinsic and extrinsic factors. Second, PV inhibition in the mPFC regulates critical period plasticity for acoustic preference, and is vulnerable to early life stress in a sex-dependent manner.

Similarities and differences in critical period regulation across brain regions

In this thesis, we have mostly focused on the similarities in the mechanisms of critical period plasticity across cortical areas. We hope to bridge our knowledge from primary sensory cortices to higher cognitive areas, such as the mouse mPFC. We found strong evidence that PV+ interneurons, which are known to control the onset of the critical period in V1, also regulate the critical period for acoustic preference. In genetic models such as *Otx2*$^{+/AA}$ and PV-α1 KO, where PV inhibition was impaired globally, we found altered critical period plasticity in primary sensory cortices as well as the mPFC (Chapter 6, V1 data not shown).

However, we should not ignore the differences between the mPFC and primary sensory areas. In humans, prefrontal areas have a late development (Chapter 1). But during aging, frontal lobe shows a faster decrease in brain volume compared with

temporal lobe (Cowell et al., 1994). The differences in development and aging suggest potential differences in critical period mechanisms.

Our results from BDNF Val/Met animals may be one example. BDNF is well known to be involved in regulating critical period plasticity in V1. Briefly, overexpression of BDNF leads to pre-maturation of PV neurons and precocious critical period in V1 (Huang et al., 1999). On the other hand, dark rearing delays the onset of the critical period in V1, in company with reduced expression of BDNF (Fagiolini et al., 1994) . The effect of dark rearing can be rescued by overexpression of BDNF (Gianfranceschi et al., 2003). Heterozygous *BDNF* knockout (*BDNF*+/-) animals show normal ocular dominance plasticity (Bartoletti et al., 2002) in V1, meaning no delay or adult plasticity. But *BDNF*+/- animals show increased anxiety behavior, similar to BDNF Met/Met males (Chen et al., 2006). In Chapter 5, we showed that BDNF Val/Met females also exhibited increased anxiety. However, we found that BDNF Val/Met females showed critical period plasticity for acoustic preference in adulthood, which is inconsistent with the normal critical period for ocular dominance plasticity in V1 in *BDNF*+/- animals (Bartoletti et al., 2002). Therefore, it is possible that reduction in BDNF will cause a delay in critical period plasticity in the mPFC, but not in primary sensory areas such as V1.

But we have to acknowledge the potential differences between BDNF+/- and BDNF Val/Met animals. Indeed, reduction of BDNF is present in both models in adulthood. But we cannot exclude the differences in their developmental trajectories, which may cause the inconsistency in critical period plasticity in V1 and the mPFC.

The differences in critical period plasticity between the mPFC and primary sensory areas, if any, may result from the differences in their inputs and outputs. The major inputs to primary sensory cortices are from their corresponding thalamic nuclei. The mPFC receives direct inputs from the mediodorsal nucleus of the thalamus, and limbic structures including the amygdala, hippocampus, hypothalamus and associated cortices (Miller and Cohen, 2001; Uylings and van Eden, 1990). In addition, the PFC is a primary target for neuromodulators, including noradrenaline, acetylcholine, serotonin, dopamine, etc. (Dembrow and Johnston, 2014). This may contribute to the complexity of critical period plasticity in the PFC. It should be pointed out that there exist distinct mechanisms for some specific forms of plasticity even within one sensory modality, due to the differences in neuromodulatory signaling. For example, expression of oxytocin receptors in inhibitory neurons in the left primary auditory cortex is necessary for the acquisition of maternal behavior in females (Marlin et al., 2015). Apparently, the right auditory cortex shows significantly less expression of oxytocin receptors, and is not involved in such behavior.

Our results also indicate that PV inhibition in the mPFC may be more susceptible to early life stress (ELS). We found a selective reduction in PV expression in the mPFC but not M1 in ELS females, in both POs and C57s. Human studies on ELS also converge on the changes in prefrontal areas. Understanding why PFC is more sensitive to early life experiences can provide insights into the mechanisms of early life stress, as well as psychiatric disorders.

Sex-specific impacts of ELS on the mPFC

Our results also highlight sexual dimorphism in the mouse mPFC. We found that the developmental time course of PV inhibition in the male and female mPFC was slightly different. Namely, females showed a significant peak in PV intensity at postnatal day (P) 35, and may be ~1 week ahead in PV intensity. Detailed mapping of critical period windows in females versus males has not been performed yet. We also showed that PV inhibition in the mPFC responded differently to early life experiences. In females, PV inhibition was reduced by ELS, but did not improve by enrichment. But in males, PV inhibition was increased by enrichment, but not affected significantly by ELS. Finally, we showed that the same genetic background in BDNF Val/Met animals yield different behaviors and critical period plasticity in females versus males.

In adult humans, frontal areas show evident sexual dimorphisms in volume. Females have larger volumes in frontal and medial paralimbic cortices, while males have a larger frontomedial cortex, amygdala and hypothalamus (Goldstein et al., 2001). During aging, age-related decreases in frontal and temporal lobe are greater in males (Cowell et al., 1994). The PFC is highly involved in emotion regulation, social behaviors, and cognitive functions. Because of sex-specific selection pressures on PFC-related behaviors, it has been hypothesized that prefrontal cortex is a candidate for sexually dimorphic evolution (Smaers et al., 2012).

Gonadal hormones have extensive impacts on sex differences in the brain (McEwen and Milner, 2017). We cannot rule out the involvement of hormonal modulation in behaviors such as anxiety and aggression (Susman et al., 1987). However, in our study, early life stress was performed in early postnatal weeks, before sexual maturation in mice. Genes on sex chromosomes can directly act in brain cells during

development to differentiate female and male brains (Arnold, 2004). For example, lateral differences in brain sexual phenotype were observed in a lateral gynandromorphic zebra finch (Wade, 2001). The study on DNA methylation in human fetal brains revealed a total of 8059 sites that showed significant differential methylation between male and female fetal brains, with most on the X Chromosome (Spiers et al., 2015). One future direction is to investigate genes (possibly on sex chromosomes) that are important for sex-specific response to early life stress.

One potential cellular mechanism underlying the sex-specific effect of early life stress could be BDNF. Decreased BDNF expression causes anxiety behavior in heterozygous BDNF +/- animals, BNDF Met/Met males (Chen et al., 2006) and BDNF Val/Met females (Chapter 5). On the other hand, restricted BDNF deletion from hippocampal area CA3 and dentate gyrus (DG), cerebellum and facial nerve nucleus in KA1-Cre animals causes aggression and social dominance but not anxiety (Ito et al., 2011). Plasma BDNF level is correlated with aggressiveness in patients with Alzheimer's disease (Nagata et al., 2014). Among schizophrenia patients, BDNF Val66Met polymorphism is also associated with aggressive behavior (Spalletta et al., 2010).

Studies have indicated interactions between BDNF and sex. The beneficial effects of 17β-estradiol on spatial learning in ovariectomized animals are abolished in BDNF+/- animals (Wu et al., 2015). In adult animals, estrogen induces the expression of BDNF in adult brains (see review(Carbone and Handa, 2013)). But in Zebra Finches, estrogen-induced BDNF expression was only observed in males but not in females (Dittrich et al., 1999). It has also been hypothesized that BDNF might contribute to sexually dimorphic

brain development from during early postnatal weeks (P0-P10) (Solum and Handa, 2001, 2002).

Evidence also points to an interplay between stress hormone glucocorticoids (GC) and BDNF (Jeanneteau and Chao, 2013). Transient increase in GC caused by acute stress leads to an increase in BDNF expression and spine turnover rate in developing and adult cortex. But chronic stress results in abnormal loss of stable spines (Liston and Gan, 2011). In depression, decreased spine density and abnormal behavior induced by chronic GC action is thought to be mediated by BDNF (Duman et al., 1997). The interaction between stress and BDNF may also be sex- and brain region-dependent. For example, in 6-7 week-old female rats (but not male rates), acute foot-shock stress increases BDNF in DG of hippocampus, while chronic stress decreases BDNF in the mPFC (Lin et al., 2009).

The sex-specific interaction between stress and BDNF could be mediated by PV+ interneurons. Tyrosine kinase B receptors (TrkB) are enriched in PV+ neurons in the cortex (Gorba and Wahle, 1999). Interestingly, male mice lacking TrkB in PV+ cells exhibit impaired fear extinction consolidation, but not females (Lucas et al., 2014). Estrogen receptor-β (ERβ) co-localizes extensively with PV+ interneurons in broad brain regions including the mPFC (Blurton-Jones and Tuszynski, 2002). And estradiol increases the expression TrkB protein in cultured hypothalamic neurons isolated from male rats, but not the neurons from females (Cambiasso et al., 2000).

BDNF expression is sensitive to early parental care. Pups receiving more licking/grooming during the first postnatal week are less stressed and show increased expression of BDNF in the hippocampus (Liu et al., 2000; Liu et al., 1997; Weaver et al.,

2004). Therefore, ELS may disrupt BDNF-GC equilibrium (Daskalakis et al., 2015). For future studies, it will be interesting to examine 1) the development of ELS females and males; 2) the sex-specific interaction of GC and BDNF in early postnatal brains; and 3) the sex-specific responses of PV+ neurons to BDNF and stress.

Critical period in psychiatric disorders

It is interesting to notice a pattern that both critical period plasticity and psychiatric disorders are thought to be caused by imbalance between excitation and inhibition. Is there any connection between critical period plasticity and mental disorders?

In Chapter 3 and our published work (Kobayashi et al., 2015), we showed that PV+ neuron cell-intrinsic *Clock* is required for the maturation of PV inhibition and the normal critical period for OD plasticity in visual cortex. Deletion of *Clock* gene from all neurons, or from PV+ neurons alone causes delayed critical period in adult animals. We have not examined the critical period plasticity in other cortical areas, including the mPFC. But it may be extremely interesting to do so because several genetic variants in *Clock* are reported to be associated with depressive disorders and seasonal affective disorder or winter depression (Partonen, 2012). There is no strong evidence of an association between *Clock* and anxiety behavior *per se*. And we did not found changes in *Clock* expression in ELS females or males (data not shown). However, genetic variants of RORB (rs7022435, rs3750420, rs1157358, rs3903529) and NR1D1 (rs2314339) are associated with manic behaviors in bipolar disorders (Partonen, 2012). And we did observe “manic” behaviors only in ELS female POs. Besides anxiety behavior, female

ELS POs showed significantly increased locomotion in behavioral tests. Interestingly, POs are known for their elaborate burrowing behaviors, which is attributed to circadian rhythm to some extent (Metz, 2015). It is possible that some *Clock* variants will increase a subject's vulnerability to ELS, which results in manic behavior.

Our results also showed a connection between anxiety behavior and critical period plasticity, linked by reduced or immature PV inhibition in the mPFC, e.g., BDNF Val/Met females. In particular, reduced PV inhibition onto subcortical projection Type A pyramidal neurons may be the key player. Interestingly, the acoustic preference behavior for testing critical period plasticity is mediated by the anxiolytic effect of music (Yang et al., 2012). The normal critical period for acoustic preference in mice happens during a pre-adolescence time window (Chapter 1). Adolescent mice, in general, show higher plasticity compared to adults. In multiple-choice reversal learning tests, juvenile mice show greater behavioral flexibility compared with adult mice (Johnson and Wilbrecht, 2011). At the same time, increased anxiety behavior in open field test and elevated plus maze has also been reported in C57BL/6J mice during P21-P60 compared to adult mice (Moore et al., 2011).

By the definition of a "critical period", it is also a time window when individuals show the greatest vulnerability to noxious experiences (Chapter 1). Abnormal plasticity in psychiatric disorders may represent increased vulnerability to external stimuli. One common hub of impairment in these illnesses is elevated oxidative stress (Do et al., 2015). In the neocortex, PV axons are also wrapped with myelin sheath (Micheva et al., 2016). But the structure of the myelination on PV axons does not seem to serve the purpose of increasing transduction speed and validity. It is possible that myelination on

PV axons is protective from oxidative stress, given the fast-spiking nature of PV+ neurons. In this thesis, we have shown in several cases that the existence of some proteins/genes blocks the extended critical period plasticity. It is possible that oxidative stress may normally be buffered by homeoproteins (Rekaik et al., 2015), like Otx2, and *Clock* genes (Kobayashi et al., 2015) in PV+ cells.

Critical period plasticity in psychiatric disorders may also represent potential opportunities for intervention. Music is reported to reduce anxiety in an anxiogenic situation ("state anxiety"), for example, clinical settings (Beccaloni, 2011; Han et al., 2010; Kemper and Danhauer, 2005; Nilsson, 2008). Recent works showed that the anxiolytic effect of music is mediated by music preference (Jiang et al., 2016; Yang et al., 2012), which is shown in mice to be formed when the animals show critical period plasticity (Yang et al., 2012). Human studies also support the higher efficacy of music therapy in children and adolescents (Jorm et al., 2004; Parslow et al., 2008). In Chapter 6, we showed that extending CP plasticity in the mPFC of $Otx2^{+/AA}$ mice enabled music to reduce anxiety in adulthood. It proves, in theory, the potential beneficial effects of pairing brain plasticity and behavioral therapy, such as music exposure.

Our results highlight the importance of mapping critical periods in psychiatric disorders, or after ELS. Human fMRI data showed early maturation of amygdala-prefrontal connectivity after maternal separation (Gee et al., 2013). In male mice, FC caused early maturation of PV+ neurons in the hippocampus and pre-matured fear behaviors (Bath et al., 2016). It is possible that critical period in the mPFC may shift earlier after ELS. In the High/Scope Perry Preschool study from 1962-1967, children born in poverty were randomly assigned to a high-quality preschool program at age 3-4.

Longitudinal analysis showed significant benefits of the preschool program, especially in female subjects (Lawrence J Schweinhart, 2005). This study agrees with our results that females may be more susceptible to ELS. It also shows that early intervention during early childhood in ELS females could be very effective. In the future studies, we have to map in details the development of the mPFC and critical period plasticity in ELS animals.

Different susceptibility to ELS among subtypes of pyramidal neurons

The neocortex contains diverse neuronal types (Molyneaux et al., 2007). Excitatory projection neurons can be divided into different subtypes based on their axonal targets, molecular profiles, intrinsic electrophysiological properties, and afferent/efferent circuits. Different subtypes of pyramidal neurons may be differently affected by early life experiences.

In our electrophysiology recordings of mPFC L5 pyramidal neurons, the distribution of Type A and Type B cells were not different in control and ELS females or males (Figures 5.6, 5.9). This suggests that the identity of pyramidal neurons may not be affected by postnatal ELS. In fact, our approach of *in vivo* reprogramming by overexpressing Fezf2 at E14.5 right after neurons became post-mitotic yielded a success rate of ~40% for reprogramming, namely, changing callosal projection neurons into subcortical projection neurons (Rouaux and Arlotta, 2013; Ye et al., 2015). The capacity of changing identity declines as neurons mature and Fezf2-overexpression alone is unable to reprogram neurons past early postnatal ages (Rouaux and Arlotta, 2013). Postnatal overexpression of Fezf2 from P3, paired with either administration of valproic acid (VPA), a histone deacetylase inhibitor, or with callosotomy as a CPN-specific injury,

only yielded a success rate of less than 10% for reprogramming (Rouaux and Arlotta, 2013). Therefore it is unlikely that early postnatal experiences will change the identity (subcortical or callosal projection) of pyramidal neurons.

However, the development of axon innervation and the refinement of axonal targets of projection neurons happen during postnatal age, and follow activity-dependent, Hebbian mechanisms (Fame et al., 2011; Grant et al., 2012). CPN axons show growth, branching, layer-specific targeting and arbor formation between P5 and P9, and develop further arborization between P9 and P15 (Mizuno et al., 2010). The adult projection pattern for CPN is established around P21 (see review (Fame et al., 2011; Innocenti and Price, 2005)). The development of CFuPN axons follows similar rules. For example, somatosensory ventrobasal complex, and motor ventrolateral nucleus are innervated by corticothalamic axons between E18.5 and P0.5, while auditory Medial geniculate nucleus (MGN) and visual dorsal Lateral geniculate nucleus (dLGN) are not fully innervated until P8 (see review (Grant et al., 2012)). This is because somatosensory and motor functions mature before visual and auditory functions. Given the time window and activity-dependent mechanisms, the development of projection neuron axons can be potentially affected by early life experiences.

In Chapter 5, we also found that there was a significant reduction in inhibitory inputs onto Type A pyramidal neurons in ELS females. Type A pyramidal neurons project to subcortical areas and have large voltage sag. In Chapter 4, we showed that Fezf2-reprogrammed L2/3 neurons, as well as L5 subcortical projection neurons, exhibited large voltage sag and received more PV inhibition. In ChIP-Seq analysis, Fezf2 directly binds to the transcriptional starting site (TSS) of *BDNF* gene. And the expression

of *BDNF* mRNA is positively regulated by Fezf2 in neural progenitor cells in 48 hrs (Lodato et al., 2014). Interestingly, we also found a decrease in *BNDF* mRNA in ELS females. These data together indicate the role of *BDNF* in recruiting PV inhibition onto subcortical projection neurons.

However, we did not detect an increase of PV inhibition in Fezf2-non-reprogrammed (NR) L2/3 CPNs. This raises two interesting questions. Firstly, both the reprogrammed and non-reprogrammed L2/3 CPNs received the same Fezf2 plasmid and over-expressed Fezf2 (measured in single-cell qPCR). This suggests that overexpression of Fezf2 alone is not enough to recruit inhibition. The recruitment of inhibition depends on the cell identity (or cell identity-specific genes). But it has not been tested whether Fezf2 is required in CFuPNs to maintain their inhibitory inputs. It will be very interesting to test in a cell-type specific way to examine whether reducing inhibition onto Type A pyramidal neurons in the mPFC will cause anxiety behavior in animals.

Secondly, in Chapter 5, we found that ELS males showed increased expression of *BDNF* mRNA and increased inhibition in Type B pyramidal neurons. Type B pyramidal neurons send callosal axons and have no obvious voltage sage. This shows that increasing *BDNF* in CPNs may be sufficient to recruit more inhibition. Compared with the Fezf2-NR data, it suggests that Fezf2 does not increase BDNF in non-reprogrammed CPNs. It is possible the effects of Fezf2 on gene regulation vary in different subtypes of neurons, or neurons in different maturation stages. After all, Fezf2-NR CPNs failed to acquire CFuPNs signature genes and intrinsic properties like iCFuPNs.

In summary, our data show that Type A pyramidal neurons in the female mPFC are susceptible to ELS. It should be noted that pyramidal neurons with different intrinsic

properties also show different vulnerabilities in neurodegenerative disorders (Roselli and Caroni, 2015). This may further indicate different susceptibility of neuronal circuits to ELS and psychiatric disorders.

References

Acampora, D., Di Giovannantonio, L.G., Di Salvio, M., Mancuso, P., and Simeone, A. (2009). Selective inactivation of Otx2 mRNA isoforms reveals isoform-specific requirement for visceral endoderm anteriorization and head morphogenesis and highlights cell diversity in the visceral endoderm. Mechanisms of development 126, 882-897.

Akbarian, S., Kim, J.J., Potkin, S.G., Hagman, J.O., Tafazzoli, A., Bunney, W.E., Jr., and Jones, E.G. (1995). Gene expression for glutamic acid decarboxylase is reduced without loss of neurons in prefrontal cortex of schizophrenics. Archives of general psychiatry 52, 258-266.

Allen, N.C., Bagade, S., McQueen, M.B., Ioannidis, J.P., Kavvoura, F.K., Khoury, M.J., Tanzi, R.E., and Bertram, L. (2008). Systematic meta-analyses and field synopsis of genetic association studies in schizophrenia: the SzGene database. Nat Genet 40, 827-834.

Amamoto, R., and Arlotta, P. (2014). Development-inspired reprogramming of the mammalian central nervous system. Science 343, 1239882.

Arlotta, P., Molyneaux, B.J., Chen, J., Inoue, J., Kominami, R., and Macklis, J.D. (2005). Neuronal subtype-specific genes that control corticospinal motor neuron development in vivo. Neuron 45, 207-221.

Arnold, A.P. (2004). Sex chromosomes and brain gender. Nat Rev Neurosci 5, 701-708.

Arnsten, A.F.T. (2009). Stress signalling pathways that impair prefrontal cortex structure and function. Nature Reviews Neuroscience 10, 410-422.

Arnsten, A.F.T. (2015). Stress weakens prefrontal networks: molecular insults to higher cognition. Nature Neuroscience 18, 1376-1385.

Avesar, D., and Gulledge, A.T. (2012). Selective serotonergic excitation of callosal projection neurons. Front Neural Circuits 6, 12.

Bale, T.L., and Epperson, C.N. (2015). Sex differences and stress across the lifespan. Nature Neuroscience 18, 1413-1420.

Barkat, T.R., Polley, D.B., and Hensch, T.K. (2011). A critical period for auditory thalamocortical connectivity. Nat Neurosci 14, 1189-1194.

Bartoletti, A., Cancedda, L., Reid, S.W., Tessarollo, L., Porciatti, V., Pizzorusso, T., and Maffei, L. (2002). Heterozygous knock-out mice for brain-derived neurotrophic factor show a pathway-specific impairment of long-term potentiation but normal critical period for monocular deprivation. J Neurosci 22, 10072-10077.

Bartolini, G., Ciceri, G., and Marin, O. (2013). Integration of GABAergic interneurons into cortical cell assemblies: lessons from embryos and adults. Neuron 79, 849-864.

Basu, S.N., Kollu, R., and Banerjee-Basu, S. (2009). AutDB: a gene reference resource for autism research. Nucleic Acids Res 37, D832-836.

Bath, K.G., Manzano-Nieves, G., and Goodwill, H. (2016). Early life stress accelerates behavioral and neural maturation of the hippocampus in male mice. Horm Behav 82, 64-71.

Beccaloni, A.M. (2011). The Medicine of Music: A Systematic Approach for Adoption Into Perianesthesia Practice. J Perianesth Nurs 26, 323-330.

Bedford, N.L., and Hoekstra, H.E. (2015). Peromyscus mice as a model for studying natural variation. Elife 4.

Belforte, J.E., Zsiros, V., Sklar, E.R., Jiang, Z., Yu, G., Li, Y., Quinlan, E.M., and Nakazawa, K. (2010). Postnatal NMDA receptor ablation in corticolimbic interneurons confers schizophrenia-like phenotypes. Nat Neurosci 13, 76-83.

Belichenko, P.V., Hagberg, B., and Dahlstrom, A. (1997). Morphological study of neocortical areas in Rett syndrome. Acta neuropathologica 93, 50-61.

Bernard, C., Kim, H.T., Torero Ibad, R., Lee, E.J., Simonutti, M., Picaud, S., Acampora, D., Simeone, A., Di Nardo, A.A., Prochiantz, A.*, et al.* (2014). Graded Otx2 activities demonstrate dose-sensitive eye and retina phenotypes. Human molecular genetics 23, 1742-1753.

Bernard, C., and Prochiantz, A. (2016). Otx2-PNN interaction to regulate cortical plasticity. Neural Plasticity 2016.

Berretta, S., Pantazopoulos, H., Markota, M., Brown, C., and Batzianouli, E.T. (2015). Losing the sugar coating: Potential impact of perineuronal net abnormalities on interneurons in schizophrenia. Schizophrenia research.

Beurdeley, M., Spatazza, J., Lee, H.H., Sugiyama, S., Bernard, C., Di Nardo, A.A., Hensch, T.K., and Prochiantz, A. (2012). Otx2 binding to perineuronal nets persistently regulates plasticity in the mature visual cortex. The Journal of neuroscience : the official journal of the Society for Neuroscience 32, 9429-9437.

Blurton-Jones, M., and Tuszynski, M.H. (2002). Estrogen receptor-beta colocalizes extensively with parvalbumin-labeled inhibitory neurons in the cortex, amygdala, basal forebrain, and hippocampal formation of intact and ovariectomized adult rats. The Journal of comparative neurology 452, 276-287.

Breslau, N., Schultz, L., and Peterson, E. (1995). Sex-Differences in Depression - a Role for Preexisting Anxiety. Psychiat Res 58, 1-12.

Brown, J.A., Ramikie, T.S., Schmidt, M.J., Baldi, R., Garbett, K., Everheart, M.G., Warren, L.E., Gellert, L., Horvath, S., Patel, S., and Mirnics, K. (2015). Inhibition of parvalbumin-expressing interneurons results in complex behavioral changes. Molecular psychiatry.

Brown, S.P., and Hestrin, S. (2009). Intracortical circuits of pyramidal neurons reflect their long-range axonal targets. Nature 457, 1133-1136.

Buhl, E.H., Halasy, K., and Somogyi, P. (1994). Diverse sources of hippocampal unitary inhibitory postsynaptic potentials and the number of synaptic release sites. Nature 368, 823-828.

Bunger, M.K., Wilsbacher, L.D., Moran, S.M., Clendenin, C., Radcliffe, L.A., Hogenesch, J.B., Simon, M.C., Takahashi, J.S., and Bradfield, C.A. (2000). Mop3 is an essential component of the master circadian pacemaker in mammals. Cell 103, 1009-1017.

Burguiere, E., Monteiro, P., Feng, G., and Graybiel, A.M. (2013). Optogenetic stimulation of lateral orbitofronto-striatal pathway suppresses compulsive behaviors. Science 340, 1243-1246.

Burguiere, E., Monteiro, P., Mallet, L., Feng, G., and Graybiel, A.M. (2015). Striatal circuits, habits, and implications for obsessive-compulsive disorder. Curr Opin Neurobiol 30, 59-65.

Caballero, A., and Tseng, K.Y. (2016). GABAergic Function as a Limiting Factor for Prefrontal Maturation during Adolescence. Trends Neurosci 39, 441-448.

Cabungcal, J.H., Steullet, P., Kraftsik, R., Cuenod, M., and Do, K.Q. (2013a). Early-Life Insults Impair Parvalbumin Interneurons via Oxidative Stress: Reversal by N-Acetylcysteine. Biol Psychiatry 73, 574-582.

Cabungcal, J.H., Steullet, P., Morishita, H., Kraftsik, R., Cuenod, M., Hensch, T.K., and Do, K.Q. (2013b). Perineuronal nets protect fast-spiking interneurons against oxidative stress. Proc Natl Acad Sci U S A 110, 9130-9135.

Calhoon, G.G., and Tye, K.M. (2015). Resolving the neural circuits of anxiety. Nature Neuroscience 18, 1394-1404.

Cambiasso, M.J., Colombo, J.A., and Carrer, H.F. (2000). Differential effect of oestradiol and astroglia-conditioned media on the growth of hypothalamic neurons from male and female rat brains. Eur J Neurosci 12, 2291-2298.

Carbone, D.L., and Handa, R.J. (2013). Sex and stress hormone influences on the expression and activity of brain-derived neurotrophic factor. Neuroscience 239, 295-303.

Cardin, J.A., Carlen, M., Meletis, K., Knoblich, U., Zhang, F., Deisseroth, K., Tsai, L.H., and Moore, C.I. (2009). Driving fast-spiking cells induces gamma rhythm and controls sensory responses. Nature 459, 663-667.

Carlen, M., Meletis, K., Siegle, J.H., Cardin, J.A., Futai, K., Vierling-Claassen, D., Ruhlmann, C., Jones, S.R., Deisseroth, K., Sheng, M.*, et al.* (2012). A critical role for NMDA receptors in parvalbumin interneurons for gamma rhythm induction and behavior. Molecular psychiatry 17, 537-548.

Carulli, D., Pizzorusso, T., Kwok, J.C., Putignano, E., Poli, A., Forostyak, S., Andrews, M.R., Deepa, S.S., Glant, T.T., and Fawcett, J.W. (2010). Animals lacking link protein have attenuated perineuronal nets and persistent plasticity. Brain 133, 2331-2347.

Champagne, F.A., Francis, D.D., Mar, A., and Meaney, M.J. (2003). Variations in maternal care in the rat as a mediating influence for the effects of environment on development. Physiol Behav 79, 359-371.

Chellappa, S.L., Gaggioni, G., Ly, J.Q., Papachilleos, S., Borsu, C., Brzozowski, A., Rosanova, M., Sarasso, S., Luxen, A., Middleton, B.*, et al.* (2016). Circadian dynamics in measures of cortical excitation and inhibition balance. Sci Rep 6, 33661.

Chemerinski, E., Ho, B.C., Flaum, M., Arndt, S., Fleming, F., and Andreasen, N.C. (2002). Insomnia as a predictor for symptom worsening following antipsychotic withdrawal in schizophrenia. Compr Psychiatry 43, 393-396.

Chen, J., Yu, J., Liu, Y.J., Zhang, L.L., and Zhang, J.X. (2015). BDNF Val66Met, stress, and positive mothering: Differential susceptibility model of adolescent trait anxiety. J Anxiety Disord 34, 68-75.

Chen, Z.Y., Ling, D.Q., Bath, K.G., Ieraci, A., Khan, T., Siao, C.J., Herrera, D.G., Toth, M., Yang, C.W., Kocsis, J.H*., et al.* (2006). Genetic variant BDNF (Val66Met) polymorphism alters anxiety-related behavior. Neuropsychopharmacol 31, S110-S111.

Chubykin, A.A., Atasoy, D., Etherton, M.R., Brose, N., Kavalali, E.T., Gibson, J.R., and Sudhof, T.C. (2007). Activity-dependent validation of excitatory versus inhibitory synapses by neuroligin-1 versus neuroligin-2. Neuron 54, 919-931.

Chugani, H.T., Behen, M.E., Muzik, O., Juhasz, C., Nagy, F., and Chugani, D.C. (2001). Local brain functional activity following early deprivation: a study of postinstitutionalized Romanian orphans. NeuroImage 14, 1290-1301.

Colombo, J. (1982). The critical period concept: research, methodology, and theoretical issues. Psychological bulletin 91, 260-275.

Cover, K.K., Maeng, L.Y., Lebron-Milad, K., and Milad, M.R. (2014). Mechanisms of estradiol in fear circuitry: implications for sex differences in psychopathology. Transl Psychiat 4.

Cowell, P.E., Turetsky, B.I., Gur, R.C., Grossman, R.I., Shtasel, D.L., and Gur, R.E. (1994). Sex-Differences in Aging of the Human Frontal and Temporal Lobes. J Neurosci 14, 4748-4755.

Crestani, F., Martin, J.R., Mohler, H., and Rudolph, U. (2000). Mechanism of action of the hypnotic zolpidem in vivo. Br J Pharmacol 131, 1251-1254.

Cruikshank, S.J., Lewis, T.J., and Connors, B.W. (2007). Synaptic basis for intense thalamocortical activation of feedforward inhibitory cells in neocortex. Nat Neurosci 10, 462-468.

Cruz-Fuentes, C.S., Benjet, C., Martinez-Levy, G.A., Perez-Molina, A., Briones-Velasco, M., and Suarez-Gonzalez, J. (2014). BDNF Met66 modulates the cumulative effect of psychosocial childhood adversities on major depression in adolescents. Brain Behav 4, 290-297.

Cunha, C., Angelucci, A., D'Antoni, A., Dobrossy, M.D., Dunnett, S.B., Berardi, N., and Brambilla, R. (2009). Brain-derived neurotrophic factor (BDNF) overexpression in the forebrain results in learning and memory impairments. Neurobiol Dis 33, 358-368.

Daskalakis, N.P., De Kloet, E.R., Yehuda, R., Malaspina, D., and Kranz, T.M. (2015). Early Life Stress Effects on Glucocorticoid-BDNF Interplay in the Hippocampus. Front Mol Neurosci 8, 68.

De la Rossa, A., Bellone, C., Golding, B., Vitali, I., Moss, J., Toni, N., Luscher, C., and Jabaudon, D. (2013). In vivo reprogramming of circuit connectivity in postmitotic neocortical neurons. Nat Neurosci 16, 193-200.

de Villers-Sidani, E., Simpson, K.L., Lu, Y.F., Lin, R.C.S., and Merzenich, M.M. (2008). Manipulating critical period closure across different sectors of the primary auditory cortex. Nature Neuroscience 11, 957-965.

Debruyne, J.P., Noton, E., Lambert, C.M., Maywood, E.S., Weaver, D.R., and Reppert, S.M. (2006). A clock shock: mouse CLOCK is not required for circadian oscillator function. Neuron 50, 465-477.

DeFelipe, J., Lopez-Cruz, P.L., Benavides-Piccione, R., Bielza, C., Larranaga, P., Anderson, S., Burkhalter, A., Cauli, B., Fairen, A., Feldmeyer, D*., et al.* (2013). New insights into the classification and nomenclature of cortical GABAergic interneurons. Nat Rev Neurosci 14, 202-216.

del Rio, J.A., de Lecea, L., Ferrer, I., and Soriano, E. (1994). The development of parvalbumin-immunoreactivity in the neocortex of the mouse. Brain research Developmental brain research 81, 247-259.

Dembrow, N., and Johnston, D. (2014). Subcircuit-specific neuromodulation in the prefrontal cortex. Front Neural Circuit 8.

Dibner, C., Schibler, U., and Albrecht, U. (2010). The mammalian circadian timing system: organization and coordination of central and peripheral clocks. Annu Rev Physiol 72, 517-549.

Dittrich, F., Feng, Y., Metzdorf, R., and Gahr, M. (1999). Estrogen-inducible, sex-specific expression of brain-derived neurotrophic factor mRNA in a forebrain song control nucleus of the juvenile zebra finch. Proc Natl Acad Sci U S A 96, 8241-8246.

Do, K.Q., Cuenod, M., and Hensch, T.K. (2015). Targeting Oxidative Stress and Aberrant Critical Period Plasticity in the Developmental Trajectory to Schizophrenia. Schizophrenia bulletin 41, 835-846.

Duman, R.S., Heninger, G.R., and Nestler, E.J. (1997). A molecular and cellular theory of depression. Arch Gen Psychiatry 54, 597-606.

Duncan, C.E., Webster, M.J., Rothmond, D.A., Bahn, S., Elashoff, M., and Weickert, C.S. (2010). Prefrontal GABA(A) receptor alpha-subunit expression in normal postnatal human development and schizophrenia. J Psychiatr Res 44, 673-681.

Eaton, N.R., Keyes, K.M., Krueger, R.F., Balsis, S., Skodol, A.E., Markon, K.E., Grant, B.F., and Hasin, D.S. (2012). An Invariant Dimensional Liability Model of Gender Differences in Mental Disorder Prevalence: Evidence From a National Sample. J Abnorm Psychol 121, 282-288.

Eaves, L.J., Silberg, J.L., Meyer, J.M., Maes, H.H., Simonoff, E., Pickles, A., Rutter, M., Neale, M.C., Reynolds, C.A., Erikson, M.T.*, et al.* (1997). Genetics and developmental psychopathology .2. The main effects of genes and environment on behavioral problems in the Virginia twin study of adolescent behavioral development. J Child Psychol Psyc 38, 965-980.

Edwards, S., Clow, A., Evans, P., and Hucklebridge, F. (2001). Exploration of the awakening cortisol response in relation to diurnal cortisol secretory activity. Life Sci 68, 2093-2103.

Egan, M.F., Kojima, M., Callicott, J.H., Goldberg, T.E., Kolachana, B.S., Bertolino, A., Zaitsev, E., Gold, B., Goldman, D., Dean, M.*, et al.* (2003). The BDNF val66met polymorphism affects activity-dependent secretion of BDNF and human memory and hippocampal function. Cell 112, 257-269.

Einon, D.F., and Morgan, M.J. (1977). A critical period for social isolation in the rat. Developmental psychobiology 10, 123-132.

Eluvathingal, T.J., Chugani, H.T., Behen, M.E., Juhasz, C., Muzik, O., Maqbool, M., Chugani, D.C., and Makki, M. (2006). Abnormal brain connectivity in children after early severe socioemotional deprivation: a diffusion tensor imaging study. Pediatrics 117, 2093-2100.

Fagiolini, M., Fritschy, J.M., Low, K., Mohler, H., Rudolph, U., and Hensch, T.K. (2004). Specific GABAA circuits for visual cortical plasticity. Science 303, 1681-1683.

Fagiolini, M., and Hensch, T.K. (2000). Inhibitory threshold for critical-period activation in primary visual cortex. Nature 404, 183-186.

Fagiolini, M., Pizzorusso, T., Berardi, N., Domenici, L., and Maffei, L. (1994). Functional postnatal development of the rat primary visual cortex and the role of visual experience: dark rearing and monocular deprivation. Vision research 34, 709-720.

Fame, R.M., MacDonald, J.L., and Macklis, J.D. (2011). Development specification, and diversity of callosal projection neurons. Trends Neurosci 34, 41-50.

Fares, R.P., Belmeguenai, A., Sanchez, P.E., Kouchi, H.Y., Bodennec, J., Morales, A., Georges, B., Bonnet, C., Bouvard, S., Sloviter, R.S., and Bezin, L. (2013). Standardized environmental enrichment supports enhanced brain plasticity in healthy rats and prevents cognitive impairment in epileptic rats. Plos One 8, e53888.

Fino, E., Packer, A.M., and Yuste, R. (2013). The Logic of Inhibitory Connectivity in the Neocortex. Neuroscientist 19, 228-237.

Fino, E., and Yuste, R. (2011). Dense inhibitory connectivity in neocortex. Neuron 69, 1188-1203.

Flechsig Of Leipsic, P. (1901). DEVELOPMENTAL (MYELOGENETIC) LOCALISATION OF THE CEREBRAL CORTEX IN THE HUMAN SUBJECT. The Lancet 158, 1027-1030.

Frank, M.G., and Cantera, R. (2014). Sleep, clocks, and synaptic plasticity. Trends Neurosci 37, 491-501.

Freund, T.F., and Katona, I. (2007). Perisomatic inhibition. Neuron 56, 33-42.

Fu, Y., Tucciarone, J.M., Espinosa, J.S., Sheng, N., Darcy, D.P., Nicoll, R.A., Huang, Z.J., and Stryker, M.P. (2014). A cortical circuit for gain control by behavioral state. Cell 156, 1139-1152.

Garvert, M.M., Moutoussis, M., Kurth-Nelson, Z., Behrens, T.E.J., and Dolan, R.J. (2015). Learning-Induced Plasticity in Medial Prefrontal Cortex Predicts Preference Malleability. Neuron 85, 418-428.

Gee, D.G., Gabard-Durnam, L.J., Flannery, J., Goff, B., Humphreys, K.L., Telzer, E.H., Hare, T.A., Bookheimer, S.Y., and Tottenham, N. (2013). Early developmental emergence of human amygdala-prefrontal connectivity after maternal deprivation. P Natl Acad Sci USA 110, 15638-15643.

Gee, S., Ellwood, I., Patel, T., Luongo, F., Deisseroth, K., and Sohal, V.S. (2012). Synaptic Activity Unmasks Dopamine D2 Receptor Modulation of a Specific Class of Layer V Pyramidal Neurons in Prefrontal Cortex. J Neurosci 32, 4959-4971.

Gianfranceschi, L., Siciliano, R., Walls, J., Morales, B., Kirkwood, A., Huang, Z.J., Tonegawa, S., and Maffei, L. (2003). Visual cortex is rescued from the effects of dark rearing by overexpression of BDNF. P Natl Acad Sci USA 100, 12486-12491.

Giedd, J.N., and Rapoport, J.L. (2010). Structural MRI of pediatric brain development: what have we learned and where are we going? Neuron 67, 728-734.

Glausier, J.R., Fish, K.N., and Lewis, D.A. (2014). Altered parvalbumin basket cell inputs in the dorsolateral prefrontal cortex of schizophrenia subjects. Molecular psychiatry 19, 30-36.

Gogolla, N., Leblanc, J.J., Quast, K.B., Sudhof, T.C., Fagiolini, M., and Hensch, T.K. (2009). Common circuit defect of excitatory-inhibitory balance in mouse models of autism. Journal of neurodevelopmental disorders 1, 172-181.

Gogolla, N., Takesian, A.E., Feng, G., Fagiolini, M., and Hensch, T.K. (2014). Sensory Integration in Mouse Insular Cortex Reflects GABA Circuit Maturation. Neuron 83, 894-905.

Goldstein, J.M., Seidman, L.J., Horton, N.J., Makris, N., Kennedy, D.N., Caviness, V.S., Faraone, S.V., and Tsuang, M.T. (2001). Normal sexual dimorphism of the adult human brain assessed by in vivo magnetic resonance imaging. Cerebral Cortex 11, 490-497.

Goldstein, P.A., Elsen, F.P., Ying, S.W., Ferguson, C., Homanics, G.E., and Harrison, N.L. (2002). Prolongation of hippocampal miniature inhibitory postsynaptic currents in mice lacking the GABA(A) receptor alpha1 subunit. Journal of neurophysiology 88, 3208-3217.

Golombek, D.A., Bussi, I.L., and Agostino, P.V. (2014). Minutes, days and years: molecular interactions among different scales of biological timing. Philos Trans R Soc Lond B Biol Sci 369, 20120465.

Gorba, T., and Wahle, P. (1999). Expression of TrkB and TrkC but not BDNF mRNA in neurochemically identified interneurons in rat visual cortex in vivo and in organotypic cultures.

Govindarajan, A., Rao, B.S.S., Nair, D., Trinh, M., Mawjee, N., Tonegawa, S., and Chattarji, S. (2006). Transgenic brain-derived neurotrophic factor expression causes both anxiogenic and antidepressant effects. P Natl Acad Sci USA 103, 13208-13213.

Grant, E., Hoerder-Suabedissen, A., and Molnar, Z. (2012). Development of the corticothalamic projections. Front Neurosci-Switz 6.

Green, C.B., Durston, A.J., and Morgan, R. (2001). The circadian gene Clock is restricted to the anterior neural plate early in development and is regulated by the neural inducer noggin and the transcription factor Otx2. Mech Dev 101, 105-110.

Greifzu, F., Pielecka-Fortuna, J., Kalogeraki, E., Krempler, K., Favaro, P.D., Schluter, O.M., and Lowel, S. (2014). Environmental enrichment extends ocular dominance plasticity into adulthood and protects from stroke-induced impairments of plasticity. P Natl Acad Sci USA 111, 1150-1155.

Greig, L.C., Woodworth, M.B., Galazo, M.J., Padmanabhan, H., and Macklis, J.D. (2013). Molecular logic of neocortical projection neuron specification, development and diversity. Nat Rev Neurosci 14, 755-769.

Grone, B.P., Chang, D., Bourgin, P., Cao, V., Fernald, R.D., Heller, H.C., and Ruby, N.F. (2011). Acute light exposure suppresses circadian rhythms in clock gene expression. J Biol Rhythms 26, 78-81.

Gunaydin, L.A., Grosenick, L., Finkelstein, J.C., Kauvar, I.V., Fenno, L.E., Adhikari, A., Lammel, S., Mirzabekov, J.J., Airan, R.D., Zalocusky, K.A*., et al.* (2014). Natural neural projection dynamics underlying social behavior. Cell 157, 1535-1551.

Han, L., Li, J.P., Sit, J.W.H., Chung, L., Jiao, Z.Y., and Ma, W.G. (2010). Effects of music intervention on physiological stress response and anxiety level of mechanically ventilated patients in China: a randomised controlled trial. J Clin Nurs 19, 978-987.

Hartig, W., Derouiche, A., Welt, K., Brauer, K., Grosche, J., Mader, M., Reichenbach, A., and Bruckner, G. (1999). Cortical neurons immunoreactive for the potassium channel Kv3.1b subunit are predominantly surrounded by perineuronal nets presumed as a buffering system for cations. Brain Res 842, 15-29.

Hashimoto, T., Nguyen, Q.L., Rotaru, D., Keenan, T., Arion, D., Beneyto, M., Gonzalez-Burgos, G., and Lewis, D.A. (2009). Protracted developmental trajectories of GABAA receptor alpha1 and alpha2 subunit expression in primate prefrontal cortex. Biological psychiatry 65, 1015-1023.

Hashimoto, T., Volk, D.W., Eggan, S.M., Mirnics, K., Pierri, J.N., Sun, Z., Sampson, A.R., and Lewis, D.A. (2003). Gene expression deficits in a subclass of GABA neurons in the prefrontal cortex of subjects with schizophrenia. The Journal of neuroscience : the official journal of the Society for Neuroscience 23, 6315-6326.

Heidbreder, C.A., and Groenewegen, H.J. (2003). The medial prefrontal cortex in the rat: evidence for a dorso-ventral distinction based upon functional and anatomical characteristics. Neurosci Biobehav Rev 27, 555-579.

Hensch, T.K. (2004). Critical period regulation. Annual review of neuroscience 27, 549-579.

Hensch, T.K. (2005). Critical period plasticity in local cortical circuits. Nature Reviews Neuroscience 6, 877-888.

Hensch, T.K., and Bilimoria, P.M. (2012). Re-opening Windows: Manipulating Critical Periods for Brain Development. Cerebrum 2012, 11.

Hensch, T.K., Fagiolini, M., Mataga, N., Stryker, M.P., Baekkeskov, S., and Kash, S.F. (1998). Local GABA circuit control of experience-dependent plasticity in developing visual cortex. Science 282, 1504-1508.

Heun-Johnson, H., and Levitt, P. (2016). Early-Life Stress Paradigm Transiently Alters Maternal Behavior, Dam-Pup Interactions, and Offspring Vocalizations in Mice. Front Behav Neurosci 10.

Hippenmeyer, S., Vrieseling, E., Sigrist, M., Portmann, T., Laengle, C., Ladle, D.R., and Arber, S. (2005). A developmental switch in the response of DRG neurons to ETS transcription factor signaling. PLoS Biol 3, e159.

Hoftman, G.D., and Lewis, D.A. (2011). Postnatal Developmental Trajectories of Neural Circuits in the Primate Prefrontal Cortex: Identifying Sensitive Periods for Vulnerability to Schizophrenia. Schizophrenia Bull 37, 493-503.

Holmes, A.J., Lee, P.H., Hollinshead, M.O., Bakst, L., Roffman, J.L., Smoller, J.W., and Buckner, R.L. (2012). Individual Differences in Amygdala-Medial Prefrontal Anatomy Link Negative Affect, Impaired Social Functioning, and Polygenic Depression Risk. J Neurosci 32, 18087-18100.

Hosang, G.M., Shiles, C., Tansey, K.E., McGuffin, P., and Uher, R. (2014). Interaction between stress and the BDNF Val66Met polymorphism in depression: a systematic review and meta-analysis. Bmc Med 12.

Huang, Z.J., Kirkwood, A., Pizzorusso, T., Porciatti, V., Morales, B., Bear, M.F., Maffei, L., and Tonegawa, S. (1999). BDNF regulates the maturation of inhibition and the critical period of plasticity in mouse visual cortex. Cell 98, 739-755.

Hubel, D.H., and Wiesel, T.N. (1970). The period of susceptibility to the physiological effects of unilateral eye closure in kittens. The Journal of physiology 206, 419-436.

Hubel, D.H., Wiesel, T.N., and LeVay, S. (1976). Functional architecture of area 17 in normal and monocularly deprived macaque monkeys. Cold Spring Harbor symposia on quantitative biology 40, 581-589.

Innocenti, G.M., and Price, D.J. (2005). Exuberance in the development of cortical networks. Nature Reviews Neuroscience 6, 955-965.

Ito, W., Chehab, M., Thakur, S., Li, J., and Morozov, A. (2011). BDNF-restricted knockout mice as an animal model for aggression. Genes Brain and Behavior 10, 365-374.

Ivy, A.S., Brunson, K.L., Sandman, C., and Baram, T.Z. (2008). Dysfunctional nurturing behavior in rat dams with limited access to nesting material: A clinically relevant model for early-life stress. Neuroscience 154, 1132-1142.

Janich, P., Pascual, G., Merlos-Suarez, A., Batlle, E., Ripperger, J., Albrecht, U., Obrietan, K., Di Croce, L., and Benitah, S.A. (2011). The circadian molecular clock creates epidermal stem cell heterogeneity. Nature 480, 209-214.

Jeanneteau, F., and Chao, M.V. (2013). Are BDNF and glucocorticoid activities calibrated? Neuroscience 239, 173-195.

Jiang, B., Huang, S., de Pasquale, R., Millman, D., Song, L., Lee, H.K., Tsumoto, T., and Kirkwood, A. (2010). The maturation of GABAergic transmission in visual cortex requires endocannabinoid-mediated LTD of inhibitory inputs during a critical period. Neuron 66, 248-259.

Jiang, J., Rickson, D., and Jiang, C.M. (2016). The mechanism of music for reducing psychological stress: Music preference as a mediator. Art Psychother 48, 62-68.

Johnson, C., and Wilbrecht, L. (2011). Juvenile mice show greater flexibility in multiple choice reversal learning than adults. Dev Cogn Neuros-Neth 1, 540-551.

Jones, N.C., Reddy, M., Anderson, P., Salzberg, M.R., O'Brien, T.J., and Pinault, D. (2012). Acute administration of typical and atypical antipsychotics reduces EEG gamma power, but only the preclinical compound LY379268 reduces the ketamine-induced rise in gamma power. Int J Neuropsychopharmacol 15, 657-668.

Jorm, A.F., Christensen, H., Griffiths, K.M., Parslow, R.A., Rodgers, B., and Blewitt, K.A. (2004). Effectiveness of complementary and self-help treatments for anxiety disorders. Med J Australia 181, S29-S46.

Kang, E., Durand, S., LeBlanc, J.J., Hensch, T.K., Chen, C., and Fagiolini, M. (2013). Visual acuity development and plasticity in the absence of sensory experience. J Neurosci 33, 17789-17796.

Karnani, M.M., Agetsuma, M., and Yuste, R. (2014). A blanket of inhibition: functional inferences from dense inhibitory connectivity. Curr Opin Neurobiol 26, 96-102.

Kemper, K.J., and Danhauer, S.C. (2005). Music as therapy. South Med J 98, 282-288.

Kessler, R.C., Sonnega, A., Bromet, E., Hughes, M., and Nelson, C.B. (1995). Posttraumatic-Stress-Disorder in the National Comorbidity Survey. Arch Gen Psychiat 52, 1048-1060.

Kilman, V., van Rossum, M.C., and Turrigiano, G.G. (2002). Activity deprivation reduces miniature IPSC amplitude by decreasing the number of postsynaptic GABA(A) receptors clustered at neocortical synapses. J Neurosci 22, 1328-1337.

Kim, H., Lim, C.S., and Kaang, B.K. (2016). Neuronal mechanisms and circuits underlying repetitive behaviors in mouse models of autism spectrum disorder. Behav Brain Funct 12, 3.

Kirkwood, A., Lee, H.K., and Bear, M.F. (1995). Co-regulation of long-term potentiation and experience-dependent synaptic plasticity in visual cortex by age and experience. Nature 375, 328-331.

Kirkwood, A., Rioult, M.C., and Bear, M.F. (1996). Experience-dependent modification of synaptic plasticity in visual cortex. Nature 381, 526-528.

Kirschbaum, C., and Hellhammer, D.H. (1989). Salivary cortisol in psychobiological research: an overview. Neuropsychobiology 22, 150-169.

Klausberger, T., Roberts, J.D., and Somogyi, P. (2002). Cell type- and input-specific differences in the number and subtypes of synaptic GABA(A) receptors in the hippocampus. J Neurosci 22, 2513-2521.

Kobayashi, Y., Ye, Z.L., and Hensch, T.K. (2015). Clock Genes Control Cortical Critical Period Timing. Neuron 86, 264-275.

Kondratov, R.V., Kondratova, A.A., Gorbacheva, V.Y., Vykhovanets, O.V., and Antoch, M.P. (2006). Early aging and age-related pathologies in mice deficient in BMAL1, the core componentof the circadian clock. Genes Dev 20, 1868-1873.

Kosten, T.A., and Nielsen, D.A. (2014). Litter and sex effects on maternal behavior and DNA methylation of the Nr3c1 exon 1(7) promoter gene in hippocampus and cerebellum. Int J Dev Neurosci 36, 5-12.

Krook-Magnuson, E., Varga, C., Lee, S.H., and Soltesz, I. (2012). New dimensions of interneuronal specialization unmasked by principal cell heterogeneity. Trends Neurosci 35, 175-184.

Kuhlman, S.J., Lu J Fau - Lazarus, M.S., Lazarus Ms Fau - Huang, Z.J., and Huang, Z.J. (2010). Maturation of GABAergic inhibition promotes strengthening of temporally coherent inputs among convergent pathways.

Kuhlman, S.J., Olivas, N.D., Tring, E., Ikrar, T., Xu, X.M., and Trachtenberg, J.T. (2013). A disinhibitory microcircuit initiates critical-period plasticity in the visual cortex. Nature 501, 543-+.

Lakshminarasimhan, H., and Chattarji, S. (2012). Stress Leads to Contrasting Effects on the Levels of Brain Derived Neurotrophic Factor in the Hippocampus and Amygdala. Plos One 7.

Lang, N., Rothkegel, H., Reiber, H., Hasan, A., Sueske, E., Tergau, F., Ehrenreich, H., Wuttke, W., and Paulus, W. (2011). Circadian modulation of GABA-mediated cortical inhibition. Cereb Cortex 21, 2299-2306.

Langfelder, P., and Horvath, S. (2008). WGCNA: an R package for weighted correlation network analysis. BMC Bioinformatics 9, 559.

Larkman, A., and Mason, A. (1990). Correlations between morphology and electrophysiology of pyramidal neurons in slices of rat visual cortex. I. Establishment of cell classes. The Journal of neuroscience : the official journal of the Society for Neuroscience 10, 1407-1414.

Lawrence J Schweinhart, J.M., Zongping Xiang, William S Barnett, Clive R Belfield, Milagros Nores (2005). Lifetime effects: The High/Scope Perry Preschool study through age 40 (High/Scope Press).

Le Magueresse, C., and Monyer, H. (2013). GABAergic interneurons shape the functional maturation of the cortex. Neuron 77, 388-405.

Lee, A.T., Gee, S.M., Vogt, D., Patel, T., Rubenstein, J.L., and Sohal, V.S. (2014). Pyramidal neurons in prefrontal cortex receive subtype-specific forms of excitation and inhibition. Neuron 81, 61-68.

Leonardo, E.D., and Hen, R. (2008). Anxiety as a developmental disorder. Neuropsychopharmacol 33, 134-140.

Letzkus, J.J., Wolff, S.B.E., Meyer, E.M.M., Tovote, P., Courtin, J., Herry, C., and Luthi, A. (2011). A disinhibitory microcircuit for associative fear learning in the auditory cortex. Nature 480, 331-U376.

Lewis, D.A., Curley, A.A., Glausier, J.R., and Volk, D.W. (2012). Cortical parvalbumin interneurons and cognitive dysfunction in schizophrenia. Trends Neurosci 35, 57-67.

Lin, Y., Ter Horst, G.J., Wichmann, R., Bakker, P., Liu, A., Li, X., and Westenbroek, C. (2009). Sex differences in the effects of acute and chronic stress and recovery after long-term stress on stress-related brain regions of rats. Cereb Cortex 19, 1978-1989.

Lisman, J. (2010). Working memory: the importance of theta and gamma oscillations. Curr Biol 20, R490-492.

Liston, C., and Gan, W.B. (2011). Glucocorticoids are critical regulators of dendritic spine development and plasticity in vivo. Proc Natl Acad Sci U S A 108, 16074-16079.

Liu, D., Diorio, J., Day, J.C., Francis, D.D., and Meaney, M.J. (2000). Maternal care, hippocampal synaptogenesis and cognitive development in rats. Nature Neuroscience 3, 799-806.

Liu, D., Diorio, J., Tannenbaum, B., Caldji, C., Francis, D., Freedman, A., Sharma, S., Pearson, D., Plotsky, P.M., and Meaney, M.J. (1997). Maternal care, hippocampal glucocorticoid receptors, and hypothalamic-pituitary-adrenal responses to stress. Science 277, 1659-1662.

Lodato, S., Molyneaux, B.J., Zuccaro, E., Goff, L.A., Chen, H.H., Yuan, W., Meleski, A., Takahashi, E., Mahony, S., Rinn, J.L., *et al.* (2014). Gene co-regulation by Fezf2 selects neurotransmitter identity and connectivity of corticospinal neurons. Nat Neurosci 17, 1046-1054.

Lodato, S., Rouaux, C., Quast, K.B., Jantrachotechatchawan, C., Studer, M., Hensch, T.K., and Arlotta, P. (2011). Excitatory projection neuron subtypes control the distribution of local inhibitory interneurons in the cerebral cortex. Neuron 69, 763-779.

Lodato, S., Shetty, A.S., and Arlotta, P. (2015). Cerebral cortex assembly: generating and reprogramming projection neuron diversity. Trends Neurosci 38, 117-125.

Lodge, D.J., Behrens, M.M., and Grace, A.A. (2009). A loss of parvalbumin-containing interneurons is associated with diminished oscillatory activity in an animal model of schizophrenia. J Neurosci 29, 2344-2354.

Lorenz, K. (1937). The Companion in the Bird's World. The Auk 54, 245-273.

Lowrey, P.L., and Takahashi, J.S. (2011). Genetics of circadian rhythms in Mammalian model organisms. Adv Genet 74, 175-230.

Lucas, E.K., Jegarl, A., and Clem, R.L. (2014). Mice lacking TrkB in parvalbumin-positive cells exhibit sexually dimorphic behavioral phenotypes. Behav Brain Res 274, 219-225.

Luth, H.J., Fischer, J., and Celio, M.R. (1992). Soybean lectin binding neurons in the visual cortex of the rat contain parvalbumin and are covered by glial nets. Journal of neurocytology 21, 211-221.

Luthi, A., and McCormick, D.A. (1998). H-current: Properties of a neuronal and network pacemaker. Neuron 21, 9-12.

Ly, J.Q., Gaggioni, G., Chellappa, S.L., Papachilleos, S., Brzozowski, A., Borsu, C., Rosanova, M., Sarasso, S., Middleton, B., Luxen, A.*, et al.* (2016). Circadian regulation of human cortical excitability. Nat Commun 7, 11828.

Madisen, L., Mao, T., Koch, H., Zhuo, J.M., Berenyi, A., Fujisawa, S., Hsu, Y.W., Garcia, A.J., 3rd, Gu, X., Zanella, S.*, et al.* (2012). A toolbox of Cre-dependent optogenetic transgenic mice for light-induced activation and silencing. Nat Neurosci 15, 793-802.

Madisen, L., Zwingman, T.A., Sunkin, S.M., Oh, S.W., Zariwala, H.A., Gu, H., Ng, L.L., Palmiter, R.D., Hawrylycz, M.J., Jones, A.R.*, et al.* (2010). A robust and high-throughput Cre reporting and characterization system for the whole mouse brain. Nat Neurosci 13, 133-140.

Maeda, N. (2015). Proteoglycans and neuronal migration in the cerebral cortex during development and disease. Frontiers in neuroscience 9, 98.

Makinodan, M., Rosen, K.M., Ito, S., and Corfas, G. (2012). A critical period for social experience-dependent oligodendrocyte maturation and myelination. Science 337, 1357-1360.

Marcheva, B., Ramsey, K.M., Buhr, E.D., Kobayashi, Y., Su, H., Ko, C.H., Ivanova, G., Omura, C., Mo, S., Vitaterna, M.H*., et al.* (2010). Disruption of the clock components CLOCK and BMAL1 leads to hypoinsulinaemia and diabetes. Nature 466, 627-631.

Marin, O. (2012). Interneuron dysfunction in psychiatric disorders. Nature Reviews Neuroscience 13, 107-120.

Markram, H., Toledo-Rodriguez, M., Wang, Y., Gupta, A., Silberberg, G., and Wu, C. (2004). Interneurons of the neocortical inhibitory system. Nature Reviews Neuroscience 5, 793-807.

Marlin, B.J., Mitre, M., D'Amour J, A., Chao, M.V., and Froemke, R.C. (2015). Oxytocin enables maternal behaviour by balancing cortical inhibition. Nature 520, 499-504.

Mason, A., and Larkman, A. (1990). Correlations between morphology and electrophysiology of pyramidal neurons in slices of rat visual cortex. II. Electrophysiology. The Journal of neuroscience : the official journal of the Society for Neuroscience 10, 1415-1428.

Masri, S., and Sassone-Corsi, P. (2010). Plasticity and specificity of the circadian epigenome. Nat Neurosci 13, 1324-1329.

Mauney, S.A., Athanas, K.M., Pantazopoulos, H., Shaskan, N., Passeri, E., Berretta, S., and Woo, T.U. (2013). Developmental pattern of perineuronal nets in the human prefrontal cortex and their deficit in schizophrenia. Biological psychiatry 74, 427-435.

Maya Vetencourt, J.F., Sale, A., Viegi, A., Baroncelli, L., De Pasquale, R., O'Leary, O.F., Castren, E., and Maffei, L. (2008). The antidepressant fluoxetine restores plasticity in the adult visual cortex. Science 320, 385-388.

McEwen, B.S., and Milner, T.A. (2017). Understanding the broad influence of sex hormones and sex differences in the brain. J Neurosci Res 95, 24-39.

McFarlane, H.G., Kusek, G.K., Yang, M., Phoenix, J.L., Bolivar, V.J., and Crawley, J.N. (2008). Autism-like behavioral phenotypes in BTBR T+tf/J mice. Genes, brain, and behavior 7, 152-163.

McGee, A.W., Yang, Y., Fischer, Q.S., Daw, N.W., and Strittmatter, S.M. (2005). Experience-driven plasticity of visual cortex limited by myelin and Nogo receptor. Science 309, 2222-2226.

McRae, P.A., Rocco, M.M., Kelly, G., Brumberg, J.C., and Matthews, R.T. (2007). Sensory deprivation alters aggrecan and perineuronal net expression in the mouse barrel cortex. J Neurosci 27, 5405-5413.

Meaney, M.J. (2001). Maternal care, gene expression, and the transmission of individual differences in stress reactivity across generations. Annual review of neuroscience 24, 1161-1192.

Mei, Y., Monteiro, P., Zhou, Y., Kim, J.A., Gao, X., Fu, Z., and Feng, G. (2016). Adult restoration of Shank3 expression rescues selective autistic-like phenotypes. Nature 530, 481-484.

Meredith, R.M., Dawitz, J., and Kramvis, I. (2012). Sensitive time-windows for susceptibility in neurodevelopmental disorders. Trends in neurosciences 35, 335-344.

Metz, H. (2015). The Genetic Basis of Behavior: Burrow Construction in Deer Mice (Genus Peromyscus). In Graduate School of Arts & Sciences (Harvard University).

Micheva, K.D., Wolman, D., Mensh, B.D., Pax, E., Buchanan, J., Smith, S.J., and Bock, D.D. (2016). A large fraction of neocortical myelin ensheathes axons of local inhibitory neurons. Elife 5.

Miller, E.K., and Cohen, J.D. (2001). An integrative theory of prefrontal cortex function. Annual review of neuroscience 24, 167-202.

Millstein, R.A., and Holmes, A. (2007). Effects of repeated maternal separation on anxiety- and depression-related phenotypes in different mouse strains. Neurosci Biobehav R 31, 3-17.

Mitsui, S., Saito, M., Mori, K., and Yoshihara, Y. (2007). A transcriptional enhancer that directs telencephalon-specific transgene expression in mouse brain. Cereb Cortex 17, 522-530.

Miwa, J.M., Ibanez-Tallon, I., Crabtree, G.W., Sanchez, R., Sali, A., Role, L.W., and Heintz, N. (1999). lynx1, an endogenous toxin-like modulator of nicotinic acetylcholine receptors in the mammalian CNS. Neuron 23, 105-114.

Miyata, S., Komatsu, Y., Yoshimura, Y., Taya, C., and Kitagawa, H. (2012). Persistent cortical plasticity by upregulation of chondroitin 6-sulfation. Nature neuroscience 15, 414-422, S411-412.

Mizuno, H., Hirano, T., and Tagawa, Y. (2010). Pre-synaptic and post-synaptic neuronal activity supports the axon development of callosal projection neurons during different post-natal periods in the mouse cerebral cortex. Eur J Neurosci 31, 410-424.

Molet, J., Heins, K., Zhuo, X., Mei, Y.T., Regev, L., Baram, T.Z., and Stern, H. (2016). Fragmentation and high entropy of neonatal experience predict adolescent emotional outcome. Transl Psychiat 6.

Molet, J., Maras, P.M., Avishai-Eliner, S., and Baram, T.Z. (2014). Naturalistic Rodent Models of Chronic Early-Life Stress. Developmental psychobiology 56, 1675-1688.

Molyneaux, B.J., Arlotta, P., Hirata, T., Hibi, M., and Macklis, J.D. (2005). Fezl is required for the birth and specification of corticospinal motor neurons. Neuron 47, 817-831.

Molyneaux, B.J., Arlotta, P., Menezes, J.R.L., and Macklis, J.D. (2007). Neuronal subtype specification in the cerebral cortex. Nature Reviews Neuroscience 8, 427-437.

Molyneaux, B.J., Goff, L.A., Brettler, A.C., Chen, H.H., Brown, J.R., Hrvatin, S., Rinn, J.L., and Arlotta, P. (2015). DeCoN: genome-wide analysis of in vivo transcriptional dynamics during pyramidal neuron fate selection in neocortex. Neuron 85, 275-288.

Mongrain, V., La Spada, F., Curie, T., and Franken, P. (2011). Sleep Loss Reduces the DNA-Binding of BMAL1, CLOCK, and NPAS2 to Specific Clock Genes in the Mouse Cerebral Cortex. PLoS One 6, e26622.

Monti, S., Tamayo, P., Mesirov, J., and Golub, T. (2003). Consensus Clustering: A Resampling-Based Method for Class Discovery and Visualization of Gene Expression Microarray Data. Machine Learning 52, 91-118.

Moore, C.L. (1995). Maternal Contributions to Mammalian Reproductive Development and the Divergence of Males and Females. Adv Stud Behav 24, 47-118.

Moore, C.L., and Morelli, G.A. (1979). Mother Rats Interact Differently with Male and Female Offspring. Journal of comparative and physiological psychology 93, 677-684.

Moore, E.M., Linsenbardt, D.N., Melon, L.C., and Boehm, S.L. (2011). Ontogenetic Differences in Adolescent and Adult C57BL/6J and DBA/2J Mice: Anxiety-Like, Locomotor, and Consummatory Behaviors. Developmental psychobiology 53, 141-156.

Morgan, R. (2002). The circadian gene Clock is required for the correct early expression of the head specific gene Otx2. Int J Dev Biol 46, 999-1004.

Morishita, H., and Hensch, T.K. (2008). Critical period revisited: impact on vision. Curr Opin Neurobiol 18, 101-107.

Morishita, H., Miwa, J.M., Heintz, N., and Hensch, T.K. (2010). Lynx1, a Cholinergic Brake, Limits Plasticity in Adult Visual Cortex. Science.

Mrdalj, J., Pallesen, S., Milde, A.M., Jellestad, F.K., Murison, R., Ursin, R., Bjorvatn, B., and Gronli, J. (2013). Early and later life stress alter brain activity and sleep in rats. Plos One 8, e69923.

Musiek, E.S., Lim, M.M., Yang, G., Bauer, A.Q., Qi, L., Lee, Y., Roh, J.H., Ortiz-Gonzalez, X., Dearborn, J.T., Culver, J.P.*, et al.* (2013). Circadian clock proteins regulate neuronal redox homeostasis and neurodegeneration. J Clin Invest 123, 5389-5400.

Nagata, T., Kobayashi, N., Shinagawa, S., Yamada, H., Kondo, K., and Nakayama, K. (2014). Plasma BDNF levels are correlated with aggressiveness in patients with amnestic mild cognitive impairment or Alzheimer disease. J Neural Transm (Vienna) 121, 433-441.

Nasca, C., Bigio, B., Zelli, D., Nicoletti, F., and McEwen, B.S. (2015). Mind the gap: glucocorticoids modulate hippocampal glutamate tone underlying individual differences in stress susceptibility. Molecular psychiatry 20, 755-763.

Nelson, C.A., 3rd, Zeanah, C.H., Fox, N.A., Marshall, P.J., Smyke, A.T., and Guthrie, D. (2007). Cognitive recovery in socially deprived young children: the Bucharest Early Intervention Project. Science 318, 1937-1940.

Nilsson, U. (2008). The anxiety- and pain-reducing effects of music interventions: a systematic review. AORN J 87, 780-807.

Nithianantharajah, J., and Hannan, A.J. (2006). Enriched environments, experience-dependent plasticity and disorders of the nervous system. Nature Reviews Neuroscience 7, 697-709.

Nowicka, D., Soulsby, S., Skangiel-Kramska, J., and Glazewski, S. (2009). Parvalbumin-containing neurons, perineuronal nets and experience-dependent plasticity in murine barrel cortex. Eur J Neurosci 30, 2053-2063.

Nusser, Z., Hajos, N., Somogyi, P., and Mody, I. (1998). Increased number of synaptic GABA(A) receptors underlies potentiation at hippocampal inhibitory synapses. Nature 395, 172-177.

Oswald, M.J., Tantirigama, M.L., Sonntag, I., Hughes, S.M., and Empson, R.M. (2013). Diversity of layer 5 projection neurons in the mouse motor cortex. Front Cell Neurosci 7, 174.

Otsuka, T., and Kawaguchi, Y. (2009). Cortical inhibitory cell types differentially form intralaminar and interlaminar subnetworks with excitatory neurons. J Neurosci 29, 10533-10540.

Packer, A.M., and Yuste, R. (2011). Dense, unspecific connectivity of neocortical parvalbumin-positive interneurons: a canonical microcircuit for inhibition? J Neurosci 31, 13260-13271.

Pantazopoulos, H., Woo, T.U., Lim, M.P., Lange, N., and Berretta, S. (2010). Extracellular matrix-glial abnormalities in the amygdala and entorhinal cortex of subjects diagnosed with schizophrenia. Archives of general psychiatry 67, 155-166.

Papaleo, F., Silverman, J.L., Aney, J., Tian, Q.J., Barkan, C.L., Chadman, K.K., and Crawley, J.N. (2011). Working memory deficits, increased anxiety-like traits, and seizure susceptibility in BDNF overexpressing mice. Learn Memory 18, 534-544.

Parslow, R., Morgan, A.J., Allen, N.B., Jorm, A.F., O'Donnell, C.P., and Purcell, R. (2008). Effectiveness of complementary and self-help treatments for anxiety in children and adolescents. Med J Australia 188, 355-359.

Partonen, T. (2012). Clock gene variants in mood and anxiety disorders. J Neural Transm 119, 1133-1145.

Paschos, G.K., Ibrahim, S., Song, W.L., Kunieda, T., Grant, G., Reyes, T.M., Bradfield, C.A., Vaughan, C.H., Eiden, M., Masoodi, M.*, et al.* (2012). Obesity in mice with adipocyte-specific deletion of clock component Arntl. Nat Med 18, 1768-1777.

Pattwell, S.S., Duhoux, S., Hartley, C.A., Johnson, D.C., Jing, D., Elliott, M.D., Ruberry, E.J., Powers, A., Mehta, N., Yang, R.R.*, et al.* (2012). Altered fear learning across development in both mouse and human. Proc Natl Acad Sci U S A 109, 16318-16323.

Paxinos, G.F., K. B. J. (2001). The Mouse Brain in Stereotaxic Coordinates (Academic Press).

Peca, J., Feliciano, C., Ting, J.T., Wang, W., Wells, M.F., Venkatraman, T.N., Lascola, C.D., Fu, Z., and Feng, G. (2011). Shank3 mutant mice display autistic-like behaviours and striatal dysfunction. Nature 472, 437-442.

Pechtel, P., and Pizzagalli, D.A. (2011). Effects of early life stress on cognitive and affective function: an integrated review of human literature. Psychopharmacology 214, 55-70.

Pedersen, C.A., Vadlamudi S Fau - Boccia, M.L., Boccia Ml Fau - Moy, S.S., and Moy, S.S. (2011). Variations in Maternal Behavior in C57BL/6J Mice: Behavioral Comparisons between Adult Offspring of High and Low Pup-Licking Mothers.

Petilla Interneuron Nomenclature, G., Ascoli, G.A., Alonso-Nanclares, L., Anderson, S.A., Barrionuevo, G., Benavides-Piccione, R., Burkhalter, A., Buzsaki, G., Cauli, B., Defelipe, J.*, et al.* (2008). Petilla terminology: nomenclature of features of GABAergic interneurons of the cerebral cortex. Nat Rev Neurosci 9, 557-568.

Pfeffer, C.K., Xue, M.S., He, M., Huang, Z.J., and Scanziani, M. (2013). Inhibition of inhibition in visual cortex: the logic of connections between molecularly distinct interneurons. Nature Neuroscience 16, 1068-U1130.

Picton, A.J., and Fisher, J.L. (2007). Effect of the alpha subunit subtype on the macroscopic kinetic properties of recombinant GABA(A) receptors. Brain Res 1165, 40-49.

Pizzorusso, T., Medini, P., Berardi, N., Chierzi, S., Fawcett, J.W., and Maffei, L. (2002). Reactivation of ocular dominance plasticity in the adult visual cortex. Science 298, 1248-1251.

Plessy, C., Fagiolini, M., Wagatsuma, A., Harasawa, N., Kuji, T., Asaka-Oba, A., Kanzaki, Y., Fujishima, S., Waki, K., Nakahara, H.*, et al.* (2008). A resource for transcriptomic analysis in the mouse brain. PLoS One 3, e3012.

Pouille, F., and Scanziani, M. (2001). Enforcement of temporal fidelity in pyramidal cells by somatic feed-forward inhibition. Science 293, 1159-1163.

Prochiantz, A., and Di Nardo, A.A. (2015). Homeoprotein signaling in the developing and adult nervous system. Neuron 85, 911-925.

Rekaik, H., Blaudin de The, F.X., Fuchs, J., Massiani-Beaudoin, O., Prochiantz, A., and Joshi, R.L. (2015). Engrailed Homeoprotein Protects Mesencephalic Dopaminergic Neurons from Oxidative Stress. Cell reports 13, 242-250.

Renger, J.J., Hartman, K.N., Tsuchimoto, Y., Yokoi, M., Nakanishi, S., and Hensch, T.K. (2002). Experience-dependent plasticity without long-term depression by type 2 metabotropic glutamate receptors in developing visual cortex. Proceedings of the National Academy of Sciences of the United States of America 99, 1041-1046.

Riga, D., Matos, M.R., Glas, A., Smit, A.B., Spijker, S., and Van den Oever, M.C. (2014). Optogenetic dissection of medial prefrontal cortex circuitry. Front Syst Neurosci 8, 230.

Roselli, F., and Caroni, P. (2015). From Intrinsic Firing Properties to Selective Neuronal Vulnerability in Neurodegenerative Diseases. Neuron 85, 901-910.

Rossignol, E. (2011). Genetics and function of neocortical GABAergic interneurons in neurodevelopmental disorders. Neural Plast 2011, 649325.

Rouaux, C., and Arlotta, P. (2010). Fezf2 directs the differentiation of corticofugal neurons from striatal progenitors in vivo. Nat Neurosci 13, 1345-1347.

Rouaux, C., and Arlotta, P. (2013). Direct lineage reprogramming of post-mitotic callosal neurons into corticofugal neurons in vivo. Nature cell biology 15, 214-221.

Roybal, K., Theobold, D., Graham, A., DiNieri, J.A., Russo, S.J., Krishnan, V., Chakravarty, S., Peevey, J., Oehrlein, N., Birnbaum, S.*, et al.* (2007). Mania-like behavior induced by disruption of CLOCK. Proceedings of the National Academy of Sciences of the United States of America 104, 6406-6411.

Sabunciyan, S., Yolken, R., Ragan, C.M., Potash, J.B., Nimgaonkar, V.L., Dickerson, F., Llenos, I.C., and Weis, S. (2007). Polymorphisms in the homeobox gene OTX2 may be a risk factor for bipolar disorder. American journal of medical genetics Part B, Neuropsychiatric genetics : the official publication of the International Society of Psychiatric Genetics 144B, 1083-1086.

Sanke, R.F. (1988). Amblyopia. American family physician 37, 275-278.

Saxena, A., Wagatsuma, A., Noro, Y., Kuji, T., Asaka-Oba, A., Watahiki, A., Gurnot, C., Fagiolini, M., Hensch, T.K., and Carninci, P. (2012). Trehalose-enhanced isolation of neuronal sub-types from adult mouse brain. BioTechniques 52, 381-385.

Seo, D., Patrick, C.J., and Kennealy, P.J. (2008). Role of Serotonin and Dopamine System Interactions in the Neurobiology of Impulsive Aggression and its Comorbidity with other Clinical Disorders. Aggress Violent Behav 13, 383-395.

Shapiro-Reznik, M., Jilg, A., Lerner, H., Earnest, D.J., and Zisapel, N. (2012). Diurnal rhythms in neurexins transcripts and inhibitory/excitatory synapse scaffold proteins in the biological clock. PLoS One 7, e37894.

Shatz, C.J., and Stryker, M.P. (1978). Ocular dominance in layer IV of the cat's visual cortex and the effects of monocular deprivation. The Journal of physiology 281, 267-283.

Shirtcliff, E.A., Allison, A.L., Armstrong, J.M., Slattery, M.J., Kalin, N.H., and Essex, M.J. (2012). Longitudinal stability and developmental properties of salivary cortisol levels and circadian rhythms from childhood to adolescence. Developmental psychobiology 54, 493-502.

Simons, S.S., Beijers, R., Cillessen, A.H., and de Weerth, C. (2015). Development of the cortisol circadian rhythm in the light of stress early in life. Psychoneuroendocrino 62, 292-300.

Smaers, J.B., Mulvaney, P.I., Soligo, C., Zilles, K., and Amunts, K. (2012). Sexual Dimorphism and Laterality in the Evolution of the Primate Prefrontal Cortex. Brain Behav Evolut 79, 205-212.

Sohal, V.S., Zhang, F., Yizhar, O., and Deisseroth, K. (2009). Parvalbumin neurons and gamma rhythms enhance cortical circuit performance. Nature 459, 698-702.

Soltesz, I., Smetters, D.K., and Mody, I. (1995). Tonic Inhibition Originates from Synapses Close to the Soma. Neuron 14, 1273-1283.

Solum, D.T., and Handa, R.J. (2001). Localization of estrogen receptor alpha (ER alpha) in pyramidal neurons of the developing rat hippocampus. Brain research Developmental brain research 128, 165-175.

Solum, D.T., and Handa, R.J. (2002). Estrogen regulates the development of brain-derived neurotrophic factor mRNA and protein in the rat hippocampus. J Neurosci 22, 2650-2659.

Somers, J.M., Goldner, E.M., Waraich, P., and Hsu, L. (2006). Prevalence and incidence studies of anxiety disorders: A systematic review of the literature. Can J Psychiat 51, 100-113.

Sommeijer, J.P., and Levelt, C.N. (2012). Synaptotagmin-2 is a reliable marker for parvalbumin positive inhibitory boutons in the mouse visual cortex. PLoS One 7, e35323.

Southwell, D.G., Froemke, R.C., Alvarez-Buylla, A., Stryker, M.P., and Gandhi, S.P. (2010). Cortical plasticity induced by inhibitory neuron transplantation. Science 327, 1145-1148.

Southwell, D.G., Nicholas, C.R., Basbaum, A.I., Stryker, M.P., Kriegstein, A.R., Rubenstein, J.L., and Alvarez-Buylla, A. (2014). Interneurons from embryonic development to cell-based therapy. Science 344, 1240622.

Spalletta, G., Morris Dw Fau - Angelucci, F., Angelucci F Fau - Rubino, I.A., Rubino Ia Fau - Spoletini, I., Spoletini I Fau - Bria, P., Bria P Fau - Martinotti, G., Martinotti G Fau - Siracusano, A., Siracusano A Fau - Bonaviri, G., Bonaviri G Fau - Bernardini, S., Bernardini S Fau - Caltagirone, C.*, et al.* (2010). BDNF Val66Met polymorphism is associated with aggressive behavior in schizophrenia.

Spatazza, J., Lee, H.H., Di Nardo, A.A., Tibaldi, L., Joliot, A., Hensch, T.K., and Prochiantz, A. (2013). Choroid-plexus-derived Otx2 homeoprotein constrains adult cortical plasticity. Cell Rep 3, 1815-1823.

Spear, L.P. (2000). The adolescent brain and age-related behavioral manifestations. Neurosci Biobehav Rev 24, 417-463.

Spiers, H., Hannon, E., Schalkwyk, L.C., Smith, R., Wong, C.C., O'Donovan, M.C., Bray, N.J., and Mill, J. (2015). Methylomic trajectories across human fetal brain development. Genome Res 25, 338-352.

Stephany, C.E., Ikrar, T., Nguyen, C., Xu, X., and McGee, A.W. (2016). Nogo Receptor 1 Confines a Disinhibitory Microcircuit to the Critical Period in Visual Cortex. J Neurosci 36, 11006-11012.

Stockard, C.R. (1921). Developmental rate and structural expression: An experimental study of twins, 'double monsters' and single deformities, and the interaction among embryonic organs during their origin and development. American Journal of Anatomy 28, 115-277.

Storch, K.F., Paz, C., Signorovitch, J., Raviola, E., Pawlyk, B., Li, T., and Weitz, C.J. (2007). Intrinsic circadian clock of the mammalian retina: importance for retinal processing of visual information. Cell 130, 730-741.

Stryker, M.P. (2014). A Neural Circuit That Controls Cortical State, Plasticity, and the Gain of Sensory Responses in Mouse. Cold Spring Harb Symp Quant Biol 79, 1-9.

Sudhof, T.C. (2008). Neuroligins and neurexins link synaptic function to cognitive disease. Nature 455, 903-911.

Sugiyama, S., Di Nardo, A.A., Aizawa, S., Matsuo, I., Volovitch, M., Prochiantz, A., and Hensch, T.K. (2008). Experience-dependent transfer of Otx2 homeoprotein into the visual cortex activates postnatal plasticity. Cell 134, 508-520.

Susman, E.J., Inoff-Germain, G., Nottelmann, E.D., Loriaux, D.L., Cutler, G.B., Jr., and Chrousos, G.P. (1987). Hormones, emotional dispositions, and aggressive attributes in young adolescents. Child Dev 58, 1114-1134.

Swadlow, H.A. (2003). Fast-spike interneurons and feedforward inhibition in awake sensory neocortex. Cereb Cortex 13, 25-32.

Takahashi, J.S., Hong, H.K., Ko, C.H., and McDearmon, E.L. (2008). The genetics of mammalian circadian order and disorder: implications for physiology and disease. Nat Rev Genet 9, 764-775.

Takesian, A.E., and Hensch, T.K. (2013). Balancing plasticity/stability across brain development. Progress in brain research 207, 3-34.

Tang, Y., Stryker, M.P., Alvarez-Buylla, A., and Espinosa, J.S. (2014). Cortical plasticity induced by transplantation of embryonic somatostatin or parvalbumin interneurons. Proc Natl Acad Sci U S A 111, 18339-18344.

Toyoizumi, T., Miyamoto, H., Yazaki-Sugiyama, Y., Atapour, N., Hensch, T.K., and Miller, K.D. (2013). A theory of the transition to critical period plasticity: inhibition selectively suppresses spontaneous activity. Neuron 80, 51-63.

Traub, R.D., Spruston, N., Soltesz, I., Konnerth, A., Whittington, M.A., and Jefferys, G.R. (1998). Gamma-frequency oscillations: a neuronal population phenomenon, regulated by synaptic and intrinsic cellular processes, and inducing synaptic plasticity. Prog Neurobiol 55, 563-575.

Tropea, D., Kreiman, G., Lyckman, A., Mukherjee, S., Yu, H., Horng, S., and Sur, M. (2006). Gene expression changes and molecular pathways mediating activity-dependent plasticity in visual cortex. Nat Neurosci 9, 660-668.

Turner, C.A., Thompson, R.C., Bunney, W.E., Schatzberg, A.F., Barchas, J.D., Myers, R.M., Akil, H., and Watson, S.J. (2014). Altered choroid plexus gene expression in major depressive disorder. Frontiers in human neuroscience 8, 238.

Uylings, H.B., and van Eden, C.G. (1990). Qualitative and quantitative comparison of the prefrontal cortex in rat and in primates, including humans. Progress in brain research 85, 31-62.

van Erp, A.M., and Miczek, K.A. (2000). Aggressive behavior, increased accumbal dopamine, and decreased cortical serotonin in rats. J Neurosci 20, 9320-9325.

Varga, C., Lee, S.Y., and Soltesz, I. (2010). Target-selective GABAergic control of entorhinal cortex output. Nat Neurosci 13, 822-824.

Verhagen, M., van der Meij, A., van Deurzen, P.A.M., Janzing, J.G.E., Arias-Vasquez, A., Buitelaar, J.K., and Franke, B. (2010). Meta-analysis of the BDNF Val66Met polymorphism in major depressive disorder: effects of gender and ethnicity. Molecular psychiatry 15, 260-271.

Vialou, V., Bagot, R.C., Cahill, M.E., Ferguson, D., Robison, A.J., Dietz, D.M., Fallon, B., Mazei-Robison, M., Ku, S.M., Harrigan, E.*, et al.* (2014). Prefrontal Cortical Circuit for Depression- and Anxiety-Related Behaviors Mediated by Cholecystokinin: Role of Delta FosB. J Neurosci 34, 3878-3887.

Vicini, S., Ferguson, C., Prybylowski, K., Kralic, J., Morrow, A.L., and Homanics, G.E. (2001). GABA(A) receptor alpha 1 subunit deletion prevents developmental changes of inhibitory synaptic currents in cerebellar neurons. J Neurosci 21, 3009-3016.

Vogt, B.A., Finch, D.M., and Olson, C.R. (1992). Functional heterogeneity in cingulate cortex: the anterior executive and posterior evaluative regions. Cereb Cortex 2, 435-443.

Wade, J. (2001). Zebra finch sexual differentiation: the aromatization hypothesis revisited. Microsc Res Tech 54, 354-363.

Wahlsten, D., Metten, P., and Crabbe, J.C. (2003). Survey of 21 inbred mouse strains in two laboratories reveals that BTBR T/+ tf/tf has severely reduced hippocampal commissure and absent corpus callosum. Brain Res 971, 47-54.

Wakamatsu, H., Yoshinobu, Y., Aida, R., Moriya, T., Akiyama, M., and Shibata, S. (2001). Restricted-feeding-induced anticipatory activity rhythm is associated with a phase-shift of the expression of mPer1 and mPer2 mRNA in the cerebral cortex and hippocampus but not in the suprachiasmatic nucleus of mice. Eur J Neurosci 13, 1190-1196.

Weaver, I.C.G., Cervoni, N., Champagne, F.A., D'Alessio, A.C., Sharma, S., Jr, S., Dymov, S., Szyf, M., and Meaney, M.J. (2004). Epigenetic programming by maternal behavior. Nature Neuroscience 7, 847-854.

Weber, E.T., and Andrade, R. (2010). Htr2a Gene and 5-HT(2A) Receptor Expression in the Cerebral Cortex Studied Using Genetically Modified Mice. Front Neurosci 4.

Weber, J.N., Peterson, B.K., and Hoekstra, H.E. (2013). Discrete genetic modules are responsible for complex burrow evolution in Peromyscus mice. Nature 493, 402-U145.

Wehr, M., and Zador, A.M. (2005). Synaptic mechanisms of forward suppression in rat auditory cortex. Neuron 47, 437-445.

Werker, J.F., and Hensch, T.K. (2015). Critical periods in speech perception: new directions. Annual review of psychology 66, 173-196.

Wiesel, T.N. (1982). Postnatal development of the visual cortex and the influence of environment. Nature 299, 583-591.

Wiesel, T.N., and Hubel, D.H. (1963). Single-Cell Responses in Striate Cortex of Kittens Deprived of Vision in One Eye. Journal of neurophysiology 26, 1003-1017.

Wisden, W., Laurie, D.J., Monyer, H., and Seeburg, P.H. (1992). The distribution of 13 GABAA receptor subunit mRNAs in the rat brain. I. Telencephalon, diencephalon, mesencephalon. J Neurosci 12, 1040-1062.

Wu, Y.W., Du, X., van den Buuse, M., and Hill, R.A. (2015). Analyzing the influence of BDNF heterozygosity on spatial memory response to 17beta-estradiol. Transl Psychiatry 5, e498.

Wulff, K., Gatti, S., Wettstein, J.G., and Foster, R.G. (2010). Sleep and circadian rhythm disruption in psychiatric and neurodegenerative disease. Nat Rev Neurosci 11, 589-599.

Wulff, P., Ponomarenko, A.A., Bartos, M., Korotkova, T.M., Fuchs, E.C., Bahner, F., Both, M., Tort, A.B., Kopell, N.J., Wisden, W., and Monyer, H. (2009). Hippocampal theta rhythm and its coupling with gamma oscillations require fast inhibition onto parvalbumin-positive interneurons. Proceedings of the National Academy of Sciences of the United States of America 106, 3561-3566.

Xiang, Z., Huguenard, J.R., and Prince, D.A. (1998). GABAA receptor-mediated currents in interneurons and pyramidal cells of rat visual cortex. The Journal of physiology 506 (Pt 3), 715-730.

Yagita, K., Horie, K., Koinuma, S., Nakamura, W., Yamanaka, I., Urasaki, A., Shigeyoshi, Y., Kawakami, K., Shimada, S., Takeda, J., and Uchiyama, Y. (2010). Development of the circadian oscillator during differentiation of mouse embryonic stem cells in vitro. Proc Natl Acad Sci U S A 107, 3846-3851.

Yakovlev, P.I., and Lecours, A.R. (1967). The myelogenetic cycles of regional maturation of the brain. In Regional Development of the Brain in Early Life, A. Minkowsky, ed. (Blackwell Scientific Publications), pp. 3-70.

Yamamoto, J., Suh, J., Takeuchi, D., and Tonegawa, S. (2014). Successful execution of working memory linked to synchronized high-frequency gamma oscillations. Cell 157, 845-857.

Yan, L., Miyake, S., and Okamura, H. (2000). Distribution and circadian expression of dbp in SCN and extra-SCN areas in the mouse brain. J Neurosci Res 59, 291-295.

Yang, E.J., Lin, E.W., and Hensch, T.K. (2012). Critical period for acoustic preference in mice. P Natl Acad Sci USA 109, 17213-17220.

Yang, M., Silverman, J.L., and Crawley, J.N. (2011). Automated three-chambered social approach task for mice. Current protocols in neuroscience / editorial board, Jacqueline N Crawley [et al] Chapter 8, Unit 8 26.

Ye, Z.L., Mostajo-Radji, M.A., Brown, J.R., Rouaux, C., Tomassy, G.S., Hensch, T.K., and Arlotta, P. (2015). Instructing Perisomatic Inhibition by Direct Lineage Reprogramming of Neocortical Projection Neurons. Neuron 88, 475-483.

Yinger, O.S., and Gooding, L. (2014). Music therapy and music medicine for children and adolescents. Child and adolescent psychiatric clinics of North America 23, 535-553.

Yizhar, O., Fenno, L.E., Prigge, M., Schneider, F., Davidson, T.J., O'Shea, D.J., Sohal, V.S., Goshen, I., Finkelstein, J., Paz, J.T.*, et al.* (2011). Neocortical excitation/inhibition balance in information processing and social dysfunction. Nature 477, 171-178.

Yu, X., Rollins, D., Ruhn, K.A., Stubblefield, J.J., Green, C.B., Kashiwada, M., Rothman, P.B., Takahashi, J.S., and Hooper, L.V. (2013). TH17 cell differentiation is regulated by the circadian clock. Science 342, 727-730.

Zhao, C., Teng, E.M., Summers, R.G., Jr., Ming, G.L., and Gage, F.H. (2006). Distinct morphological stages of dentate granule neuron maturation in the adult mouse hippocampus. J Neurosci 26, 3-11.

Zhou, X.M., and Merzenich, M.M. (2012). Environmental noise exposure degrades normal listening processes. Nat Commun 3.

Zhou, X.M., Panizzutti, R., de Villers-Sidani, E., Madeira, C., and Merzenich, M.M. (2011). Natural Restoration of Critical Period Plasticity in the Juvenile and Adult Primary Auditory Cortex. J Neurosci 31, 5625-5634.

Zuccotti, A., Le Magueresse, C., Chen, M., Neitz, A., and Monyer, H. (2014). The transcription factor Fezf2 directs the differentiation of neural stem cells in the subventricular zone toward a cortical phenotype. Proc Natl Acad Sci U S A 111, 10726-10731.